

Molecular Detection & Identification Using Laser Mass Spectrometry.

**Joseph Sander
Department of Physics and Astronomy
University of Glasgow**

**Presented as a thesis for the degree of Doctor of
Philosophy
in the University of Glasgow**

© Joseph Sander, April 1994.

ProQuest Number: 11007930

All rights reserved

INFORMATION TO ALL USERS

The quality of this reproduction is dependent upon the quality of the copy submitted.

In the unlikely event that the author did not send a complete manuscript and there are missing pages, these will be noted. Also, if material had to be removed, a note will indicate the deletion.



ProQuest 11007930

Published by ProQuest LLC (2018). Copyright of the Dissertation is held by the Author.

All rights reserved.

This work is protected against unauthorized copying under Title 17, United States Code
Microform Edition © ProQuest LLC.

ProQuest LLC.
789 East Eisenhower Parkway
P.O. Box 1346
Ann Arbor, MI 48106 – 1346

GLASGOW
UNIVERSITY
LIBRARY

Thesis
9804
copy 1

***To
Mum and Dad***

Acknowledgements

I would at this point like to mention a number of people who have assisted and encouraged me in the experimental work and the analysis of the data, which has resulted in the completion of this thesis.

Dr. Kenneth Ledingham, for close supervision and an open door at all times for all types of problems.

Dr. Ravi Singhal, for sharing his insight of theoretical calculations.

Dr. Archie Marshall, for encouragement and guidance in the experimental work and proof reading the thesis.

Dr. Alastair Clark, for lucid explanations of experimental and theoretical concepts.

Dr. Costas Kosmidis, for help in interpretation and analysis of data.

Colin Scott, Rong-er Zheng, Robert Deas, Wei-jie Jia and Weixian Peng for companionship and friendly bantering.

Tom McCanny and Bob Maxwell for valuable technical assistance and lively philosophical discussions.

To the various members of the Mechanical and Electronic Workshops for the construction of various types of apparatus.

The S.E.R.C for financial support.

Publications

Marshall A, Clark A, Jennings R, Ledingham KWD, **Sander J** and Singhal RP

Laser-induced Dissociation, Ionisation and Fragmentation Processes in Nitroaromatic Molecules.

Int. J. Mass Spectrom. and Ion Proc., 116 (1992) 143

Clark A, Ledingham KWD, Jennings R, Marshall A, **Sander J** and Singhal RP

Atomic pathways in the fragmentation of nitroaromatic molecules.

RIS 92, Inst. Phys. Conf. Ser. No 128: Section 5 (1992) 189

Marshall A, Clark A, Jennings R, Ledingham KWD, **Sander J** and Singhal RP

Laser Ionisation and Fragmentation Processes in Nitrobenzene.

RIS 92, Inst. Phys. Conf. Ser. No 128: Section 5 (1992) 181

Zheng R, Campbell M, Ledingham KWD, Clark A, Jennings R, Marshall A, **Sander J** and Singhal RP

A laser based procedure for the detection of NO and NO₂ in both vacuum and atmospheric conditions.

Proceedings of Miconex 92, the 5th Multinational

Instrumentation Conference on Instrumentation and Total

Quality Management, 22-25 Sept. 1992, Beijing, P.R. China, 442-447.

Clark A, Ledingham KWD, Marshall A, **Sander J** and Singhal RP

Attomole detection of nitroaromatic vapours using Resonance Enhanced Ionisation Mass Spectrometry.

Analyst 118 (1993) 601

Marshall A, Clark A, Ledingham KWD, **Sander J** and Singhal RP

Laser Ionisation Studies of Nitroaromatic and NO_x (x=1,2) Molecules in the region 224-237nm.

Int. J. Mass Spectrom. and Ion Proc. 124 (1993) R15-R20

Campbell M, Javaud S, Zheng R, Ledingham KWD, Singhal R P, Borthwick I S, Clark A, Marshall A and **Sander J**

Attenuation characteristics of an all-silica UV fibre.

SPIE 1712 Proceedings of the 14th Symposium on Photonic Measurements, 1-3 June 1992, Sopron, Hungary, 150-159.

Clark A, Kosmidis C, Deas RM, Ledingham KWD, Marshall A, **Sander J** and Singhal RP

Multiphoton processes in open atmosphere in the wavelength region 224-230nm.

J. Phys. D: Appl. Phys. 26 (1993) 2107-2111

Clark A, Deas RM, Kosmidis C, Ledingham KWD, Marshall A, **Sander J**, Singhal RP, Campbell M and Zheng R

A laser-based sensor system for trace NO_x (x=1,2) detection in atmospheric air.

Sensors VI: Technology, Systems and Applications, Adam Hilger, Ed KTV Grattan, 57 (1993)

Clark A, Kosmidis C, Ledingham KWD, Marshall A, **Sander J**, Singhal RP and Campbell M

Resonant ionization of oxygen and hydrogen atoms following laser induced photodissociation of nitrobenzene vapour.

J. Phys. B: At. Mol. Opt. Phys., 26 (1993) L665-L670

Marshall A, Clark A, Ledingham KWD, **Sander J**, Singhal RP, Deas RM and Kosmidis C

Detection and Identification of Explosives Compounds using Laser Ionisation Techniques.

Submitted for publication to Rapid Communications in Mass Spectrometry.

Marshall A, Clark A, Ledingham KWD, **Sander J**, Singhal RP,
Deas RM and Kosmidis C

Sensitive atmospheric pressure detection of nitroaromatic and
NO_x compounds using Resonance Enhanced Multiphoton
Ionisation.

Submitted for publication to The Analyst.

Kosmidis C, Ledingham KWD, Clark A, Marshall A, Jennings R,
Sander J and Singhal RP

On the dissociation pathways of nitrobenzene.

Submitted for publication to The Journal of Chemical Physics.

Summary

Chapter 1 gives a brief review of the advent of laser based techniques for atomic and thereafter molecular detection. The laser based techniques have been used in conjunction with mass spectrometers and other spectroscopic instruments, with the system based on a Time-of-flight mass spectrometer. The essence of the thesis is to show results pertaining to detection of explosive type molecules and currently deployed techniques in this area are discussed in this chapter.

Chapter 2 gives detailed insight into the laser interaction with matter and the fragmentation mechanisms which result in the production of atomic and molecular species. The pros and cons of some ionisation schemes are put forward and a discussion of those deployed in our experiments is carried out.

Chapter 3 is an exposition of the various components of the apparatus used.

Chapter 4 highlights the presence of an impurity, viz., benzene in our nitrobenzene sample and also demonstrates the potency of our technique as a sensitive analytical instrument. A number of different techniques were used by the author in order to show the presence of the contaminant. These techniques provided inconclusive evidence to support our prediction, unlike the information provided by the TOF system. This system has shown both the presence and further the unambiguous identification of the contaminant.

Chapter 5 deals with nitrobenzene and o-nitrotoluene which are the simplest compounds of the nitroaromatic group. It describes the typical fragmentation patterns observed and a thorough discussion of the most prominent fragment, namely, the NO ion. Also a computer program written by the author is used to compare the experimental with theoretical results.

The origins and significance of this ion for sensitivity and selectivity purposes is investigated. Measurements from the nitrobenzene sample have demonstrated that parts per billion sensitivity levels can be attained.

Chapter 6 pursues the investigation of the fragments concentrating on the atomic species of oxygen & hydrogen which are analysed by Dr Marshall and the author. An analysis of the possible pathways leading to the oxygen ion formation are discussed.

The second half this chapter looks at the various higher mass fragments obtained from nitrobenzene. From the presence of the higher mass fragments, interpretations of the possible fragmentation pathways has been elucidated by Dr Kosmidis. Of primary significance in this analysis was the first recorded presence of the nitrobenzene parent ion in a laser photolysis experiment.

Chapter 7 discusses results from a variety of commonly used explosive compounds obtained by Dr Marshall and the author. Their analysis is undertaken using the modified sample entry system. This allows the variation in signal heights against temperature to be recorded which were subsequently plotted. The identification of the individual species is sought from the mass spectra obtained which were also used to determine sensitivity levels.

Contents

<u>Frontspiece</u>	(i)
<u>Acknowledgements</u>	(iii)
<u>Publications</u>	(iv)
<u>Summary</u>	(vii)
<u>Contents</u>	(ix)

Chapter 1.Introduction.

(1) Historical Background.	1
(2) Two Dimensional Analysis.	2
(3) Glasgow Groups Experiments.	3
(i) Desirable Properties.	3
(4) Alternative Techniques.	4
(i) ECD Device.	5
(ii) Ion Mobility Spectrometry.	6
(iii) X-Rays.	9
(iv) Nuclear Devices.	9

Chapter 2.Theory.

(1) Introduction.	11
(2) Semi-Classical Description.	12
(i) Photon-Atom Mathematical Evaluation.	12
(3) Line Width.	17
(i) Natural Line Broadening.	18
(ii) Doppler Broadening.	20
(iii) Pressure Broadening.	21
(iv) Classification of Mechanisms.	21
(4) Ionisation Schemes.	22
(5) Effect of Radiation Intensity on Ionisation Schemes.	24
(6) Intensity Dependence.	25
(7) Ionisation of Molecules.	26
(i) Typical Experimental Parameters.	27

(ii) Methods and Regimes of Multiphoton Ionisation of Molecules.	28
(8) Detection of Molecules by Multistep & Multiphoton Resonant Ionisation.	31
(i) Fragmentation.	31
(9) Intensity of Vibrational-Electronic Spectra: The Franck Condon Principle.	32
(10) Dissociation Energy & Products.	34
(11) Predissociation.	35

Chapter 3. Experimental Set-Up 37

(1) Method.	37
(2) The Excimer Laser.	39
(3) The Dye Laser.	40
(i) Theory of Operation.	41
(4) The Compuscan.	44
(5) Autotracker.	44
(6) Optical Attenuator.	45
(i) Principle of Operation.	45
(7) Time of Flight Mass Spectrometer.	45
(8) Ionivac.	47
(9) Pyroelectric Joulemeter.	48
(10) Gentec Joulemeter.	48
(11) Data Acquisition.	49
(12) Electron Multiplier.	50

Chapter 4. The Role of REMPI Mass Spectrometry In Trace Analysis. 51

(1) Mass & Wavelength Dependent Data of Nitrobenzene.	52
(2) UV Absorption Spectra.	53
(3) Comparison of Absorption Spectra of Benzene with Wavelength Dependence of Nitrobenzene Fragments.	55
(4) Search for Benzene Contaminant.	56
(5) Interpretation of Results.	60
(6) Conclusions.	61

Chapter 5.Nitrobenzene & Nitrotoluene. 63

(1) Introduction.	63
(2) Results Obtained.	64
(3) Nitrobenzene and O-Nitrotoluene Investigation.	65
(4) Laser Induced Fragmentation In Nitroaromatics.	65
(5) Significance of NO Ion.	67
(6) Comparison Using Computational Analysis.	71
(7) Interpretation of Data.	72
(8) Determining Origins Of The NO Signal.	72
(9) Sensitivity Measurements.	73
(10) Conclusions.	76

Chapter 6.Analysis of Fragments Other Than NO⁺ & Photodissociation Pathways. 77

(1) Spectroscopy of Oxygen & Hydrogen.	77
(2) Oxygen Data.	78
(i) Analysis.	79
(ii) Origin Of The Oxygen Ion Signal.	80
(3) Hydrogen Atom Production.	81
(4) Conclusions.	82
(i) Future.	83
(5) Photodissociation Pathways of Nitrobenzene.	84
(6) Resume of Possible Photodissociation Pathways.	85
(7) Technique And Application.	86
(8) Results and Discussion.	87
(i) Dissociation and Ionisation.	88
(ii) Ionisation Dissociation	91
(9) Conclusion.	92

Chapter 7.Explosives. 93

(1) Introduction.	93
-------------------	----

(2) Experimental Set-Up.	94
(3) Results and Discussion.	95
(4) Mass Spectra.	96
(5) Temperature Dependencies.	97
(6) Sensitivity Measurements.	100
(7) Conclusions.	102
<u>Chapter8. Conclusions</u>	103
<u>References</u>	107

1.Introduction

(1)Historical Background

Resonance Ionisation Spectroscopy is an exceptionally powerful and versatile analytical tool which is capable of single atom detection. Also it holds great potential for the very sensitive and selective detection of molecular species, although as yet single molecule detection is not possible. It was discovered independently in the early 1970's by Sam Hurst at the Oak Ridge national Laboratory in the US and Vladilen Letokhov of the Russian Academy of Sciences Institute of Spectroscopy at Troitsk near Moscow(1). Both Hurst and Letokhov realised the enormous potential of a tuneable source of laser light to selectively ionise a pre-determined atomic species in a sample and leave any other species unchanged.(2,3) It is the case that charged particles are a very convenient entity for detection by any ultra sensitive technique owing to their high collection efficiency, usually brought about by applying strong electric fields, and their direct conversion to a laboratory signal. The viability and interest in this technique was also precipitated by a review paper by Hurst et al in 1974 (4).

Following the work of Bohr in 1913 it was evident that photons could excite an atom to a high-lying electronic state which is subsequently excited above the ionisation potential in a sequential absorption process. A condition for this process to succeed is that the photon flux is high enough such that the excited state photoionisation occurs at a rate competitive with other process which remove excited state population. Such processes include predissociation which is a common population loss mechanism in polyatomic molecules, with rates as high as 10^{14}sec^{-1} , Other processes will be looked at later in the thesis and their significance explained. Because of this flux requirement, resonant two-photon ionisation (R2PI) was not actively investigated until the advent of high intensity pulsed lasers in the middle 1960's.

Intense lasers can also cause non-linear or multi-photon events, which follow an I^N dependence (where I is the photon flux and N the number of photons absorbed). This dependence describes the situation when absorption of photons proceed through virtual states in the atom or molecule and is referred to as multiphoton ionisation. When the ionisation process proceeds through real intermediate excited states, the cross section for this process is increased by several orders of magnitude over the non-resonant case. This phenomenon is referred to as Resonance Enhanced Multiphoton Ionisation (REMPI) and has been utilised in our experiments with molecules. Molecules like atoms have a resonant structure but in their case, the resonant structure is much more complicated because of vibrations and rotations for any specific molecule. In order to ameliorate the effects of this problem techniques such as supersonic jet cooling have been deployed to narrow and simplify the molecular resonances and thereby improve selectivity.

(2) Two Dimensional Analysis

Mass Spectroscopy and Resonance Enhanced Multiphoton Ionisation when used in conjunction provide both mass and spectral information simultaneously. The potential of this approach is reviewed as an analytical and spectroscopic tool for the study of atoms and molecules by Letokhov(5). Ions are created efficiently only when the laser is tuned to specific excited states of the selected molecule. The ionisation spectrum can be used to form a spectral wavelength-dependent fingerprint of the molecule, and mass analysis of the resulting ions also allows direct identification. Charged particles can be detected with very high sensitivity, with single electron charges being detectable using the appropriate electronics. With such selectivity possible, there exists the possibility of detecting signals from any specific rovibronic state.

It is therefore proposed that REMPI in conjunction with time of flight (TOF) mass spectrometry can be used as a very sensitive

and highly selective tool for the trace detection of explosive molecules in normal atmospheric conditions. These compounds are used by both the military and commercial sector for a variety of roles. Because of their widespread use and ease of availability some have inevitably fallen into the wrong hands. It is for this reason that the sensitive detection of explosive compounds has become one of the most important problems in analytical science today. (6,7)

(3) The Glasgow Experiments

The research carried out in this thesis is under vacuum conditions but the interfacing of this technique to atmospheric pressure conditions remains a possibility. The problem of interfacing has not been dealt with in this thesis but rather the optimisation of conditions such as to obtain the greatest sensitivity and the unambiguous detection of explosive materials has been pursued. Because of the very low vapour pressures associated with these compounds ($<10^{-6}$ Torr), very high sensitivity levels are a prerequisite to their detection.

The work of this thesis is concerned with developing and optimising a procedure using a laser based system for the detection of explosive molecules. Detection of hidden explosives has become an important social requirement as terrorist groups have increasingly adopted the technique of using hidden explosive devices as a convenient weapon to pursue their aims. With the use of plastic explosives terrorists have found light weight materials which have powerful explosive yields, also the malleability of such materials allow them to be concealed with consummate ease. These properties have meant that the detection using conventional methods are becoming inadequate.

(4) Desirable Properties

A suitable detector must therefore be sufficiently sensitive to be able to detect relatively small amounts of materials when

concealed in luggage containers. It must be very selective, so that alarms are not raised for innocuous substances and thereby minimising the disturbance to normal business practices, such as airports etc. Finally, it must be capable of detecting a potentially dangerous material in a relatively short time (short real time analyses) and should be as efficient at the end of an extended search as at the beginning.

All of the explosive molecules dealt with fall into the category of nitro-compounds, therefore the procedure developed should have the properties of not only detecting the nitro-compounds but have the ability to distinguish between individual species. Otherwise the device would respond to innocent compounds such as perfumes, musks etc. which would render the viability of the instrument in doubt.

The research is carried out in high vacuum conditions, therefore difficulty is envisaged on the applicability of the instrument in normal atmospheric conditions. The interfacing of the technique to ambient conditions will add to the complexity and possibly the analysis time, but for the time being our research is dedicated to finding a wavelength dependent fingerprint in order to allow unambiguous identification.

(5) Alternative Techniques

A description of some current devices in operation used for explosive detection are discussed and comments made on their pros and cons.

Animals are one kind of "sniffer" detector, being sensitive to the vapour from an explosive substance. Other basic techniques for detecting such explosives vapours include plasma chromatography, chemiluminescence, and electron capture devices (ECD).

Techniques which do not rely on detecting the vapour but rather concentrate on bulk detection include X-ray, thermal neutron activation etc.

(i) ECD Device (8, 9) (Fig 1.1)

This involves the unit sucking air through a sampling probe and through a concentrator using a vacuum pump. At the end of the pump time, the concentrator is transferred from the absorb port to the desorb port where heated carrier gas (nitrogen) drives off the sample of vapours and transfers it to the analysis system.

The analysis involves using a column separator on the mixture of vapours transferred from the concentrator. The package of vapours is moved by the carrier gas stream through the chromatography column. The column offers a greater restriction to the passage vapours of large molecular size or materials of high polarity than to vapours of small molecular size and low polarity, and so each is delayed in the column for a different time.

Retention times are monitored using the electrical output of the ECD. This detector consists of a stainless-steel tube with a ^{63}Ni radioactive foil around its inner face and an electrode running along its axis. When the body of the ECD is pulsed with a voltage we attract the ions within the electric field region to the electrodes, which subsequently induces a current which is monitored. Under normal conditions the passing carrier gas allows a reference current to be generated between the foil and the electrode. This current varies with its response being a characteristic of the vapour passing, each vapour producing a peak on the flat baseline. The time of appearance of a peak indicates its chemical composition, and, by gating the output to provide a signal only when the timing is between predetermined limits, the detection system can be made to respond and provide an alarm-only when the vapours searched for are present.

The ECD electrical output is amplified and fed to the microprocessor, which stores information regarding the components appearing at specific retention times. At the end of the cycle the stored information is analysed, and if vapours are present at the retention times similar to those stored in the memory corresponding to dangerous materials an alarm is initiated.

One of the disadvantages of such a system is that because the system relies on the times of materials passing through the column it is found that a number of materials have the same exit time thus giving an unacceptable level of false alarms. As most of the nitroaromatics have similar chemical composition containing the benzene ring with associated radicals attached to it this could lead to difficulties as far as the selectivity is concerned.

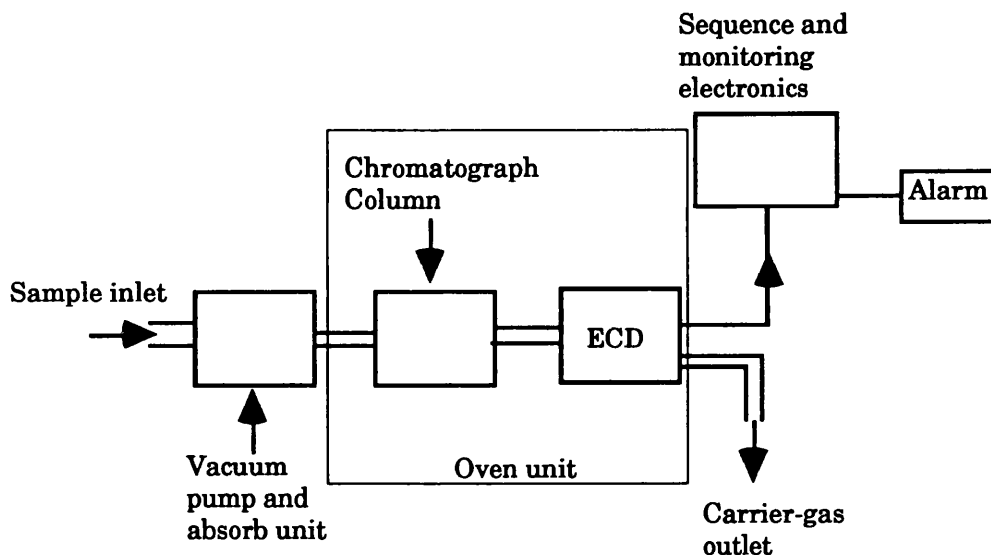


Fig 1.1 Schematic Diagram Of Portable Explosive Detector.

(ii) Ion Mobility Spectrometry (9,10,11)

From the earliest days of interest in explosives vapour detection, ion mobility spectrometry (IMS) has been considered a viable candidate for exploitation as a sensor. IMS is used as an

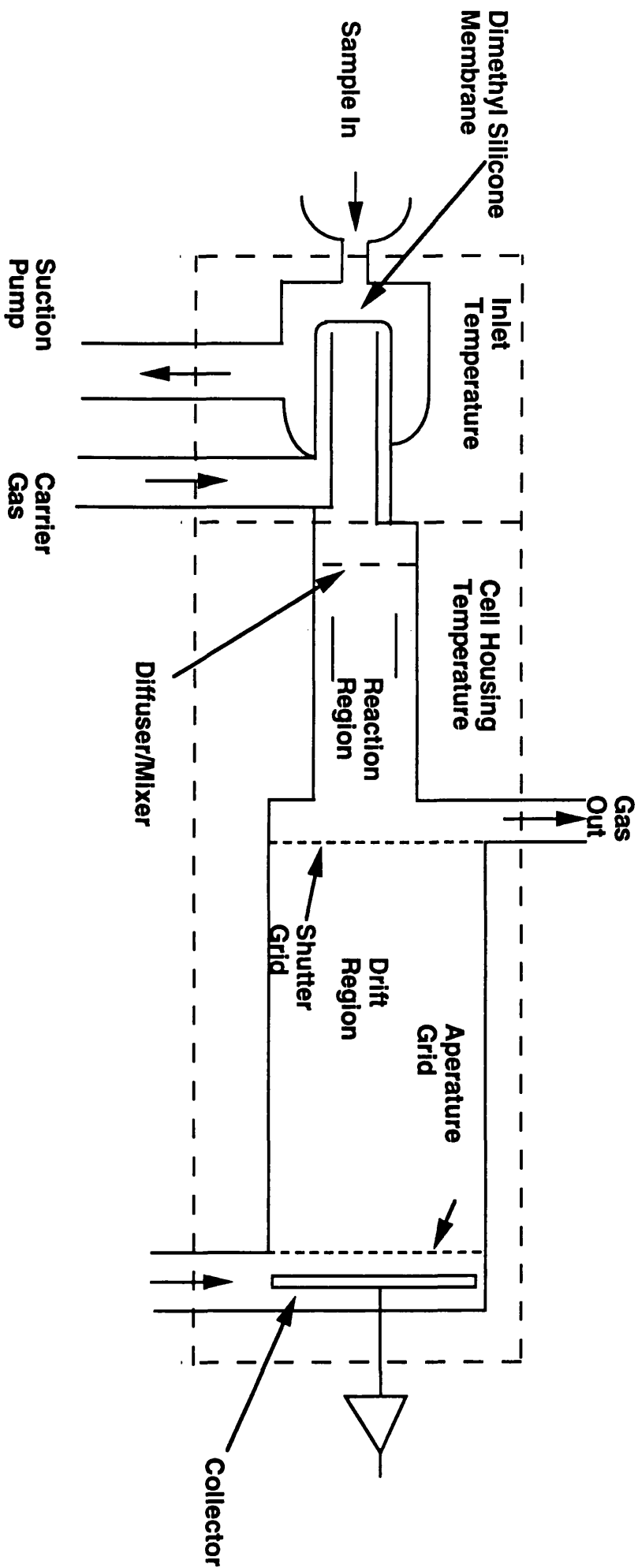


Fig 1.2 Ion Mobility Spectrometer (IMS)
Schematic

analytical instrument for the identification of chemical vapours by measuring their ionic mobilities in an unreactive drift gas. The attractiveness of its capabilities lies in the area of extreme sensitivity and the ability to resolve one compound from another. IMS has the ability to give quick results in real time analyses which is a well sought after commodity as far as explosive detectors are concerned. Another major advantage that IMS holds is being able to operate at atmospheric conditions, obviating the need to employ complicated vacuum systems. The Glasgow group has recently acquired an IMS which will be used in conjunction with a laser system.

In the traditional set-up the neutral sample is introduced into the system where it is ionised using a radioactive ^{63}Ni source. A series of ion/molecule reactions take place, resulting in product ions which can be extracted from the reactor by means of an accelerating field. Under the influence of the drift field, the ions extracted from the reactor arrive at the collector as a continuous background signal. In order to obtain bona fide signals from this continuum, a shutter grid periodically allows a small sample of the mixed ions into the drift region. In the drift region, the ion mixture is separated into its constituent parts as each ion species passes down the length of the drift column with a characteristic velocity. This temporal spread is characteristic of the individual species of ions present and a note of the times of arrival can lead to the identification of unknown substances.

When using the modified system, the radioactive source would be removed and a tuneable laser used to carry out the ionisation procedure. This enables the technique to be more selective as to which ions will be formed.

Despite these attractions, certain deficiencies of IMS have been noted. Some of the more important deficiencies include:

- a) The system is not very robust being susceptible to knocks and bumps which alter its working efficiency, especially when it may have to be used in hostile environments.
- b) The output spectrum shows results which vary according to the concentration of the sample introduced, making it less reliable in terms of sensitivity.
- c) Innocent samples are difficult to discriminate against and may lead to a number of false alarms arising.

(iii) X-Rays (9)

The familiar X-ray machine deployed at airports is currently the accepted method for inspection of carry-on luggage for concealed weapons. This sort of detector is more suited to the detection of weapons such as guns which may be used to carry out hijackings.

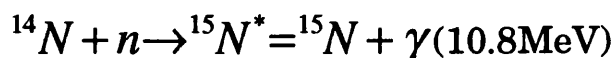
The degree of attenuation of X-rays in matter is primarily determined by its density times its atomic number (Z). X-ray images are therefore dominated by objects with high densities, while substances with relatively low densities (e.g. explosives or plastic materials) are transparent to X-rays.

Objects with high atomic numbers attenuate more X-rays, masking the explosives: a metal baking sheet in a suitcase easily fools a simple X-ray machine.

Several methods have evolved to get round this. The first is to use X-Rays of two different energies simultaneously. Each material attenuates the two sets of X-rays differently. By comparing the attenuated beams, the system can estimate the materials atomic number. In this way the machine can distinguish between dense organic material- bombs - and dense inorganic materials such as metals, and between bombs and other less dense organic material.

(iv) Nuclear Devices (9,12,13)

These techniques use high energy neutrons as probes to look inside luggage and concealed containers. Most chemical explosives are composed of high concentrations of nitrogen and oxygen. It is the presence of both oxygen and nitrogen in high densities which is used as the signature for the presence of bomb material. Nuclear techniques can pick up the presence of these elemental concentrations very efficiently. Thermal-neutron analysis (TNA) is currently the only nuclear technique incorporated in a practical and tested explosives-detection system. In TNA, the material to be inspected is placed in a thermal-neutron flux, with each element in the material having a known reaction rate to these neutrons. The compound nucleus on absorbing the high energy neutron has an excess energy, which it dispenses by giving off a gamma ray.



It is from an analyses of these emitted gamma rays that inferences as to what the original material is composed off can be gleaned. A nucleus which has absorbed a neutron will emit gamma-rays of characteristic energy at a known rate. For example, a nitrogen nucleus will emit a 10.8 MeV gamma-ray when it absorbs a neutron in a radioactive capture process. By knowing the number of gamma-rays received in a detector, the number of neutrons bombarding the sample, and the known reaction rates for the elements in the sample, the amount of a particular element ion in the sample can be determined. The most important element for detecting commercial and military explosives is nitrogen, because these explosives have a nitrogen abundance which is much greater than for other materials.

The use of neutrons and high-energy gamma-rays is advantageous because they penetrate typical luggage materials well, but the disadvantage is that they will penetrate detector materials as well. Thus in order to get reasonable detector

Chapter 1

efficiency, it is necessary to use relatively large detectors, thereby adding to the bulkiness of the apparatus.

Chapter 2 goes on to describe the theory behind the use of the laser based approach for molecular detection.

2.Theory

(1) Introduction

The purpose of this chapter is to give an account of the various processes which may arise as atoms/molecules interact with laser light. Such interactions can lead to either the ionisation of the species or formation of various daughter fragments. The mechanisms by which the molecule will disperse its energy such as dissociation and predissociation will be explained. The spectroscopy of both molecular and atomic species will be considered, with an account of the line broadening mechanisms which may arise in atoms as well as their causes being given.

Resonant photoionisation spectroscopy is based on the principle that when the photon energy matches the energy difference between excited states, the molecule readily ionises. To obtain the maximum detection sensitivity it is necessary that the probability of such excitation should be as close to 100% as is possible. In order to gain an understanding of the characteristics of photoionisation spectroscopy, we should consider first of all the resonant excitation of particles upon their interaction with laser radiation. The situation where only a two level system is considered will be dealt with in detail. However consideration should be given not only to the simple case of excitation of a two-level systems by one-quantum transitions, but also to the excitation of a multiple-level quantum system under the effect of multiple frequency laser radiation and multiple-photon excitation of high-lying states. This provides a more realistic approach for the qualitative analysis of most experimental situations.

Therefore consideration will be given to a simple two-level system interacting with a resonant light field in the absence of damping and relaxation processes. This model makes it possible to reveal the specific features of the coherent resonant interaction of a quantum system with a light field.

(2) *Semi-Classical Description*

The radiation incident upon an atom is described by a classical electromagnetic (EM) plane wave

$$E = A_0 \cos(\omega t - kz) \quad (1)$$

where E , A_0 , ω and k are the electric field, amplitude, angular frequency and wave number respectively.

The atom, is treated quantum mechanically with eigenstates E_a and E_b . Fig 2.1

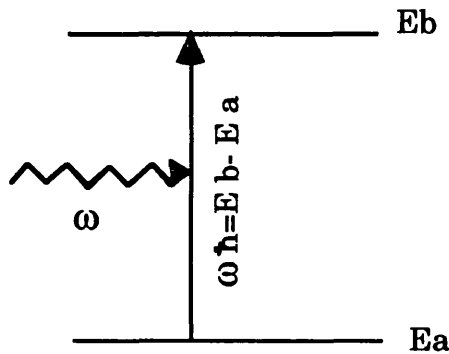


Fig 2.1 Two-level system with energies E_a and E_b , interacting with a monochromatic field.

For wavelength (λ) of the incoming photon, with $\lambda \gg d$ where d is the atomic diameter the phase of the E.M wave does not change significantly within the volume of an atom, therefore we can neglect the spatial derivative of the field amplitude.

(i) *Photon-Atom Mathematical Evaluation* (14)

This section gives insight as to why there is an increase in the ion signal when resonance conditions are satisfied.

Using the technique of separation of variables the Schroedinger Equation (SE) reduces to a time dependent and time independent form. Because the perturbation Hamiltonian is time dependent the time dependent SE is considered.

$$\hat{H}\Psi = i\hbar \frac{\partial \Psi}{\partial t} \quad (2)$$

The Hamiltonian operator

$$\hat{H} = \hat{H}_0 + \hat{V} \quad (3)$$

can be written as a sum of the unperturbed Hamiltonian \hat{H}_0 of the free atom plus the perturbation operator

$$\hat{V} = \underline{\hat{p}} \cdot \underline{E} = \underline{\hat{p}} \cdot \underline{A}_0 \cos \omega t \quad (4)$$

which describes the interaction of the atom with the E.M field.

The general solutions $\Psi(\underline{r}, t)$ of (2) can be expressed as a linear superposition

$$\Psi(\underline{r}, t) = \sum_{n=1}^{\infty} c_n(t) \phi_n(\underline{r}, t) \quad (5)$$

of the eigenfunction of the unperturbed atom, for a non-degenerate system, where

$$\phi_n(r, t) = u_n(\underline{r}) \exp(-iE_n t / \hbar) \quad (6)$$

The spatial parts $\phi_n(r, t)$ of these eigenfunctions are solutions of the time dependent Schrodinger equation.

$$\hat{H}_0 u_n(\underline{r}) = E_n u_n(\underline{r}) \quad (7)$$

and satisfy the orthonormality relations

$$\int u_i^* u_k d\tau = \delta_{ik} \quad (8)$$

For our two-level system with eigenstates a and b and energies E_a and E_b , the expansion of (5) reduces to a sum of two terms

$$\Psi(\underline{r}, t) = a(t)u_a \exp(-iE_a t/\hbar) + b(t)u_b \exp(-iE_b t/\hbar) \quad (9)$$

The coefficients $a(t)$, $b(t)$ are the time-dependent probability amplitudes of the atomic states E_a , E_b . This means that the value $|a(t)|^2$ gives the probability of finding the system in level a at time t , if decay into other levels is neglected.

Substituting (9) into (2) gives

$$\begin{aligned} i\hbar \dot{a}(t)u_a \exp(-iE_a t/\hbar) + i\hbar \dot{b}(t)u_b \exp(-iE_b t/\hbar) &= a\hat{V}u_a \exp(-iE_a t/\hbar) \\ &+ b\hat{V}u_b \exp(-iE_b t/\hbar) \end{aligned} \quad (10)$$

where (7) has been used to cancel equal terms on both sides. Multiplication with $u^*_n (n=a, b)$ and spatial integration results in the following two equations

$$\dot{a}(t) = -(i/\hbar) \left[a(t)V_{aa} + b(t)V_{ab} \exp\left\{i(E_a - E_b)t/\hbar\right\} \right] \quad (11)$$

$$\dot{b}(t) = -(i/\hbar) \left[b(t)V_{bb} + a(t)V_{ba} \exp\left\{i(E_a - E_b)t/\hbar\right\} \right] \quad (12)$$

The spatial integral

$$V_{ik} = \int u_i^* \hat{V} u_k d\tau = -e \underline{E} \int u_i^* \underline{r} u_k d\tau \quad (13)$$

$$= -e \underline{E} \underline{R}_{ik} \quad \text{with} \quad \underline{R}_{ik} = \underline{R}_{ki} = \int u_i^* \underline{r} u_k d\tau$$

matrix element of the interaction operator

$$\hat{V} = \underline{\tilde{p}} \cdot \underline{E} \quad (14)$$

Since \underline{r} has odd parity the integrals V_{aa} vanish when integrating over all co-ordinates from $\pm\infty$.

Using (1) for the E.M field, (15) & (16) with abbreviations

$$\omega_{ba} = (E_b - E_a)/\hbar = -\omega_{ab} \quad (15) \quad \text{and} \quad P_{ab} = -e \underline{R}_{ab} \underline{A}_0 / \hbar = P_{ba} \quad (16)$$

reduce to

$$\dot{a}(t) = (i/2) P_{ab} [\exp\{i(\omega_{ab} - \omega)t\} + \exp\{i(\omega_{ab} + \omega)t\}] b(t) \quad (17)$$

$$\dot{b}(t) = (i/2) P_{ab} [\exp\{-i(\omega_{ab} - \omega)t\} + \exp\{-i(\omega_{ab} + \omega)t\}] a(t) \quad (18)$$

These are the basic equations which must be solved to obtain the probability amplitudes $a(t)$ and $b(t)$.

Suppose that the atoms are in the lower state E_a at time $t=0$, which implies that $a(0)=1$ and $b(0)=0$. We assume the field amplitudes A_0 to be sufficiently small that for times $t < T$ the population of E_b remains small compared with that of E_a , i.e.

$$|b(t < T)|^2 \ll 1$$

Under this weak-field condition we can solve (17) & (18) with an iterative procedure starting with $a=1$ and $b=0$.

With these assumptions the first approx. of (17) & (18) gives

$$\dot{a}(t) = 0 \quad (19)$$

$$\dot{b}(t) = (i/2)P_{ab}[\exp i(\omega_{ba} - \omega)t + \exp i(\omega_{ba} + \omega)t] \quad (20)$$

With the initial conditions $a(0)=1$ and $b(0)=0$ integration of (19) & (20) yields

$$a(t) = a(0) = 1 \quad (21)$$

$$b(t) = (P_{ab}/2) \left[\frac{\exp i(\omega_{ba} - \omega)t - 1}{\omega_{ba} - \omega} + \frac{\exp i(\omega_{ba} + \omega)t - 1}{\omega_{ba} + \omega} \right] \quad (22)$$

In the optical frequency range this implies that $[\omega_{ba}-\omega] \ll \omega_{ba}$. The second term of (22) is then small compared to the first and may be neglected. This is called the rotating-wave approximation.

$$b(t) = (P_{ab}/2) \frac{\exp i(\omega_{ba} - \omega)t - 1}{\omega_{ba} - \omega} \quad (23)$$

we obtain for the probability $|b(t)|^2$ that the system is at time t in the upper level E_b

$$|b(t)|^2 = (P_{ab}/2)^2 \left(\frac{\sin(\omega_{ba} - \omega)t/2}{(\omega_{ba} - \omega)/2} \right)^2 \quad (24)$$

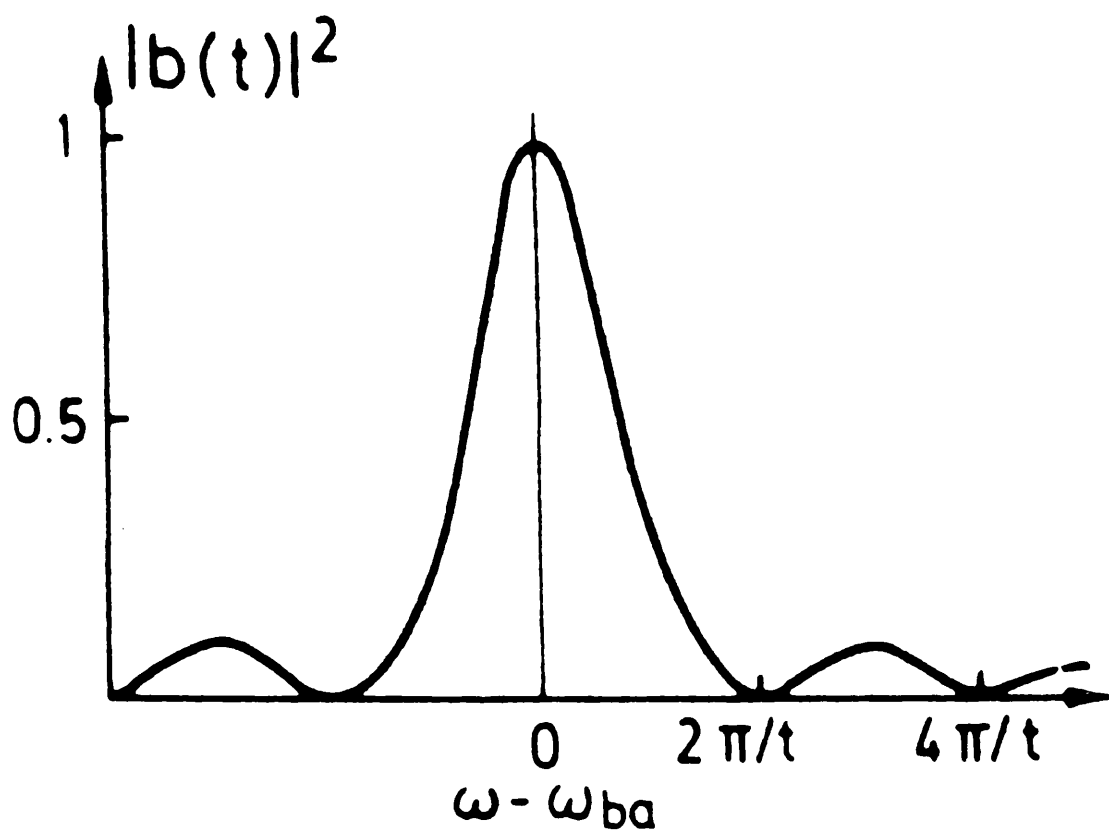


Fig 2.2 The probability distribution of a transition to the E_b eigenstate from the E_a state is given as a function of the detuning $\Delta\omega = \omega - \omega_{ba}$.

Since we had assumed that the atom was at $t=0$ in the lower level E_a , (24) gives the transition probability for the atom to go from E_a to E_b during the time t .

Fig 2.2 illustrates this transition probability as a function of the detuning $\Delta\omega = \omega - \omega_{ba}$ of the field frequency ω from the eigenfrequency ω_{ba} . It can be seen that when the resonance condition is fulfilled the maximum probability of the transition taking place arises. This is the basis of the principle involved behind Resonance Ionisation Spectroscopy.

(3) Line Width

The ubiquitous use of the word "line" to describe an experimentally observed transition goes back to the early days of observations of visible spectra with spectroscopes. Although, nowadays, observations tend to be in the form of a plot of some measure of the intensity of the transition against wavelength, frequency or wavenumber, we still refer to peaks in such a spectrum as lines

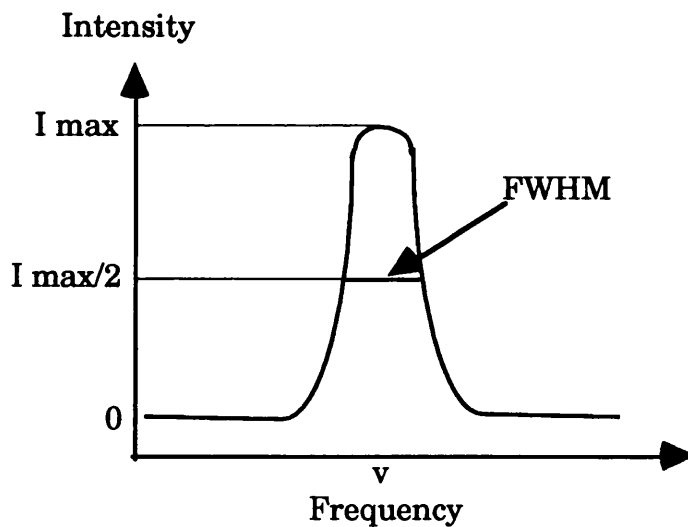


Fig 2.3

Fig 2.3 above shows, for a sample in the gas phase, a characteristic absorption line with its FWHM (Full-Width Half-Maximum). The FWHM of the emission line has been chosen as the distance between points when the intensity of the line drops by a 1/2. The line is not infinitely narrow even if we assume that the instrument used for observation has not imposed any broadening of its own. Three important factors which may contribute to the line width and shape will be considered.

(i) Natural Line Broadening

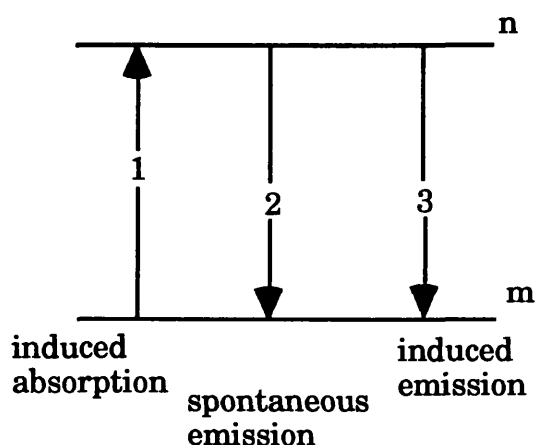


Fig 2.4 Absorption and emission processes between states m and n.

If the state n in Fig 2.4 is populated by absorption in excess of its Boltzmann population, the species M^* in this state will decay to the lower state until the Boltzmann population is regained. The decay is a first-order process so that

$$-\frac{dN_n}{dt} = kN_n$$

where k is the first-order rate constant and N_n is the total number in the n state and is given by

$$\frac{1}{k} = \tau$$

Here τ is the time taken for N_n to fall to $1/e$ of its initial value (e is the base of the natural logarithms) and is referred to as the lifetime of state n . If spontaneous emission is the only process by which M^* decays, then

$$k = A_{nm}$$

where A_{nm} is an Einstein coefficient.

The Heisenberg uncertainty principle in the form

$$\tau \Delta E \geq \hbar$$

relates the lifetime to the energy width, of the state n . This equation illustrates the point that state n has an exactly defined energy only if τ is infinite, but, since this is never the case, all energy levels have finite width with resulting line broadening.

The Einstein coefficient (14) can be related to the transition probability

$$A_{nm} = \frac{64 \pi^4 \nu^3}{(4 \pi \epsilon_0) 3 h c^3} |R^{nm}|^2$$

using the uncertainty principle, where R^{nm} is the electric dipole matrix and ν is the frequency of the transition.

$$\Delta \nu \geq \frac{32 \pi^3 \nu^3}{(4 \pi \epsilon_0) 3 h c^3} |R^{nm}|^2$$

The dependence of $\Delta\nu$, the frequency spread, on ν^3 results in a much larger value for an excited electronic state, typically 30 MHz, than for an excited rotational state which is typically 10^4 to 10^5 Hz.

The equation above illustrates what is called the natural line broadening. Since each atom or molecule behaves, identically in this respect it is an example of homogenous line broadening which results in a characteristic Lorentzian line shape.

Natural line broadening is usually very small compared to other causes of broadening.

(ii) Doppler Broadening

Whether radiation is being absorbed or emitted the frequency at which it takes place depends on the velocity of the atom or molecules relative to the detector. The effect is known as the Doppler effect.

If an atom or molecule is travelling towards the detector with a velocity V_a , then the frequency ν_a at which a transition is observed to occur is related to the actual transition frequency ν in a stationary atom or molecule by

$$\nu_a = \nu \left(1 - \frac{V_a}{c} \right)^{-1}$$

where c is the speed of light. Because of the usual Maxwell velocity distribution at a temperature T there is a spread of values of ν_a and a characteristic line broadening given by

$$\Delta\nu = \frac{\nu}{c} \left(\frac{2kT \ln 2}{m} \right)^{\frac{1}{2}}$$

where m is the mass of the atom or molecule. At room temperature v_a is normally far greater than the natural line width. The broadening is inhomogeneous, since not all atoms or molecules in a particular sample behave in the same way, and results in a line shape similar to a Gaussian.

(iii) Pressure Broadening

When collisions occur between gas phase atoms or molecules there is an exchange of energy which leads effectively to a broadening of energy levels. If α is the mean time between collisions and each collision results in a line broadening $\Delta\nu$ of the transition where

$$\Delta\nu = (2\pi\alpha)^{-1}$$

derived from the uncertainty principle equation.

This broadening is, like natural line broadening, homogeneous and usually produces a Lorentzian line shape except for transitions at low frequencies when an asymmetrical line shape results.

(iv) Classification of Mechanisms

Broadening mechanisms in general can be classified into two categories, homogeneous and inhomogeneous. Homogeneous mechanisms occur when every atom in the collection has the same transition centre frequency and same resonance lineshape.

Inhomogeneous mechanisms involve the collection of atoms exhibiting different resonance frequencies or lineshapes. In this case the atom responds to a larger range of frequencies than the linewidth of any single atom.

Pressure and natural line broadening are described as homogeneous and the Doppler broadening is inhomogeneous.

The five basic Resonance Ionisation schemes

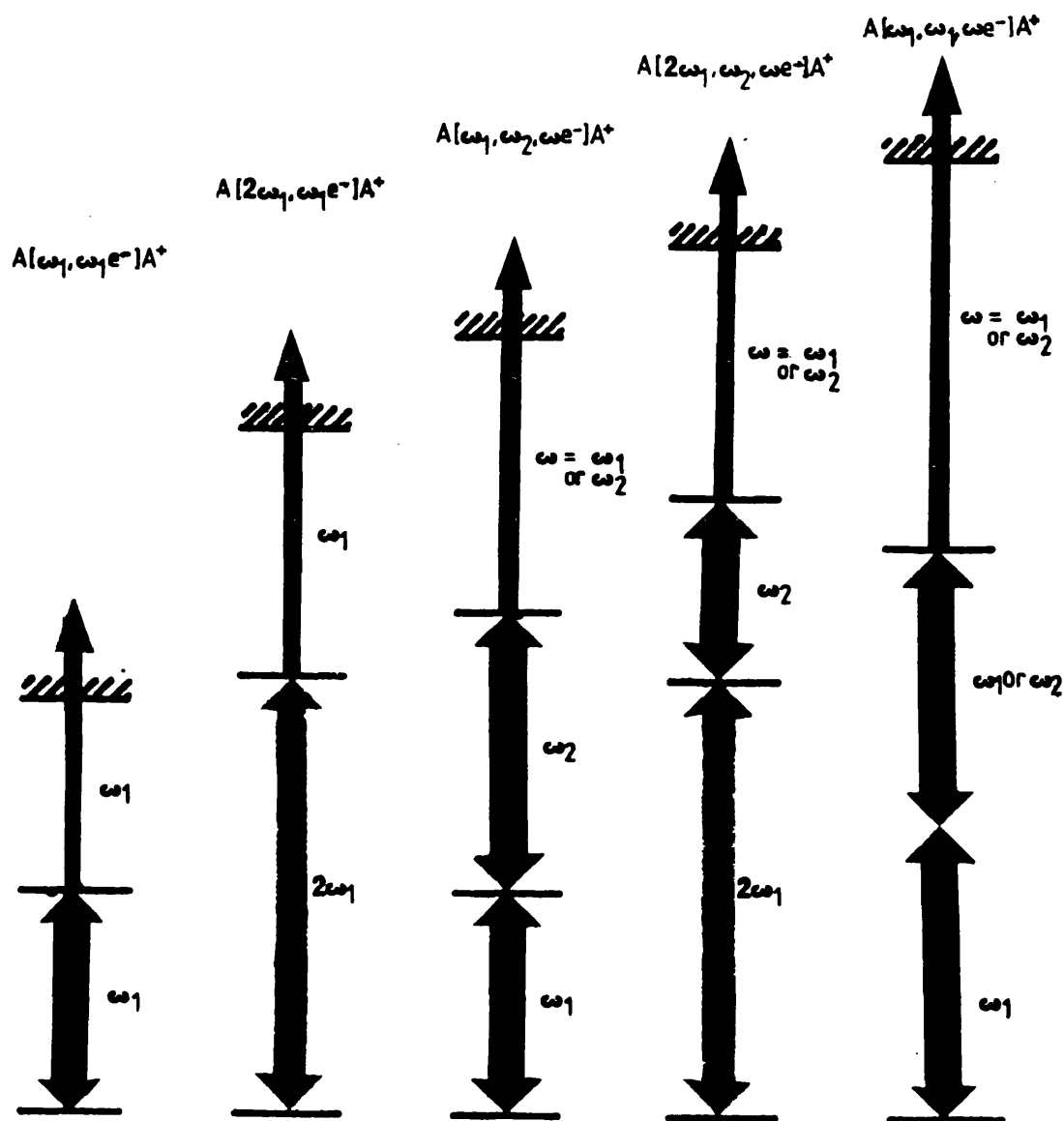


Fig 2.5 The 5 laser ionisation schemes predicted as the means to ionise most of the elements of the periodic table.

The line shapes associated with homogeneous mechanisms are Lorentzian in shape whereas inhomogeneous broadening mechanisms give rise to Gaussian line shapes.

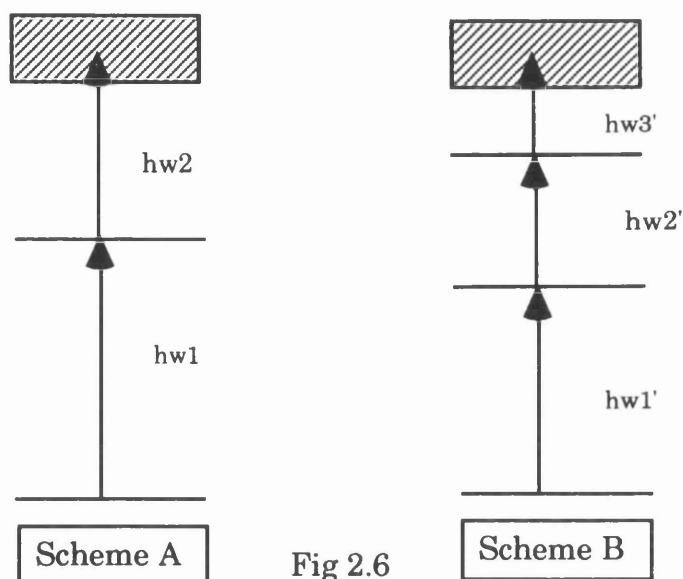
(4) Ionisation Schemes (15)

At the time when the five laser ionisation schemes were devised which allowed ionisation of most of the elements within the periodic table. (Fig 2.5) the optics and crystals for extending the wavelength attainable by dye laser systems were not commonly supplied with commercial systems.

With the advance of laser technology the commercial sector can now supply nearly everything needed to extend the range of tuneability to the point where only elements with ionisation potentials higher than 11eV need special techniques for their efficient ionisation. Since the use of frequency doubling, frequency sum and difference mixing are now standard with commercial dye lasers, one no longer needs to distinguish between ionisation methods which differ only in the details used to generate the light.

If a strong one-photon transition exists for photon energy less than 11eV, a very plausible ionisation scheme using commercially available lasers can start with a one-photon transition to an excited state. (Fig 2.6) Following this initial excitation there are two general alternatives. In scheme A another photon, usually at another wavelength, completes the ionisation process, known as resonance two photon ionisation.

With scheme B another tuneable dye laser promotes the first excited state population to a higher level which could, for example, be ionised with the fundamental of the Nd-Yag laser.



Also comparisons of the practicality of the above schemes for RIS using commercial laser systems are now discussed.

Scheme A involves only one resonance step and could be carried out with a single colour. It is however preferable to use a two colour process in order to avoid loss of selectivity due to strong pumping of the resonance state. The two colour scheme is referred to as R2PI (Resonance Two Photon Ionisation), although it should be noted that it can take place with photons of the same frequency.

In Scheme B two resonant steps are used in order to improve selectivity or to avoid the necessity of *exciting* a state with a small photo-ionisation cross section.

There are several reasons why one might choose scheme B. Firstly the only available first excited states might be "s" states, which typically have very small photoionisation cross-sections. A second reason for using two resonance steps is to improve the selectivity and make possible the use of non-tuneable red or infra-red lasers for the ionisation step. There are only four or five elements in the periodic table which cannot be ionised effectively by using this method.

Scheme A allows the possibility of achieving ionisation with the use of a single dye laser, with the first step initiated by a frequency doubled photon and the ionising step induced by either another doubled photon or the fundamental component.

(5) Effect of Radiation Intensity on Ionisation Schemes

It is possible to characterise the different types of photoionisation schemes involved into separate categories depending on the intensity of radiation used in the visible or UV regions.

1) Resonance two-step (or more) photoionisation in weak fields. In this situation we have a number of photons selectively exciting electronic states which ultimately lead to the ionisation of the molecule. The power-law dependence of the yield of photoions on the radiation intensity is a function of the number of absorbed photons, and the yield of ions itself greatly depends on the properties of the intermediate electronically excited states.

2) Resonance stepwise photoionisation in strong fields. This is an important case in that it allows the possibility of photoionising molecules approaching a 100% efficiency. However, on reaching the first ionisation potential, the molecule as a rule continues to absorb energy, and this leads to their subsequent fragmentation. Fragmentation of molecules under the action of intense laser radiation, first observed in experiments on multiphoton ionisation(16), have become the object of a large number of investigations from the points of view of studying the physics of the processes that occur and of finding the optimum conditions for photoionisation detection of molecules.

3) Multiphoton ionisation. This involves the molecule absorbing a number of photons before reaching the ionisation continuum. The intermediate states through which transitions take place are known as virtual states and are characterised by their very low

cross-sections. Because of the overall very low cross-section for the ionisation very high intensity beams are required which subsequently can lead to complete breakdown of the molecule into its constituent atoms.

(6) Intensity Dependence

The laser intensity dependence observed in multiphoton transitions can be classified into two kinds. One type originates from the intrinsic laser intensity dependence, which is involved in the expression of the transition probability, and the other type from geometrical effects of the focused laser beam in the region of molecule-photon interaction. In some cases the measured intensity dependence is governed by both effects.

The transition rate constant for the n -photon process is proportional to the n^{th} order of laser intensity

$$k^{(n)} = (\sigma^{(n)} I^n) / (\hbar \omega_r)^n$$

where $\sigma^{(n)}$, I , and ω_r are the n^{th} order transition cross section (strength) in units of $\text{cm}^2 \text{s}^{-1}$, the laser irradiance in units of $\text{cm}^{-2} \text{s}^{-1}$, and the laser frequency, respectively.

The I^n dependence of the transition probability for the n -photon process is called the formal intensity law. The intensity dependence originating from geometrical effects in focused laser experiments is sometimes called the 3/2 power law.

The formal intensity law, I^n -intensity dependence of the observed quantities, has been utilised to determine the orders of multiphoton processes such as excitation, ionisation and/or dissociation of molecules.

(7) Ionisation of Molecules (17)

The situation with molecules, however, is much more complicated than that with atoms. In spite of the fact that selective laser photoionisation of atoms has been extensively developed, the method of laser photoionisation spectroscopy of atoms cannot be directly transferred to molecules for a number of reasons.

1) When considering polyatomic molecules, it is the case that their excited states are of a much more complicated nature and their molecular absorption spectra sometimes display little structural information which could be utilised for identification purposes. All of these features render the possibility of selectively ionising polyatomic molecules much more difficult.

2) Unlike atoms, molecules when excited to an intermediate state have a number of possible relaxation processes which they can undergo. These processes include dissociation, predissociation etc. which will affect the ability of the molecule to subsequently absorb more photons and consequently affecting the ionisation rate. These will be discussed later in this chapter.

3) When considering the irradiation of molecules with intense laser radiation, various fragmentation processes leading to a number of different fragment ions can take place. The fragment ions can only be analysed using a mass spectrometric approach. It has been realised that the different fragmentation branches which may open are a function of both the wavelength and power of laser light used.

4) Molecular bound cross sections, are in general several orders of magnitude smaller than the atomic photoionisation cross sections, which make it necessary to use more powerful sources of radiation. At the same time, the molecular absorption and photoionisation spectra usually lie in the UV and VUV regions,

where it has been more difficult to generate tuneable laser radiation.

In recent years, considerable progress has been made in the development of photoionisation laser spectroscopy of molecules (18,19). This is due to the progress in laser technology, especially the development of lasers operating in the UV and VUV regions, providing greater power. The second and most important aspect of laser ionisation has been the implementation of mass spectrometric techniques. This has lead to a "two dimensional approach" to analyse the ions, whereby both the spectroscopic and mass information are being utilised.

(i) Typical Experimental Parameters

An important factor in all experiments on resonance photoionisation of molecules is the use of intense laser radiation, which permits attaining quite high ionisation efficiency in multistep photoionisation via an intermediate electronically excited state; in order to achieve saturation of the optical transition in the first step, the energy fluence of the first radiation pulse $\Phi_1(\omega_1)$ must satisfy the condition

$$\Phi_1(\omega_1) \geq \Phi_{sat}^{(1)} \approx 1/(2\sigma_{exc})$$

where σ_{exc} and $\Phi_{sat}^{(1)}$ are the cross section for resonant excitation and saturation fluence respectively (17). Where saturation is defined as being the condition when all the molecules within the laser beam are excited. This relation is valid in the case when the duration of the exciting pulse τ_p is shorter than the relaxation time of the excited state, T_1 . Appreciable depletion of the excited electronic state due to stimulated transitions into the ionised state is achieved with an energy fluence Φ_2 in the second photon with frequency ω_2

$$\Phi_2(\omega_2) \geq \Phi_{sat}^{(2)} \approx 1/\sigma_{ion}$$

where σ_{ion} is the cross section for the transition from the excited state into the ionisation continuum. For characteristic cross sections of excitation and ionisation of molecules of 10^{-17} - 10^{-18} cm² and lifetimes of intermediate excited states $T_1 \cong 10^{-8}$ - 10^{-10} s, typical energy densities and intensities required for saturation to occur in optical transitions are respectively, 0.1-1 J/cm² and 10^7 - 10^9 W/cm².

In the case of non-resonant multiphoton ionisation, the characteristic cross section of two- and three- photon transitions constitute, 10^{-30-34} cm⁴sec and 10^{-43-49} cm⁶sec² so that in order to achieve an acceptable ionisation efficiency it is necessary to use radiation intensities $I > 10^{10} - 10^{11}$ W/cm² (for a 10 nsec laser pulse).

The other important requirements imposed on the laser radiation sources in experiments on multistep photoionisation are related to the spectral characteristics of the molecules. The electronic absorption bands of most molecules are situated in the ultraviolet region of the spectrum, so that photon energies greater than 4eV are required in order to excite electronic states. The ionisation potentials of polyatomic molecules usually lie in the range 8-12 eV, so that efficient photoionisation of molecules out of electronically excited states in a single step requires photons energies $\hbar\omega = 4$ -8eV.

The experiments carried out mainly use the resonance 2-photon ionisation schemes. Therefore the molecular species which are examined must have absorption bands at energies greater than 1/2 the ionisation potential.

(ii) Methods and Regimes of Multiphoton Ionisation of Molecules

Several basic schemes of multistep excitation can be used for the resonance photoionisation of molecules. (Fig 2.7)

Two-step photoionisation via intermediate excited electronic-vibrational states is the simplest type of selective stepwise photoionisation of molecules. (Fig 2.7.1) This is the type of scheme deployed for the ionisation of neutral NO_2 and NO gas discussed later, commonly referred to as Resonance Two Photon Ionisation (R2PI).

Since with excitation of electronic states the energy required to ionise molecules decreases by several electron volts, the quantum energy of the ionising radiation $\hbar\omega_2$ is selected so as to just cross the ionisation level. (Fig 2.7.1) The selectivity aspect of the process arises because of the unique energy level of the intermediate state which is excited in the first step of the ionisation process. The first experiments in this direction were performed using two independent lasers tuned to the frequency of the first and second steps (20).

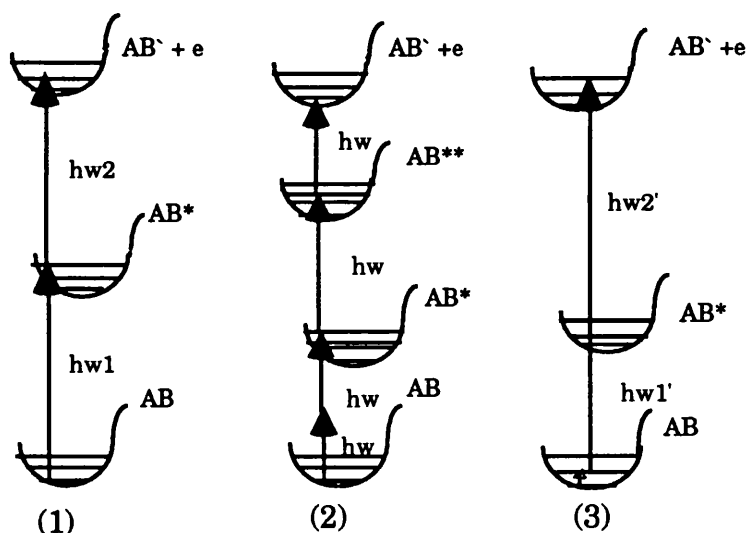


Fig 2.7 Scheme of resonance laser photoionization of molecules: (1) via an intermediate excited electronic state (two-color resonant photoionization); (2) via two intermediate resonances, and (3) via a vibrationally excited state (IR-UV photoionization).

For most molecules the bands of intense electronic excitation are situated in the ultra-violet region of the spectrum ($\lambda < 300\text{nm}$). Methods of multiphoton ionisation of molecules have been

extensively developed. Some of these methods are based on the use of frequency doubling tuneable dye lasers with sharp focusing of the radiation down to the diffraction limit using quartz lenses (21,22). Frequency doubling involves the use of doubling crystals such as BBO (Beta Barium Borate) which are aligned at the correct angles to the incoming beams for maximum conversion into doubled frequencies. In such cases it is possible to reach radiation intensities exceeding 10^{10} W/cm^2 at the focal point. At these powers the multiphoton absorption and ionisation processes of molecules proceed efficiently. As the wavelength of the radiation is tuned, resonances arise at the doubled or tripled frequency of the laser with subsequent simple one or two-photon ionisation of the molecules (Fig 2.7.2). The presence of intermediate resonances greatly increases the yield of ions, and as a result, a wavelength dependent multiphoton ionisation spectrum can be formed. This method turns out to be very effective for investigating the spectra of excited electronic states of molecules, especially those that are forbidden for single photon transitions. For example, a transition between levels with identical parity is forbidden for single-photon transitions but is allowed for two-photon transitions. Thus spectroscopic data obtained with multiphoton ionisation schemes supplement the usual single-photon spectroscopy.

Vibrational spectra provide the most significant characteristic features of polyatomic molecules, therefore schemes involving two-step photoionisation via intermediate vibrationally excited states (Fig 2.7.3) must in principle have higher selectivity than the schemes via the electronic states. In this scheme however because the infra red photon only increases the relative energy of the excited molecule above the ground state by 0.1-0.3eV, ionisation of ground state molecules can occur when the second photon is used to ionise, this can lead to an increase in the background signal.

(8) Detection of Molecules by Multistep & Multiphoton Resonant Ionisation

It is much more difficult to detect single molecules than single atoms. The basic method of identifying trace quantities of molecules is the mass-spectrometric analysis.

The analysis of matter by the mass-spectroscopic method is based on the transformation of the molecules of a sample into ions that can be further separated and analysed due to their different mass-to-charge ratios. Analytical scientists have always been trying to create ion sources with high ionisation efficiencies and moderate molecular fragmentation. The situation is somewhat worse for selectivity. As a rule, molecular mass spectra are the result of fragment ions. Despite the fact that an analysis of the fragments yields valuable information on the molecular structure, it is rather difficult to analyse multi-component mixtures.

Therefore, we are tempted to try to combine the existing methods for detection and identification of complex molecules with selective molecular photoionisation techniques. The technique deploys both of these features in conjunction and is referred to as Resonance Enhanced Multi-Photon Ionisation Mass Spectrometry.(REMPI/MS)

(i) Fragmentation Processes

The relative yield of different fragment ions in laser photoionisation is related qualitatively to their appearance potentials: peaks of fragment ions with low appearance potentials have the highest intensity in the mass spectrum.

Studies have shown that a substantial degree of ion fragmentation can take place and the relative yield of molecular ions is small even when low laser radiation intensities are used.

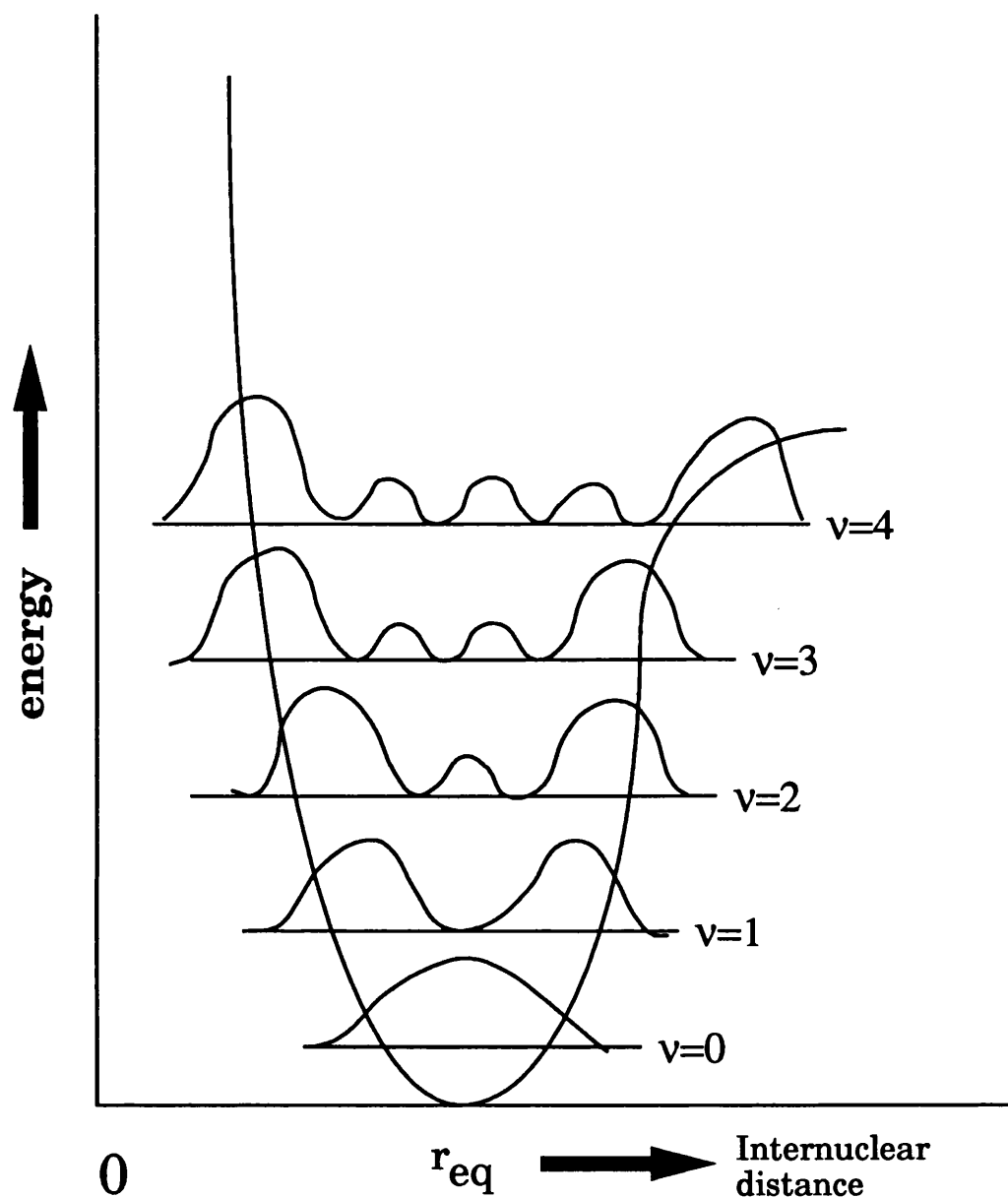


Fig 2.8 The probability distributions of electrons in vibrational states in a diatomic molecule according to the quantum theory. The nuclei are most likely to be found at separations given by the maxima of the curve for each vibrational state.

This is related to the dissociation of molecules accompanying excitation into intermediate electronic states and the main ionisation channel generally is the photoionisation of neutral molecular fragments.

If the dissociation time of the molecule in the intermediate excited state is much shorter than the duration of the laser pulse, then a high level of dissociation will take place resulting in the effective suppression of direct stepwise photoionisation of molecules. The neutral molecular fragments which absorb at the frequency of the laser radiation, can then be ionised during the same laser pulse. However, ionisation of neutral molecular fragments can play an important role in the formation of the photoionisation mass spectrum of polyatomic molecules, even in the presence of stable intermediate states. The transition of a molecule into a state above the ionisation limit from the electronically excited state with a large reserve of vibrational energy or with the nuclear configuration of this state differing considerably from the configuration of the ion, can result in a sharp increase in the fraction of dissociating molecules and, correspondingly, drop in the yield of molecular ions.

(9) Intensity of Vibrational- Electronic Spectra: The Franck Condon Principle

A description of how the energies are associated within a transition can be represented by Morse curves which are used to describe the electronic, vibrational and rotational energies contained within a molecular transition. (Fig 2.8) The height of the curves on the energy diagram gives a representation of the electronic energy it contains, the vibrational bands are represented by lines that run across the curve, with the rotational states superimposed on them. (14) The electron is considered bound if the vibrational state in which it is located is confined by two sides of the curve. The probability of finding the electron within this region is given by its wavefunction. These have been calculated using quantum mechanics and typical probability distributions are drawn on Fig 2.8.

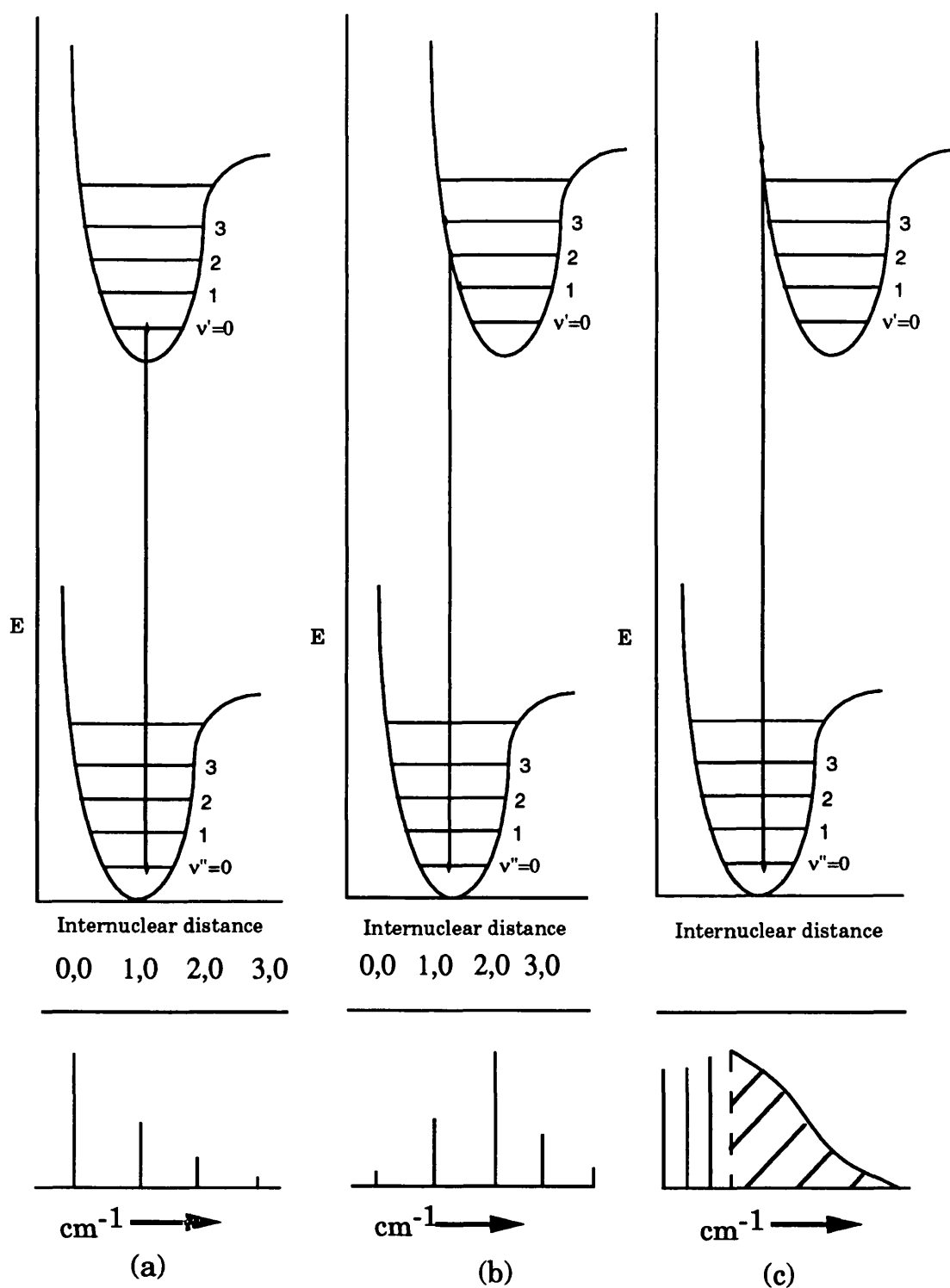


Fig 2.9 The operation of the Franck Condon principle for (a) internuclear distances equal in upper and lower states, (b) upper-state internuclear distance a little greater than that in the lower state, and (c) upper -state distance considerably greater.

Although quantum mechanics imposes no restrictions on the change in the vibrational quantum number during an electronic transition, the vibration lines in a progression are not all observed to be of the same intensity. (Fig 2.9) In some spectra the (0,0) transition is the strongest, in others the intensity increases to a maximum at some value of v' , while in yet others only a few vibrational lines with high v' are seen, followed by a continuum. All these types of spectra are readily explicable in terms of the Franck-Condon principle which states that an electronic transition takes place so rapidly that a vibrating molecule does not change its internuclear distance appreciably during the transition. (23)

If a diatomic molecule undergoes a transition into an upper electronic state in which the excited molecule is stable with respect to dissociation into its atoms, then the upper state can be represented by a Morse Curve similar in outline to that of the ground electronic state. There will probably (but not necessarily) be differences in such parameters as vibrational frequency, equilibrium internuclear distance, or dissociation energy between the states, but this simply means that each excited molecule should be considered as a new molecule with a different, but also rather similar, Morse curve.

Fig 2.9 shows three possibilities. In (a) is shown the upper electronic state having the same equilibrium internuclear distance as the lower.

Now the Franck Condon principle suggests that a transition occurs vertically on this diagram, since the internuclear distance does not change, and so if we consider the molecule to be initially in the ground state both electronically (ϵ'') and vibrationally ($v''=0$), then the most probable transition is that indicated by the vertical line. Thus the strongest spectral line of the $v''=0$ progression will be the (0,0).

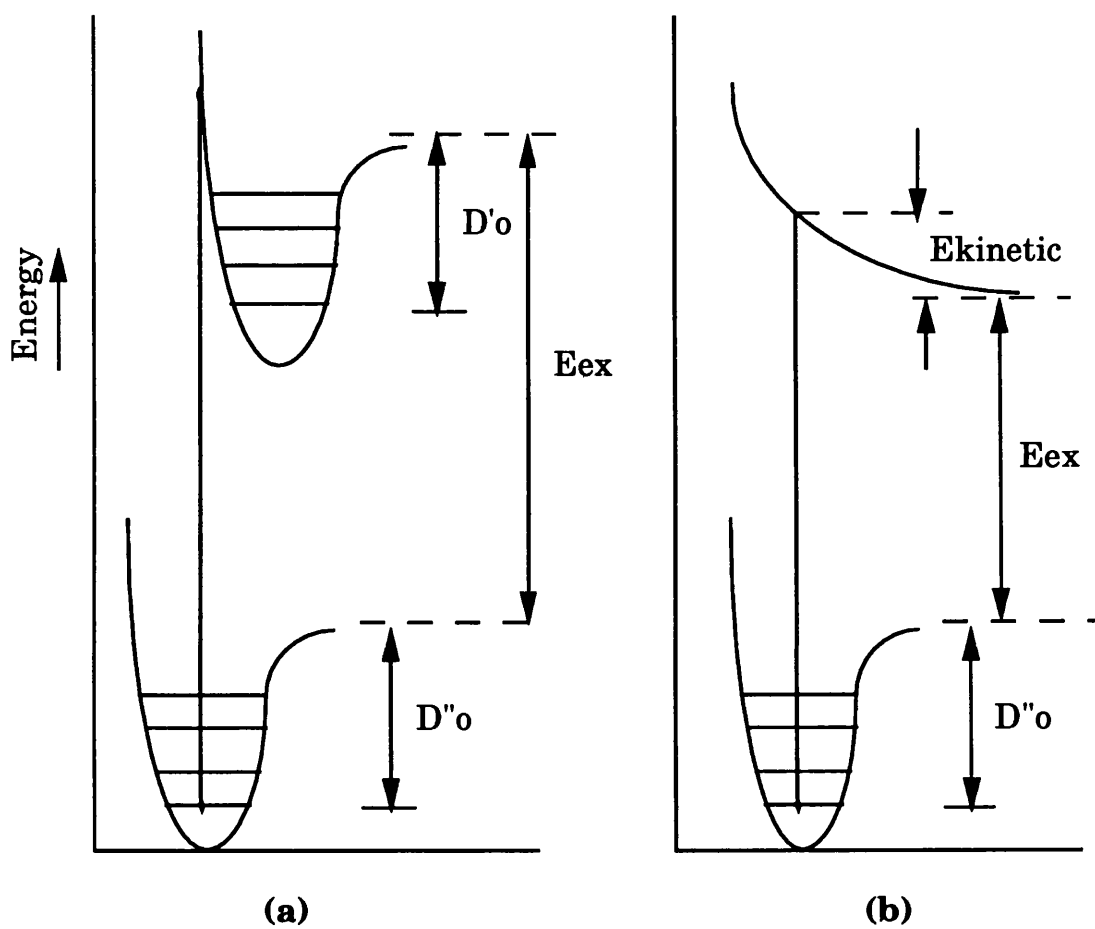


Fig 2.10 Illustrating dissociation by excitation into (a) a stable upper state, and (b) a continuum upper state.

However, quantum theory predicts the probability of finding the oscillating atom is greatest at the equilibrium distance in the $v''=0$ state- it allows some, although small, chance of the atom being near the extremities of its vibrational motion. Hence there is some chance of the transition starting from the ends of the $v''=0$ state and finishing in the $v''=1,2$ etc. states. The $(1,0)$, $(2,0)$ etc. lines diminish rapidly in intensity, see Fig 2.9 (a).

The diagram, Fig 2.9 (b) shows the case where the excited electronic state has a slightly greater internuclear separation than the ground state. A vertical transition from the $v''=0$ level will most likely occur into the upper vibrational state $v'=2$, transition to lower and higher v' states being less likely; in general the upper state most likely to be reached will depend on the difference between the equilibrium separations in the lower and upper states. Fig 2.9 (b)

In (c) the upper state separation is drawn as considerably greater than that in the lower state and we see that, firstly, the vibrational level to which a transition takes place has a high v' value. Further, transitions can now occur to a state where the excited molecule has energy in excess of its own dissociation energy. From such states the molecule will dissociate without any vibrational states being excited and since the atoms which are formed may take up any value of kinetic energy, the transitions are not quantized and a continuum results. Fig 2.9.

(10) Dissociation Energy & Products

Fig 2.10 shows two of the ways in which electronic excitations can lead to dissociation of a molecule.

Fig 2.10 (a) represents the case where the equilibrium nuclear separation in the upper state is considerably greater than that in the lower. The dashed line limits of the Morse curve represent the dissociation energies of the normal and excited molecules into fragments; the dissociation energies being D''_0 and D'_0 from

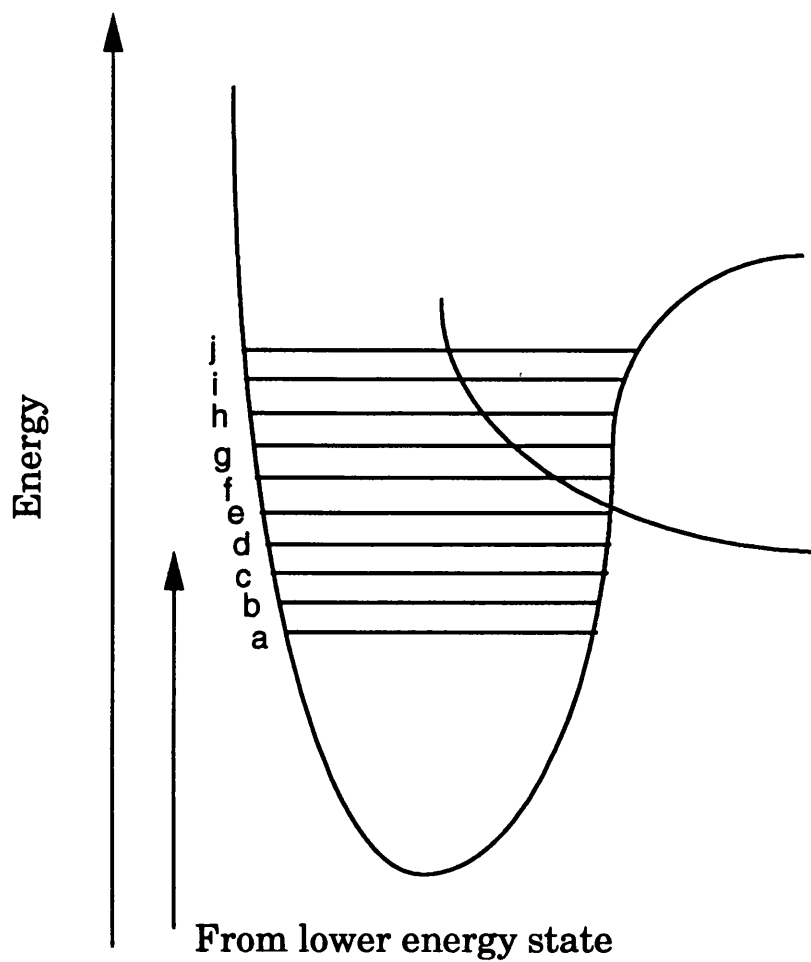


Fig 2.11 Showing the occurrence of predissociation during transitions into a stable upper state intersected by a continuum state.

the first vibrational states in the ground and electronic states. The total energy of the dissociation products from the upper state is greater by an amount E_{ex} , than that of the products of dissociation in the lower state. This energy is the excitation energy of one (or rarely both) of the atoms produced on dissociation.

(b) Illustrates the case in which the upper electronic state is unstable: there is no minimum in the energy curve and, as soon as a molecule is raised to this state by excitation, the molecule dissociates into products with total excitation energy E_{ex} . The products fragment with kinetic energy E_{kinetic} which represents the excess energy in the final state above that needed just to dissociate the molecule. Since E_{kinetic} is not quantized the whole spectrum for this system will exhibit a continuum the lower limit of which (if observable) will be precisely the energy $D'' + E_{\text{ex}}$.

(11) Predissociation

Predissociation can arise when the Morse curves of a particular molecule have two different excited states intersecting. (Fig 2.11) One of the excited states is stable, since it has a minimum in the curve, and the other is continuous. Some of the vibrational levels are also shown, and let us suppose a transition takes place from some lower state into the vibrational levels alphabetically labelled on the left. Now if a transition takes place into the levels labelled a, b, or c a normal vibrational electronic spectrum is complete with rotational fine structure.

If the transition is to levels d, e, or f there is a possibility that the molecule will "cross over" on to the continuum curve and thus dissociate. In general, transitions from one curve to another in this way (a so-called radiationless transfer since no energy is absorbed or emitted in the process) is faster than the time taken by the molecule to rotate (10^{-10}s) but usually slower than the vibrational time (10^{-13}s). Thus predissociation will occur before the molecule rotates (and thus all rotational fine structure will

be destroyed in the spectrum), while the vibrational structure is usually not affected.

On the other hand, transitions into levels g, h, \dots will give rise to normal vibrational-electronic spectrum including rotational fine structure once more. As observed before, (Fig 2.8) when v is large the molecule spends most time at the extreme ends of its vibrational motion, and very little time in between. When moving in the vibrational states g, h, \dots the molecule spends insufficient time near the cross-over point for appreciable dissociation to occur and a large parent mass results.

3.Experimental Set-up

(1) Method

The main purpose of the experiments described in this thesis was to acquire a wavelength dependent fingerprint, power dependencies and mass spectral data from various parent and fragment ions produced in laser interaction with sample vapours. The nitro-aromatics studied in detail so far are nitrobenzene & nitrotoluene.

Recently work has also involved looking at the mass spectra of more complex explosives structures. Due to the lower vapour pressures of these compounds modifications have been carried out on the sample entry system. (Fig 7.2) This alteration to the system is described fully in the explosives chapter where results from its implementation have been discussed.

Laser Systems

A Lumonics TE-860 XeCl excimer laser (Fig 3.1) was used to pump a Lumonics EPD-330 dye laser which could be operated using a variety of different dyes depending upon the wavelength region required for the particular investigation. A number of dyes allow the output of the laser to cover the range from 320-950nm. The laser could be operated at a variety of repetition rates , with the typical rate of 10Hz used.

The dye laser output was frequency doubled by a BBO crystal in order to span the range 223-262nm, with wavelength tracking being accomplished using an Inrad Model 5-12 second harmonic generation autotracking system. The output beam intensity is controlled by a Newport optical attenuator.

In general except when otherwise stated, experiments carried out have both the fundamental and second harmonic laser beams focused using a 30cm quartz lens into the high vacuum chamber.

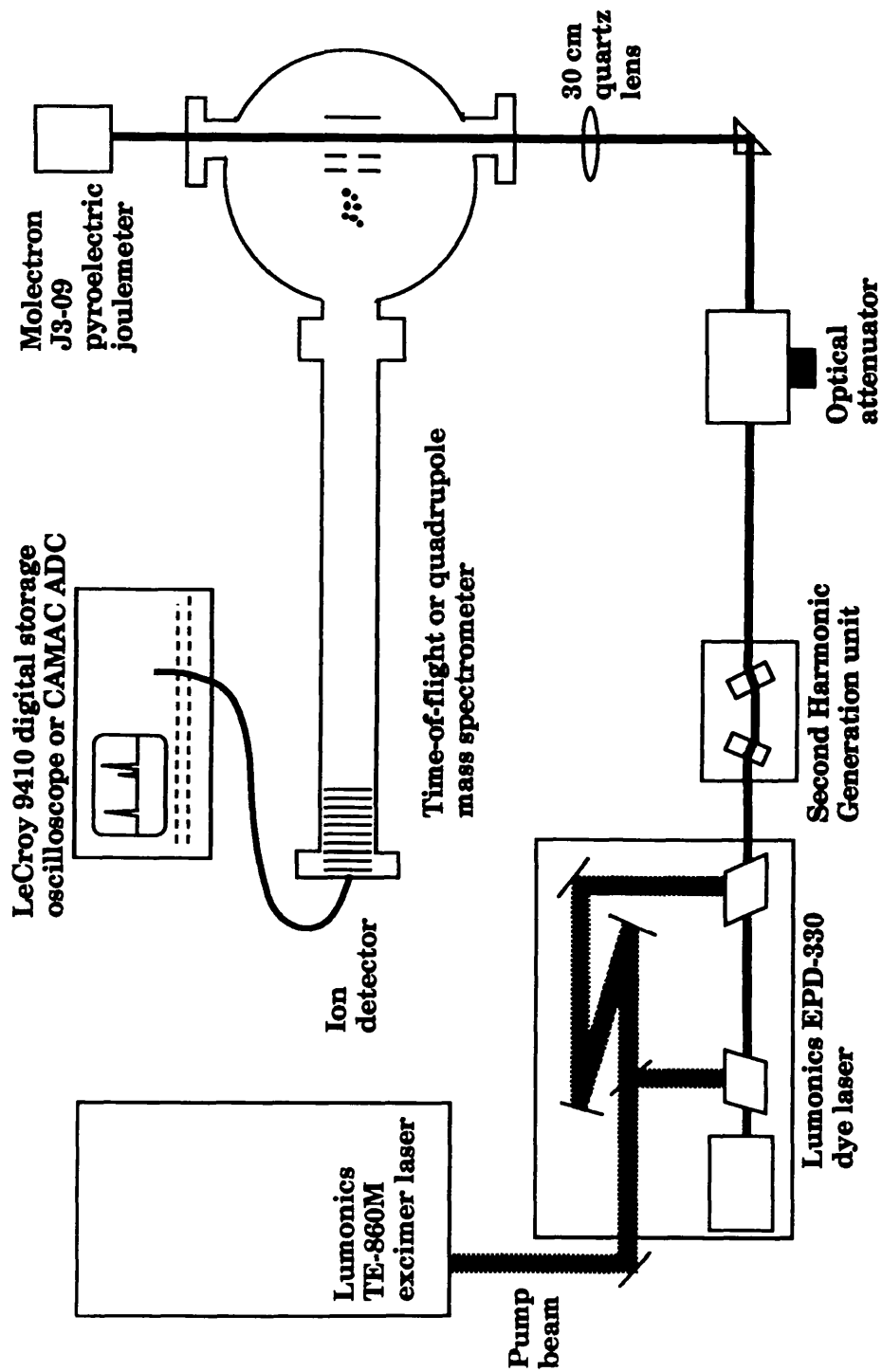


Fig 3.1 The experimental set-up is shown with the apparatus used to conduct the experiments.

This typically produces a laser spot in the extraction region of the ion optics of 200 μ m diameter and energy of ~20mJ/mm². On passing through the chamber, the beams were separated using a prism and the pulse energy of the UV beam was measured using a Molectron J3-09 pyroelectric joulemeter.

The stainless steel custom built chamber is operated at a base pressure of typically 10⁻⁸ mbar being pumped by a single Balzers TCP 310 turbo molecular pump backed by a rotary pump.

The samples are introduced into the system via a stainless steel capillary tube which is connected to the pusher plate. The samples pass through the pusher plate via 0.5mm diameter hole into the extraction region.

The phial which contains the sample and the inlet line may be heated to attain sufficient analyte concentration in the laser interaction region.

Laser sample interaction occurred in front of the sample stub, with the optimal distance being 1mm from the pusher plate face. The ions produced are extracted using a conventional double field system into a 1.20m drift region, where they are separated temporally and detected by a standard Thorn-EMI 18-dynode electron multiplier. The ion optics are of a Wiley Maclaren (24) design to optimise the mass resolution of the signal obtained. The TOF mass spectrometer was operated at a resolution of 220 measured at m/z 77, with the ion transmission factor from interaction region to detector estimated to be ~10⁻⁵.

For wavelength dependent measurements, signals from both the electron multiplier and the joulemeter were amplified and recorded simultaneously by a CAMAC based ADC system. In fixed wavelength measurements, TOF mass spectra were accumulated by taking the output of the multiplier directly to a Lecroy 9410 digitising oscilloscope where signals were averaged over typically 600 laser shots.

In order to give a more concise description of the experimental apparatus, each instrument in turn will be investigated and a detailed account of its specifications given.

(2) The Excimer Laser

The excimer laser used in our experiments is the Lumonics TE-860-3 series. Excimer lasers generate intense pulses of radiation at wavelengths from the vacuum ultra-violet to the visible region of the spectrum, depending on the operating gas mix, by transitions from excited molecules in a high pressure electrical discharge.

An excimer is a dimer which is stable only in an excited electronic state but dissociates readily in the ground state. Therefore it is possible to create a population inversion and obtain laser action between the two states, since any molecules in the repulsive ground state have an extremely short lifetime, typically of a few picoseconds. A laser operating by this mechanism is a two-level laser with population of the upper state not due to pumping of the ground state. Molecules in the upper state are created in a discharge by collisions between two atoms, one or both of which may be in an excited state. If one or both of the excited-state atoms are rare-gas atoms, the amount of excitation energy is extremely large. Therefore the metastable excimer state is very useful for storing high energies. With the efficiency of such lasers being quite high at about 20%.

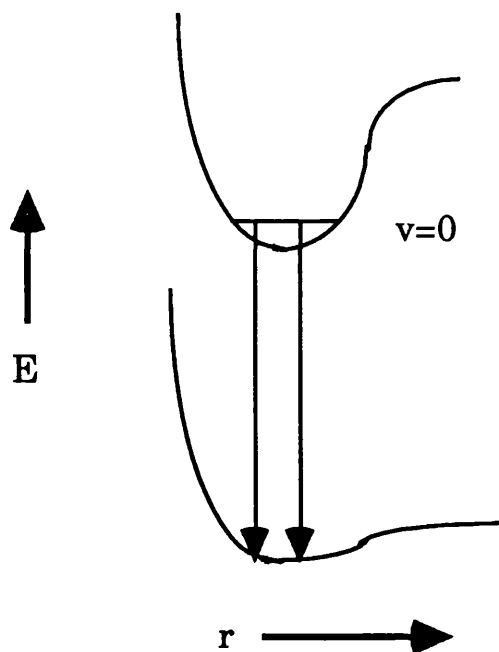


Fig 3.2 Potential curves for a weakly bound ground state and a strongly bounded excited state of a noble gas halide.

(3) *The Dye Laser*

The dye laser used is the Lumonics EPD-330 series. Dye lasers are sources of tuneable narrow bandwidth radiation which can be operated from 320nm to approximately 950nm by choosing the appropriate dye. As such, they are useful in a variety of photochemical and spectroscopic experiments-any application requiring a tuneable light source of extremely narrow bandwidth throughout the optical band, including techniques such as Resonance Ionisation Spectroscopy.

Organic dye molecules are the lasing species and are dissolved in an appropriate solvent and circulated by a pump through the lasing volume. These molecules absorb short wavelength light from a pump laser, and fluoresce at longer wavelengths. Under appropriate conditions, the fluorescence can be sufficiently bright that gain is available along the dye laser axis.

Broadband lasing action at a wavelength near the peak of the fluorescence curve can then be achieved by aligning the cavity

mirrors to this gain region. With the addition of a reflective grating into the cavity, narrow line width radiation can be obtained at any wavelength covered by the fluorescence band of the dye, simply by rotating the reflective grating. The single most important advantage of the dye laser over other lasers is the relatively large tuning range. In comparison, gas or solid-state lasers can be tuned only within a very small range, essentially the width of the gain profile.

The laser consists of an oscillator and simple amplifier stage, together with necessary optics to guide the pump beam into the cells. The use of a single amplifier allows rapid alignment and simple operation without loss of efficiency.

(i) Theory Of Operation:

One characteristic property of dyes is their colour, due to absorption, from the ground electronic state S_0 to the first excited singlet state S_1 , lying in the visible region. Also typical of a dye is a high absorbing power characterised by a value of the oscillator strength close to 1, and also a value of the fluorescence quantum yield close to 1.

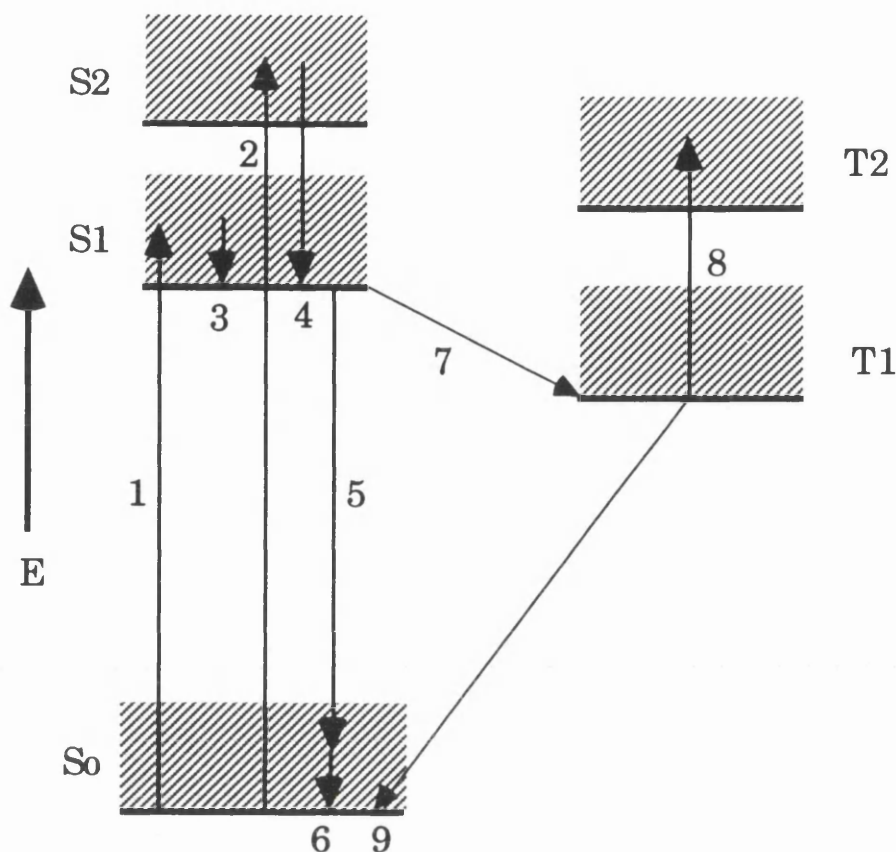


Fig 3.3 Energy level scheme for a dye molecule showing processes important in laser action.

The diagram shows a typical energy level diagram of a dye molecule including the lowest electronic states S_0 , S_1 , S_2 , in the singlet manifold and T_1 and T_2 in the triplet manifold. Associated with each of these states are vibrational and rotational sub-levels broadened to such an extent by collisions in the liquid that they form a continuum. As a result the absorption spectrum, is typical of a liquid phase spectrum showing almost no structure within the band system.

Depending on the method of pumping, the population of S_1 may be achieved by S_1 - S_0 or S_2 - S_0 absorption processes, labelled 1 and 2. Following either process, collisional relaxation to the lower vibrational levels of S_1 is rapid by process 3 or 4: e.g. the vibrational-rotational relaxation of process 3 takes the order of 10ps. The laser transition occurs between a state near the

bottom of the S_1 and an intermediate state in S_0 . Since there are many vibrational-rotational sublevels within S_0 and S_1 , the resulting emission line is very broad.

The state S_1 may decay by radiative or non-radiative processes, labelled 5 and 7 respectively. Process 5 is the fluorescence which forms the laser radiation and the figure shows it terminating in a vibrationally excited level of S_0 . The fact that it does so is vital to the dye being used as an active medium. The fluorescence lifetime for spontaneous emission from S_1 is typically of the order of 1ns while the relaxation process 6, like process 3, takes only about 10ps. The result is that, following processes 1 and 3, there is a population inversion between the zero-point level of S_1 and vibrationally excited levels of S_0 to which emission may occur, provided that these levels are sufficiently highly excited to have negligible thermal population.

The triplet states T_1 and T_2 are not involved directly in the laser action, but they play an important role, nevertheless. There is a small probability that the forbidden transition S_1 - T_1 (process 7) known as intersystem crossing will occur. Process 9 is also spin forbidden, thereby tending the molecules to pile up in the T_1 state. However the transition T_1 - T_2 is allowed and, unfortunately, the range of frequencies for this transition coincides almost exactly with the range of laser transition frequencies. If a significant number of molecules have made the S_1 - T_1 transition, the T_1 - T_2 absorption can quickly reduce the laser gain and quench laser action. For this reason the dye is circulated through the lasing medium and the lasers operate on a pulsed basis. The pulse duration is shorter than the time it takes for the population of the T_1 state to reach a significant value.

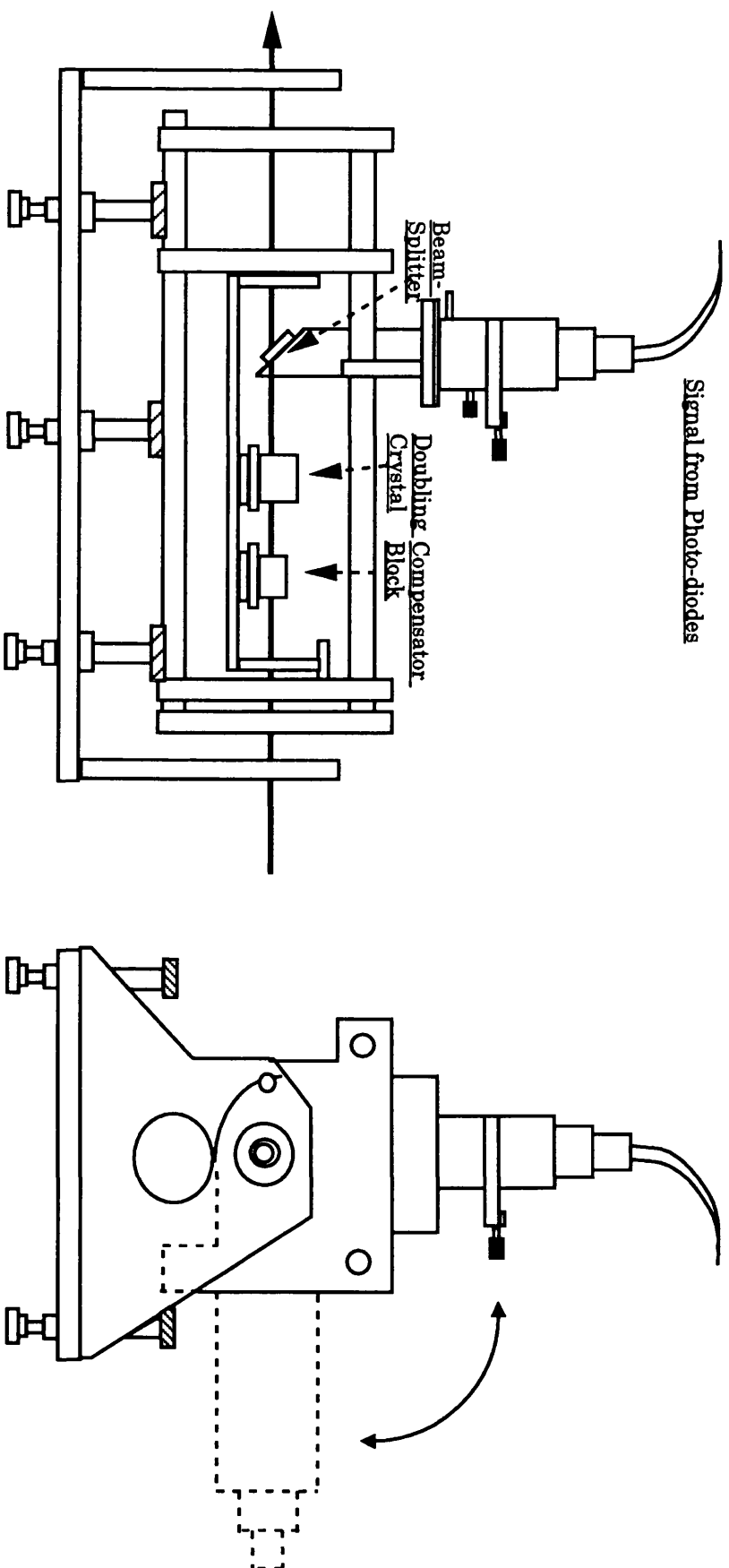


Fig 3.4 Autotracker showing both the side and end elevation. With the direction of the incoming and output beam indicated.

(4) *The Compuscan*

The addition of the EPD-50 motor drive and EPD-60 Compuscan to the dye laser provides the ability to control the wavelength parameters through a keyboard interface. The motor drive consists of a stepping motor together with a micro-step drive module offering extremely smooth (25000 step/rev) motion. This motor drive unit controls the rotation of a mirror in the optical cavity which alters the angle of the laser beam incident upon the holographic grating. The angle of incidence upon the holographic grating determines the lasing wavelength which is most efficient.

Once calibrated, the system will follow all wavelength changes, constantly updating in angstroms. Two modes of scanning are possible i.e. continuous or burst, as well as a toggle switch which allows manual control over the wavelength position, allowing the user to home in on a peak.

The system also has the ability to remove any backlash from the wavelength drive, before carrying out any wavelength scans to ensure reliable and accurate wavelength measurements.

(5) *Autotracker*

The Inrad Model 5-12 SHG Autotracking System consists of an optical assembly and an electronic control box. Fig 3.4

The autotracker works on the principle that the incoming laser beam is directed through a compensation block and then a doubling crystal. The compensation blocks purpose is to correct any displacement the beam may suffer on passing through the doubling crystal. A variety of doubling crystals exist such as BBO, KDP etc. which have different optimum wavelength regions in which they operate.

A small component of the doubled beam on passing through the crystal is split off by the beamsplitter. This component is monitored using two photo-diodes, which relay signals back to

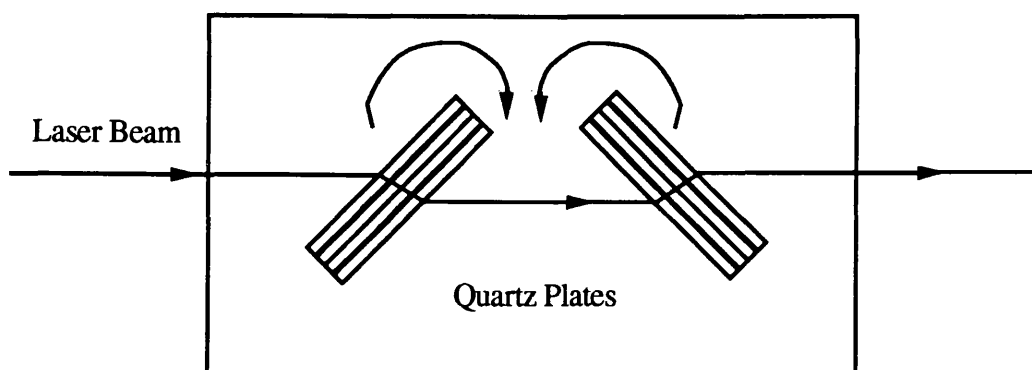


Fig 3.4a. Plan view of the attenuator showing the direction of movement of the quartz plates.

the motor unit controlling the doubling crystal turntable in order to optimise the phase matching condition, and thus the output of the doubled beam. The active feedback design of the autotracker system also allows accommodation of crystal temperature changes, produced by either ambient or laser induced heating, by altering the angle of the crystal appropriately. The Inrad Model 5-12 Autotracker, therefore, provides a practical way to achieve stable second harmonic outputs from a fixed frequency or variable frequency laser source.

(6) Optical Attenuator

The optical attenuator used in our experiments is the Newport 935-10 Model, which features a 10mm clear aperture.

(i) Principle of Operation

The attenuator works based on the Fresnel equations. Thus attenuation of the laser beam arises as it passes through a series of quartz plates, with the degree of attenuation being a function of the angle of incidence upon the plates and the number of plates used. In order to compensate for beam displacement as the beam passes through the plates the geometry of the set-up is such that the net displacement is zero.(Fig 3.4a)

(7) Time Of Flight Mass Spectrometer

Although the time-of-flight mass spectrometer based on the Wiley-McLaren pulsed two-grid ion source has been available since the early 1960's (24), its application has been limited by low resolving power and sensitivity. The renaissance of interest in this instrument is, in part, a consequence of the development of new ionisation techniques such as laser ionisation which take advantage of the TOF spectrometer's unique ability to provide a complete mass spectrum per event, and its high mass range. This has led to design developments which give major improvements

in instrument performance with promise to yield rich rewards particularly in the study of large molecules.

Advantages of TOF/MS

- Complete mass spectrum for each ionisation event
- Spectra can be obtained for very small amounts of sample
- Ideal where ionisation is pulsed or spatially confined
- Unlimited mass range
- Fast repetition rates up to 100kHz
- Performance dependent on electronic rather than mechanical alignment
- Relatively low cost

(i) Basic Principles of TOFMS

TOFMS operates on the basis that if a packet of gas phase ions of differing m/z ratios is rapidly accelerated through a constant electric field, V , then the ions will possess individual velocities, u , proportional to the ^{inverse} square root of their m/z ratio:

$$u = \left(\frac{2zeV}{m} \right)^{1/2}$$

As the ions tra - verse a fixed distance to the detector, l , then they separate in time according to their m/z ratio, those ions with the lowest m/z reaching the detector first and vice versa:

$$\text{Time - Of - Flight} = \frac{l}{u} = \left(\frac{l^2}{2Ve} \right)^{1/2} \cdot \left(\frac{m}{z} \right)^{1/2}$$

To utilise this "time of flight" separation to provide mass spectra the ion packets must be pulsed into the flight tube. Each pulse of laser light creates a packet of ions which travels down the flight tube, spreading out according to mass. Thus each packet or ion-generating event yields a complete mass spectrum. (Fig 3.5)

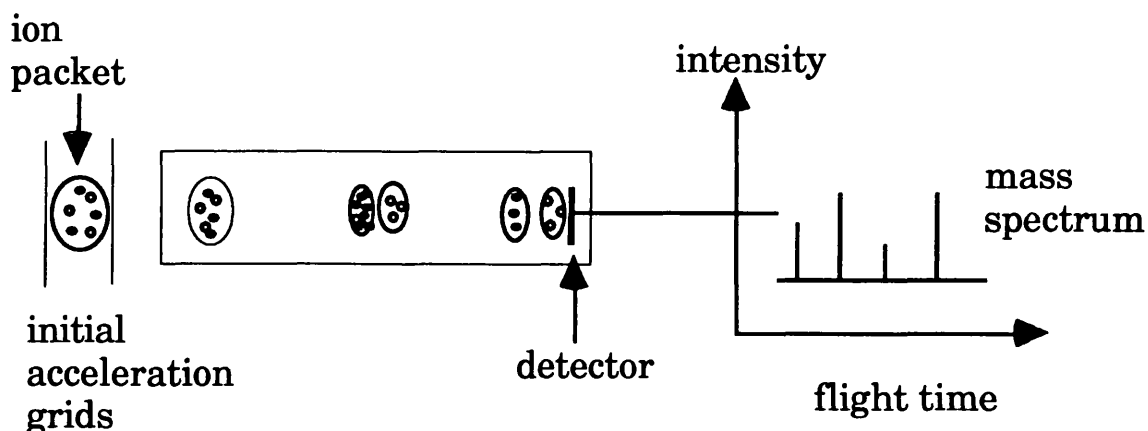


Fig 3.5 Time-of-flight separation of ions with different masses.
 • = light • = heavy ions

Since the ions traverse what is essentially empty space, the TOFMS has a high transmission capability and thus high sensitivity for single event monitoring. It is these attributes which make the TOFMS such an attractive choice for pulsed ionisation techniques.

(8) Ionivac

The accurate measurement of pressure readings is very important as this gives us an indication of the number of molecules within our interaction region and thereby quantifying our sensitivity measurements. The Ionivac IM210 is used which is a hot cathode ionisation vacuum gauge which uses a Bayard-Alpert gauge head for reliable vacuum measurements in the range from 10^{-10} to 10^{-2} mbar.

Main Features:

- Large measuring range with linear or logarithmic pressure reading over 7 decimal ranges.
- High accuracy
- Degassing of the gauge head without interrupting the process of measurements.

(9) Pyroelectric Joulemeter

The joulemeter is used to record the UV component of the beam after being separated from the fundamental using a quartz prism. The J3 Pyroelectric Joulemeter is a calibrated, fast response pulsed-energy detector which operates in the wavelength range from x-rays to far infra-red.

It relies on a crystal of lithium tantalate absorbing the photon energy, which then subsequently rapidly heats up and becomes electrically polarised. This polarisation produces a surface charge whose integrated value gives us an indication of the pulse energy.

The joulemeter is designed for operation with pulse widths ranging from picoseconds to 250 μ s. The output of the J3 is a linearly rising voltage during the radiation pulse, with a more slowly decaying fall time. The peak amplitude of the leading edge is proportional to the total radiation pulse energy. The output is displayed on the digital scope with measurements of the height of the pulse giving us the value of energy recorded.

(10) Gentec Joulemeter

The gentec is used to monitor the output power of the excimer beam. The model used is suitable for use with any 1M Ω input resistance monitoring system such as an oscilloscope. A combination of rugged construction, high sensitivity and fast reading capability makes Gentec joulemeters very useful instruments for EM pulse energy measurements.

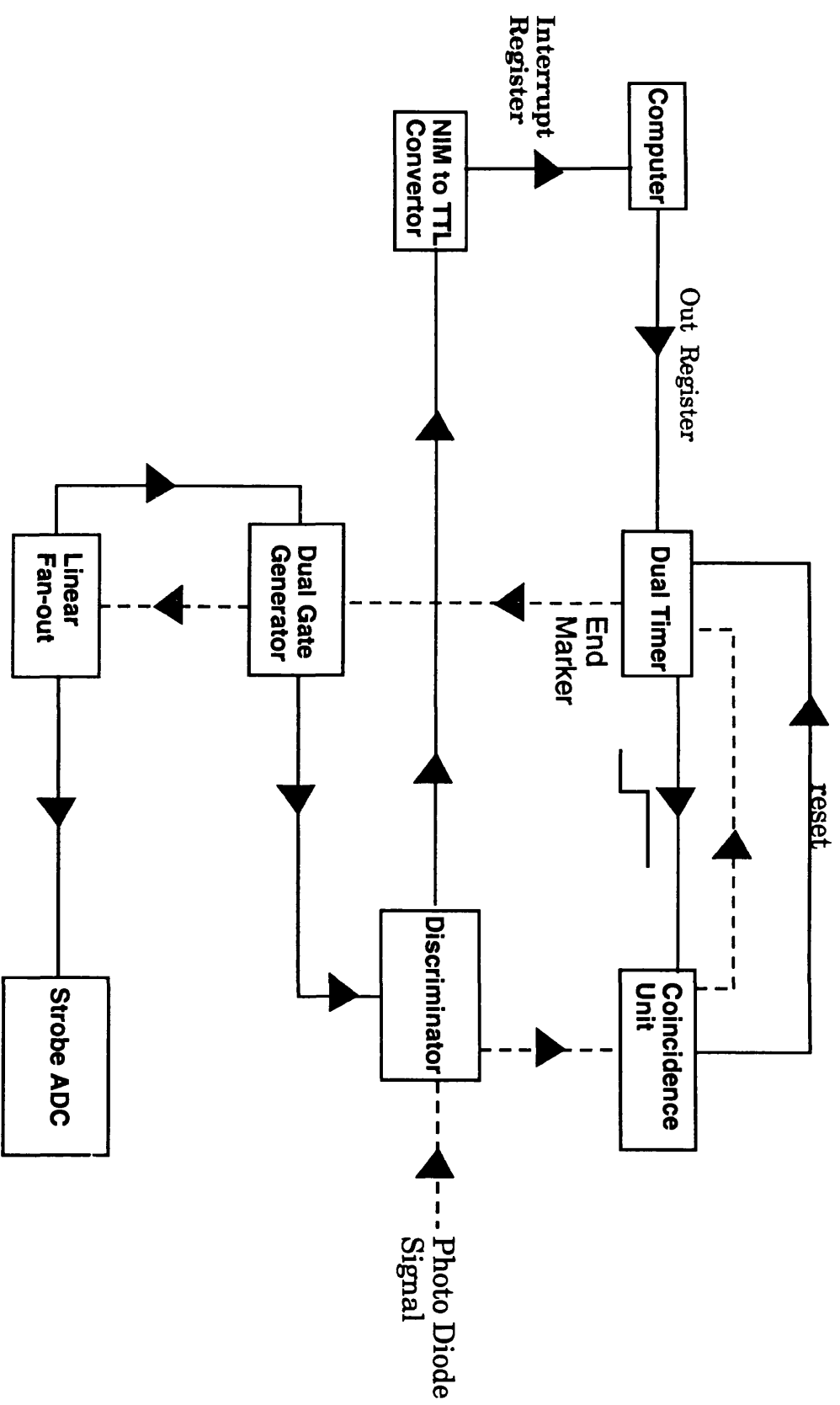


Fig 3.6 Flow diagram showing the routes taken by the signals in the data acquisition system.

Theory

The detector head is composed of a pyroelectric ceramic and an optical absorptive coating. Laser radiation is transformed into heat that flows through the ceramic to the heat sink. The ceramic then produces a voltage which is proportional to the average temperature variation of the ceramic.

Since pyroelectric detectors are heat sensitive, the main purpose of the absorptive coating is to transform the optical energy into heat.

(11) Data Acquisition (Fig 3.6)

The data acquisition system involves using the LSI-11 computer to start the electronics. The computer sends out a ready pulse which when coincident with a photo diode pulse from the laser starts the timing mechanism. This mechanism involves producing a pulse of variable delay and width using the dual timer and dual gate generator respectively. By varying the delay with respect to the photodiode signal it is possible to select any specific ion for investigation. The ADC gate is placed on the oscilloscope to observe the ADC gate and the ion signal simultaneously. In this way wavelength dependent spectra can be recorded by scanning through the appropriate wavelength region and recording the variation of the ion signal onto a 5"1/4' floppy disk. This information is transferred to the Mackintosh where Cricket Graph is used to plot the wavelength scan.

Mass spectra are recorded by printing directly from the digital Lecroy 9410 oscilloscope using a plotter.

(12) Electron Multiplier

A Thorn-EMI 18 dynode electron multiplier is used for ion detection. The detector works on the principle that an ion strikes the dynode releasing two electrons. The liberated electrons are accelerated through an electric field and strike more dynodes thus resulting in an avalanche effect. The net gain of this system is $\sim 10^5$.

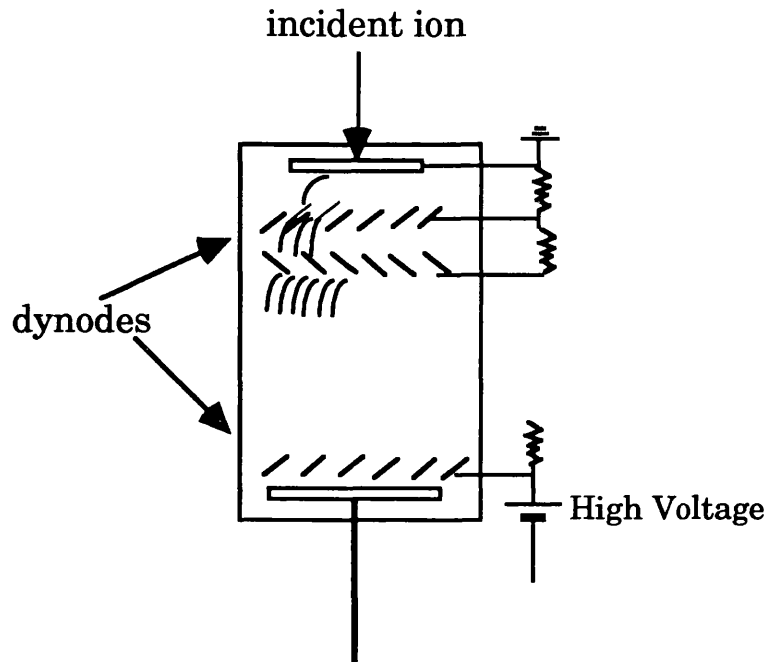


Fig 3.7

4. The Role Of REMPI Mass Spectrometry In Trace Analysis

Laser based systems have been used extensively for mass spectroscopic analysis of environmentally hazardous as well as explosive materials (25-28). Although RIS and REMPI have proved to be very important laboratory based analytical techniques, there have been few applications which are operating in an industrial environment.

The following results have been obtained with a system built in-house at Glasgow University and used for the sensitive detection of NO₂ containing molecules (29-31). These are of great strategic importance since many explosive compounds fall into the categories of nitroaromatics, nitroamines and nitrate esters. Recently a number of research groups have used this approach for analysing and monitoring a variety of vapour-phase nitro-compounds (29-35). One important aspect of this work is to establish a means of detecting explosive molecules in the presence of other similar impurities which may also exist in the surroundings. These innocent compounds such as perfumes and musks also belong to the nitroaromatic family and pose formidable problems as far as selectivity is concerned.

This chapter describes the wavelength-dependent yield of some of the positively charged ions resulting from the interaction of UV laser beam with both nitrobenzene and nitrotoluene gaseous vapours in a high vacuum chamber. Both mass spectra at fixed wavelengths and wavelength dependence of the hydrocarbon fragment ions have been investigated. In the course of this study, the nitrobenzene sample was investigated for possible benzene contamination. The following sections describe approaches used to clarify this assumption.

It is noted from the mass spectra of the nitroaromatics taken at various wavelengths that a number of hydrocarbon groups are created (Fig 4.1). In previous studies the wavelength dependence

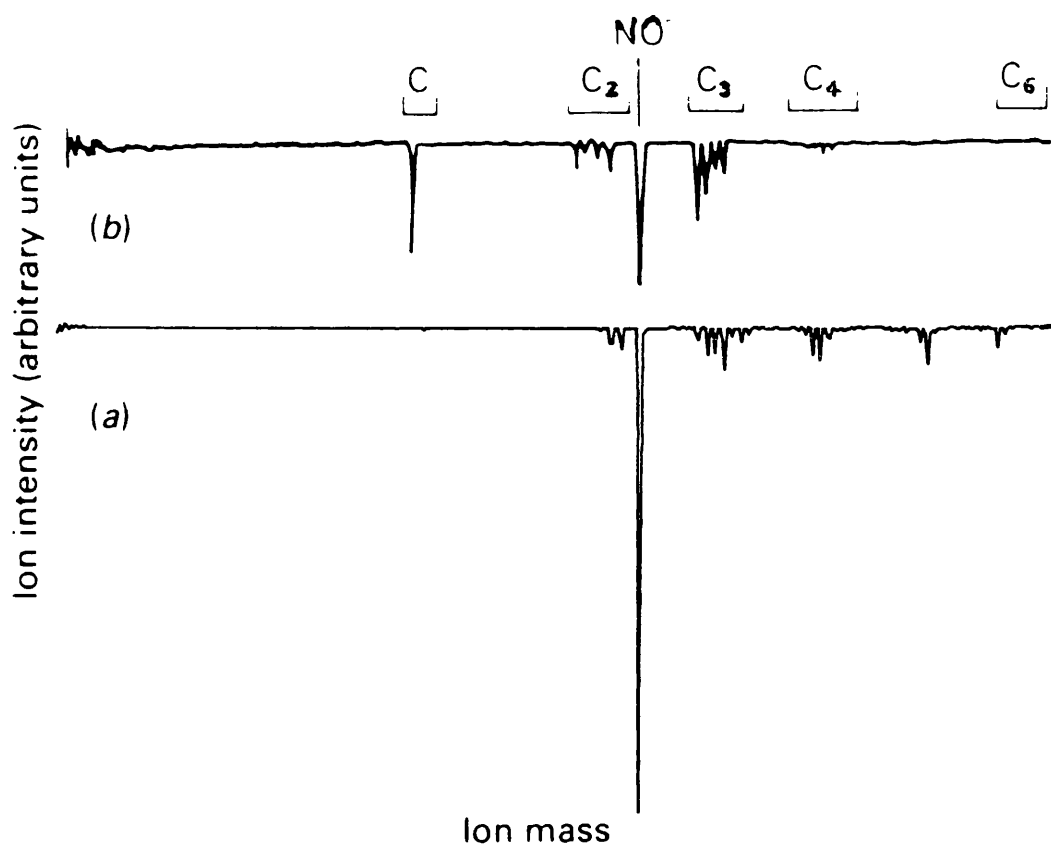


Fig 4.1 Time-of-flight mass spectra of (a) nitrobenzene at 247nm and (b) o-nitrotoluene at 247.5nm. Both show various hydrocarbon groups as well as a strong NO ion.

of the hydrocarbon fragments of nitrobenzene and nitrotoluene were described and it was shown that the two compounds could be distinguished using this procedure (Fig 4.2).

In the course of subsequent research into the benzene molecule, wavelength dependence of the hydrocarbon fragments from nitrobenzene were compared with the single photon absorption spectrum of benzene, with very close similarities being noted.

Because of the marked similarity in the comparison of the spectra it was thought that benzene impurity may exist in the sample of nitrobenzene obtained from BDH.

Consequently a number of different techniques were deployed in order to investigate this situation. These have involved carrying out UV absorption spectra of nitrobenzene and benzene, gas chromatography and electron impact experiments.

In order to discount the possibility that the contamination may arise from the analysing system itself, two samples from different manufacturers were investigated (BDH & Aldrich), with only one of the samples showing evidence of benzene impurity.

Conclusive evidence for the presence of this impurity is realised through experiments carried out using the laser based system.

(1) Mass & Wavelength Dependent Data of Nitrobenzene

Firstly, a brief description of the various fragments which have been observed in the mass spectra of nitrobenzene will be presented. The mass spectra show a number of hydrocarbon groups ranging from the C₁ to C₆ group, as well as showing a prominent NO ion signal (Fig 4.1). Atomic resonance signals of the hydrogen and oxygen ions have also been observed but these will be discussed later.

The identification of higher masses such as C₆H₅O and the parent ion are of particular importance, since the presence of these ions elucidate possible pathways leading to the formation

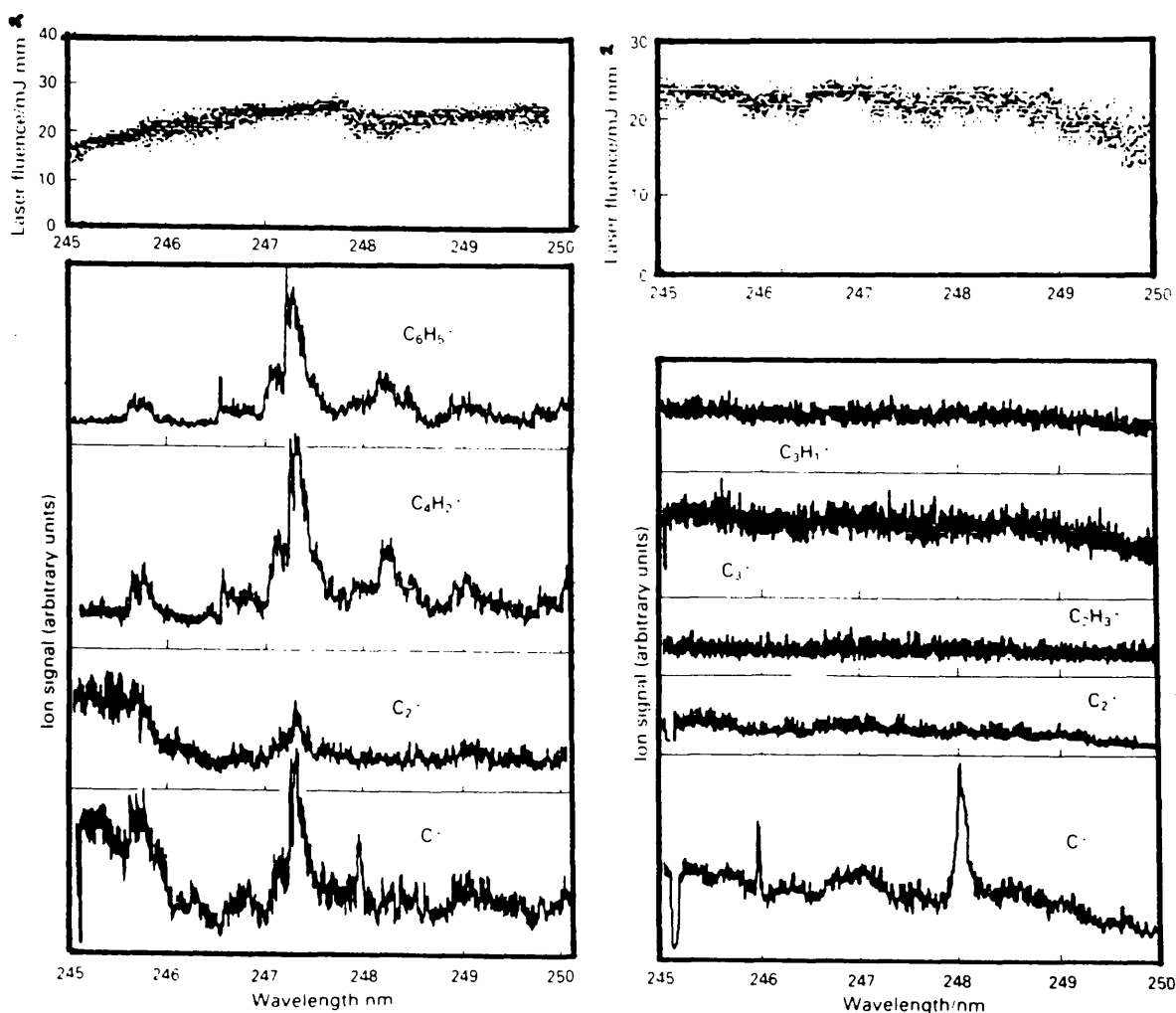


Fig 4.2 The wavelength dependence of the fragment ions between 245 and 250nm from nitrobenzene and o-nitrotoluene are shown. All the fragments from nitrobenzene show similar resonance structure whereas fragments from o-nitrotoluene exhibit no resonance structure. The dye profiles for both spectra over this region are shown above.

of the various lower mass ions. This will also be discussed at a later stage. The various masses have been identified with a time of flight mass spectrometer using their times of arrival as recorded by the digital oscilloscope. With the acquisition of a new digital oscilloscope with a floppy disc storage facility, it has been possible to store the complete spectra to be analysed at a later time. The mass calibration of the peaks in the spectra was performed using the NO ion as the reference marker, as this ion is the most readily identified.

Previous wavelength scans of the hydrocarbon fragments in nitrobenzene in the region 245-250nm have been taken. These scans show broad resonance structures which are indicative of molecular transitions (Fig 4.2). One important feature to note from the spectra is that all of the hydrocarbon fragments have similar wavelength dependencies. This would suggest that the fragment ions have originated from the break-up of the same parent molecule or ion. This property could be utilised to increase sensitivity measurements by recording the total ion signal as a function of wavelength, rather than separating the masses in a spectrometer, thus allowing a larger signal for detection purposes.

The primary reason for the investigation of the wavelength dependence of the hydrocarbons is to aid the identification procedure. By recording the wavelength fingerprint of the hydrocarbons it should be possible to set up a library of spectra which could be consulted in order to distinguish between individual nitroaromatics.

(2) UV Absorption Spectra

In order to gain more insight into the transitions involved in the fragmentation and ionisation processes the UV absorption spectra of nitrobenzene and benzene were recorded using a Beckman UV 5270 spectrophotometer with a resolution of 0.05nm (Fig 4.3 & 4.4).

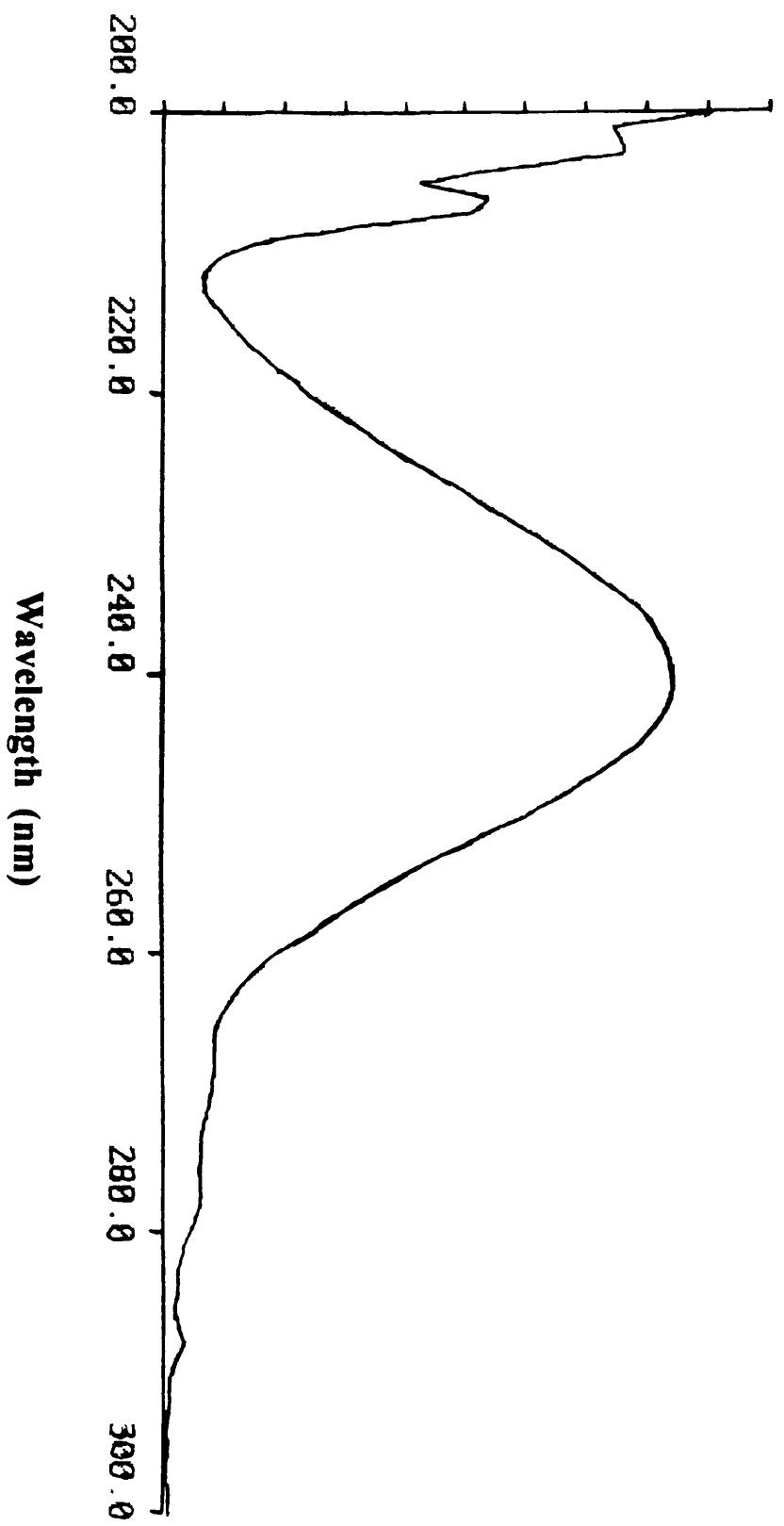


Fig 4.3 The UV absorption spectrum of nitrobenzene is shown.

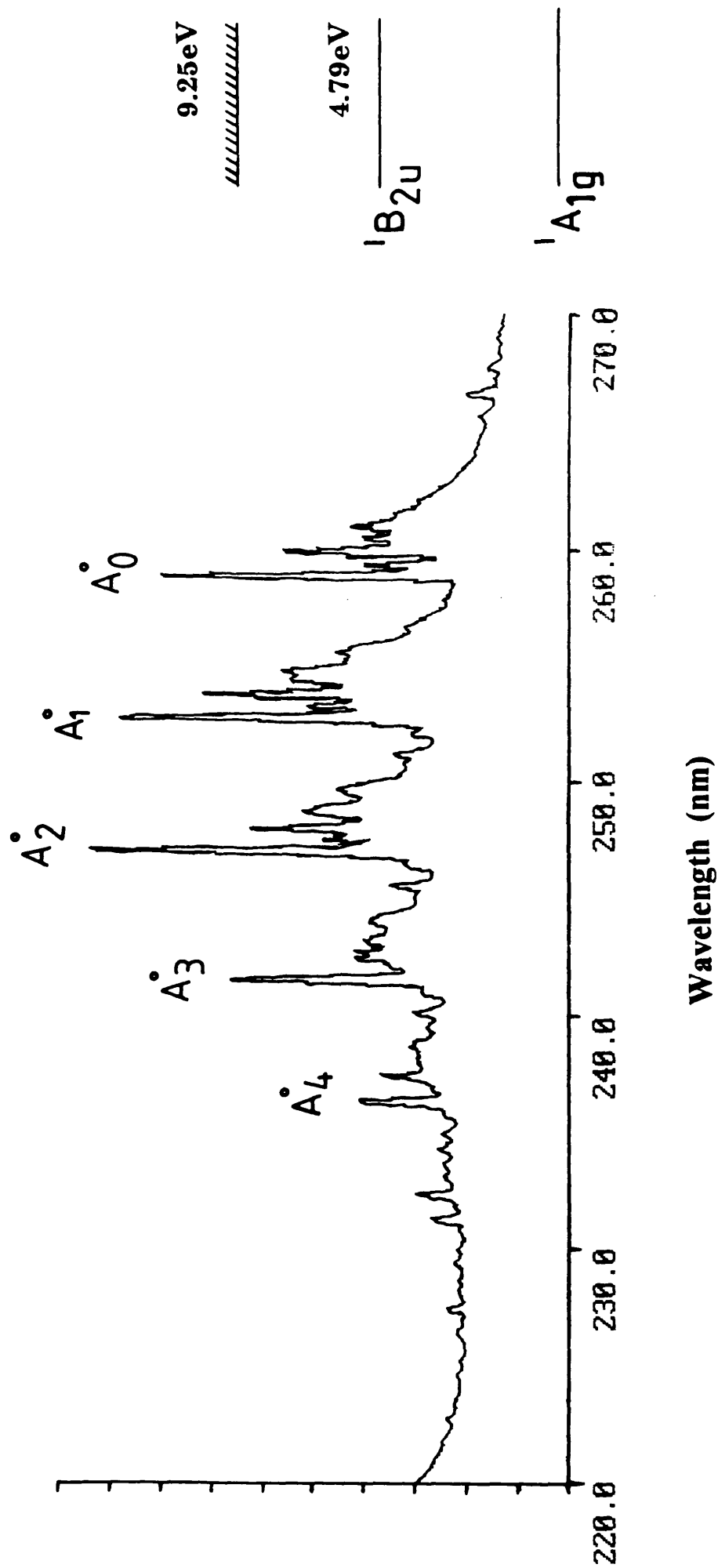


Fig 4.4 UV absorption spectrum of benzene gas at approximately 10-3Torr. The spectrum shows a number of prominent peaks associated with the $1B_{2u} \rightarrow 1A_{1g}$ transition.

The nitrobenzene absorption spectrum, shows no structure but instead has a broad continuous absorption intensity peaking at 240nm whereas in contrast the benzene spectrum shows a number of prominent peaks associated with the ${}^1B_{2u} \rightarrow {}^1A_{1g}$ transition. The vibrational bands are marked and have measured wavelengths in close agreement with those of Atkinson and Parmenter (36).

It is a characteristic feature of explosive molecules that a number of NO_2 groups are bonded to either carbon or nitrogen atoms. These groups are often responsible for the structureless absorption spectrum in the UV of these molecules, pointing to the fact that photodissociation is taking place.

This observation can be supported from two points of view.

Firstly, in the UV absorption spectrum of benzene strong resonance structure is observed whereas in nitrobenzene no structure is observed and the only structural difference in these compounds is the addition of an NO_2 radical to the benzene ring. Thus suggesting that the presence of this radical has suppressed the resonance structure.

Secondly, the NO_2 radical is electro-negative therefore causing a charge transfer process which subsequently perturbs the transitions allowed in the benzene ring.

In previous REMPI experiments, it was possible to obtain the identity of the molecular species by comparing the ionisation spectrum with the single-photon absorption spectrum (37). Such a comparison can be made if the REMPI process involves an ionisation scheme with the intermediate resonance step not being saturated and the ionisation step having no wavelength dependence.

A comparison of the nitrobenzene absorption spectra with the wavelength dependence of the fragments shows no similarities.

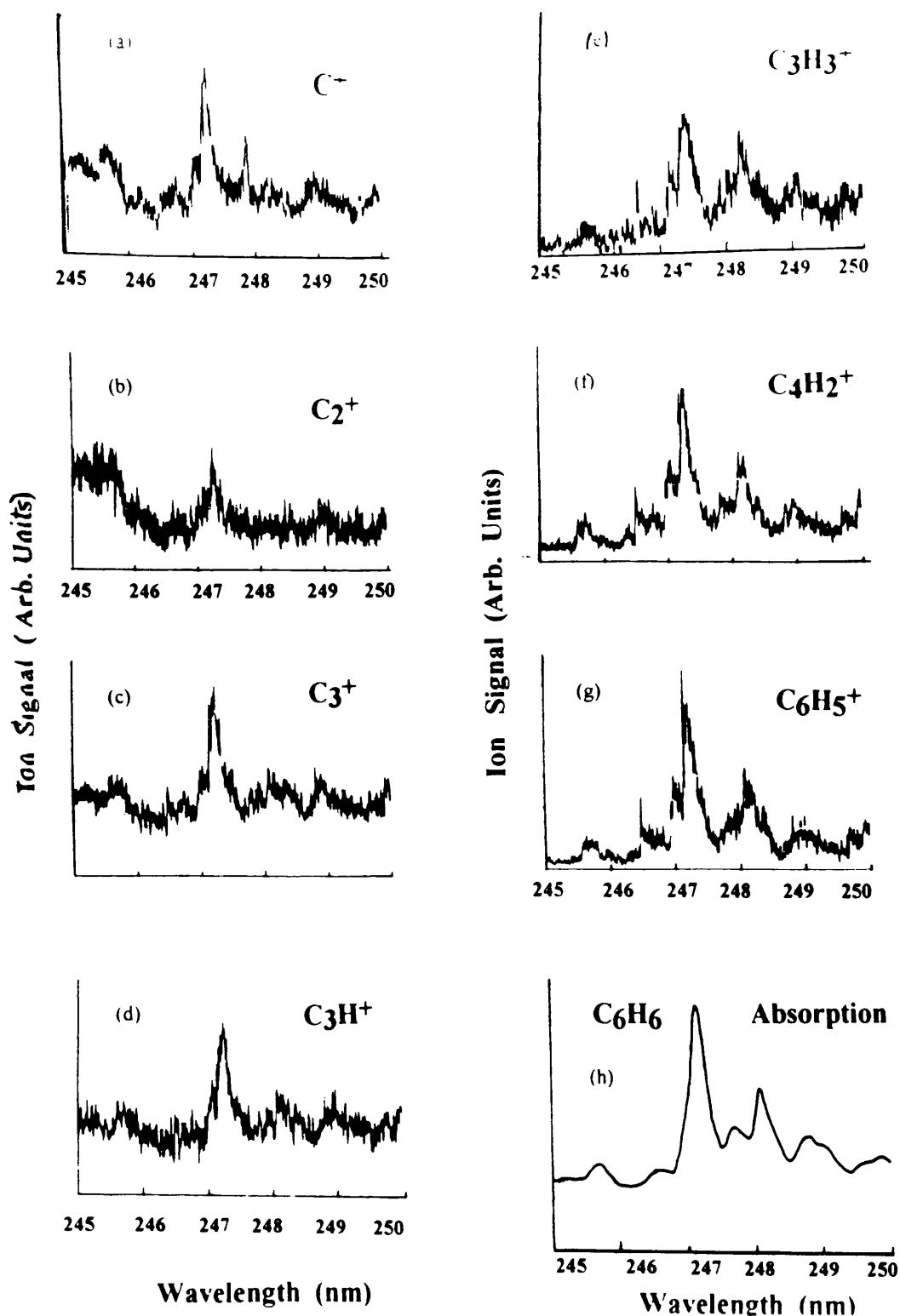
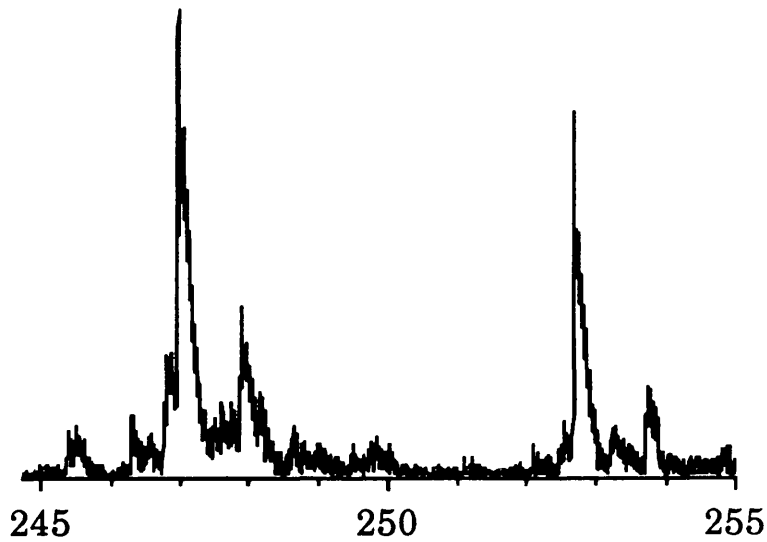
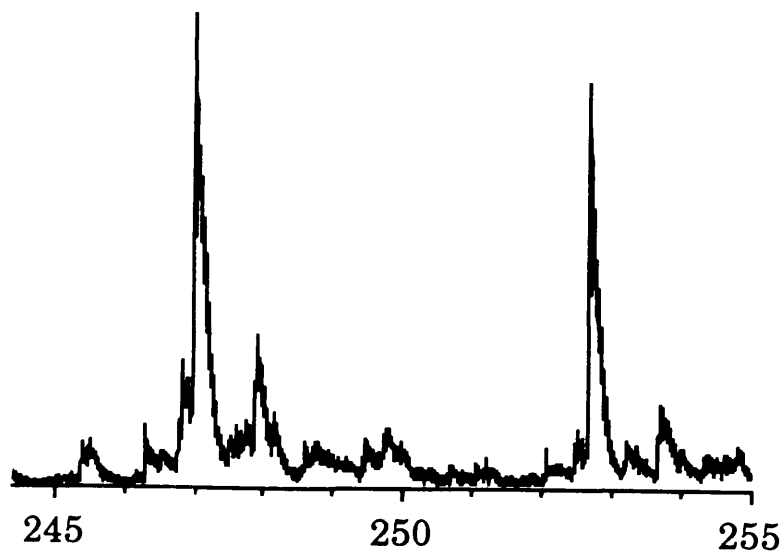


Fig 4.5 (a-g) The C_nH_m fragments wavelength dependence from nitrobenzene in the wavelength range 245-250nm is shown. The dependence of the ion signal on the dye profile has been linearly normalised. (h) shows the benzene single photon absorption spectrum.

Nitrobenzene Sample



Benzene Sample



Wavelength(nm)

Fig 4.6 The wavelength dependence of both the fragments from nitrobenzene and benzene samples are shown top and bottom respectively. The benzene fragment shows a wavelength dependence as predicted by the UV absorption spectrum of benzene, with the nitrobenzene fragment ion also following a similar dependence.

This difference could be explained by acknowledging that the intermediate state of nitro-compounds have a very small lifetime (~picoseconds), thus rapidly dissociating on absorbing a UV photon. This would lead to the formation of neutrals or ions which subsequently would absorb at different wavelengths and hence have different structural bands compared to the original parent.

(3) Comparison of Absorption spectra of Benzene with wavelength dependence of Nitrobenzene Fragments

It was at this stage that the similarity between the UV absorption spectrum of benzene and the hydrocarbon wavelength dependence from a sample of nitrobenzene taken in earlier studies was realised (Fig 4.5). This observation prompted us to repeat experiments carried out on the hydrocarbon ions of nitrobenzene. Wavelength scans along the 245-255nm region have been repeated showing improved signal to noise statistics.

The wavelength dependence of the hydrocarbon group from a pure sample of benzene was also carried out. Transitions predicted by the UV absorption spectrum, were observed as expected. Between 245-255nm the spectrum of the REMPI ions produced from the BDH nitrobenzene sample and the absorption spectrum of benzene were almost identical, with both the A_2^0 and A_1^0 absorption bands of benzene present (Fig 4.6).

It can be concluded from the evidence produced so far that the UV absorption spectrum of benzene is the same as that produced by the fragment ions produced from the nitrobenzene sample. At this stage in our experiments it was believed that because the fragment ions did not mimic the behaviour of the nitrobenzene UV absorption spectra, that on absorption of photons the nitrobenzene molecule dissociated into neutral fragments. Thereafter any ions produced would reflect the characteristics of the neutral fragments formed and not the original parent. One such neutral fragment which may form in the intermediate state is phenyl (C_6H_5).

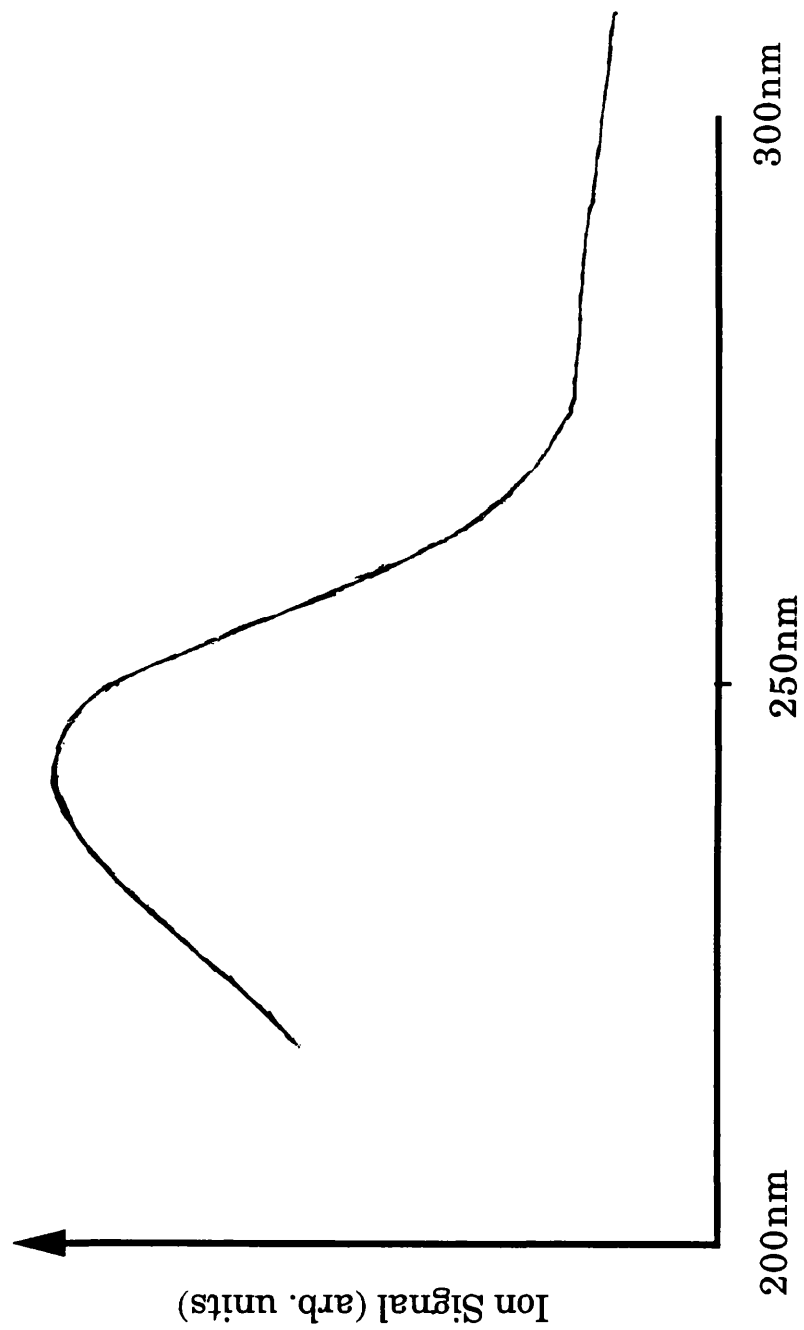


Fig 4.7 The UV absorption spectrum of phenyl is shown with a broad continuous profile peaking at approx. 250nm.

The first interpretation of the results was that the electronic structures of C_6H_6 and C_6H_5 must be very similar in nature accounting for the marked similarity in the spectra. Both molecules have similar ionisation potentials of 9.25eV and 9.35eV respectively and hence a resonant two photon absorption process with wavelengths $<265\text{nm}$ will cause ionisation in both molecules.

The interpretation of the data obtained to date implies that under laser irradiation in the wavelength range 224-260nm, nitrobenzene dissociates to yield phenyl radicals which absorb further photons producing phenyl ions and daughter fragments. The phenyl radical are likely to be produced in their ground electronic states and have electronic transitions similar to C_6H_6 . However, a UV absorption spectrum of phenyl is reported (38) which shows a broad structureless profile akin to the nitrobenzene spectrum with a peak at 245nm (Fig 4.7). The features in this spectrum are unlike the REMPI spectrum of the ions recorded which infers that the fragment ions do not originate from the neutral phenyl radical.

(4) Search For Benzene Contaminant

As the evidence for benzene contamination was growing it was decided that other techniques should be used in an attempt to detect the impurity. The following techniques were used:

a)

The UV absorption spectra of nitrobenzene was taken, which showed no evidence of benzene structure (Fig 4.3). In this series of experiments both benzene and nitrobenzene compounds were studied (Fig 4.8). Quartz cells were used to hold both samples. Introduction of the sample into the cell was accomplished by first evacuating the cell using a rotary pump. Thereafter, the cell was filled with the sample. The cell was then taken to the absorption spectrometer and the UV absorption spectra recorded.

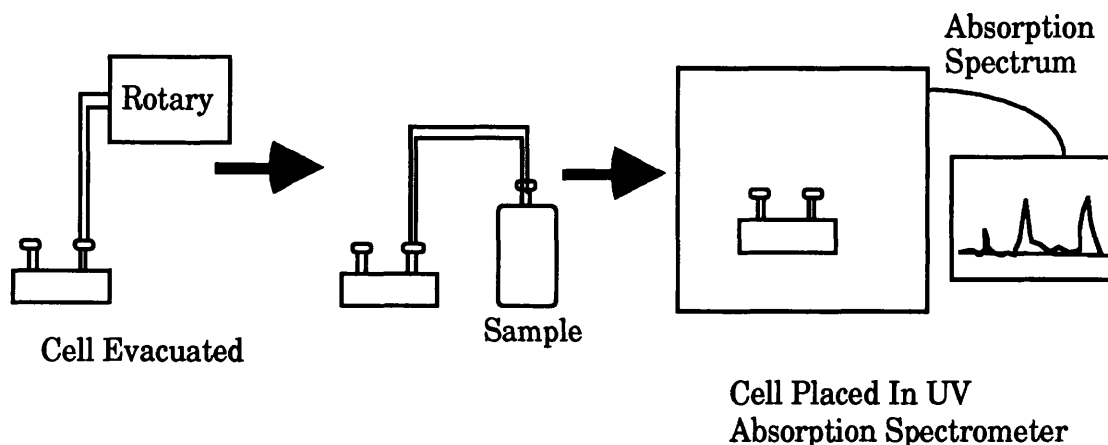


Fig 4.8

The UV spectrum of the samples showed the characteristic features associated with both nitrobenzene and benzene, i.e. the broad structureless absorption spectrum associated with the spectrum of nitrobenzene and the prominent peaks associated with the ${}^1B_{2u} \rightarrow {}^1A_{1g}$ transitions of benzene (Fig 4.3 & 4.4). At first only the vapour from the nitrobenzene bottle was analysed which gave no evidence of contamination, thereafter up to 20 drops of nitrobenzene was introduced into the cell and the spectra recorded again showing no benzene signal. The quantity of the sample introduced is increased in order to increase the absolute amount of any benzene contaminant that may exist. If benzene's high saturated vapour pressure (122 torr) can be maintained within the sample cell, then a large proportion of the gaseous sample will be benzene and should show itself in the UV absorption profile.

b) (The following analysis was carried out by the GC unit in the Chemistry Department.)

From the various mass spectra recorded the times of arrival of the various ions were noted. By using the flight time of the NO ion to calibrate the data, the times of the C_6H_6 ion could be predicted. But from the mass spectra it was not possible to distinguish unequivocally between the C_6H_6 and C_6H_5 ions.

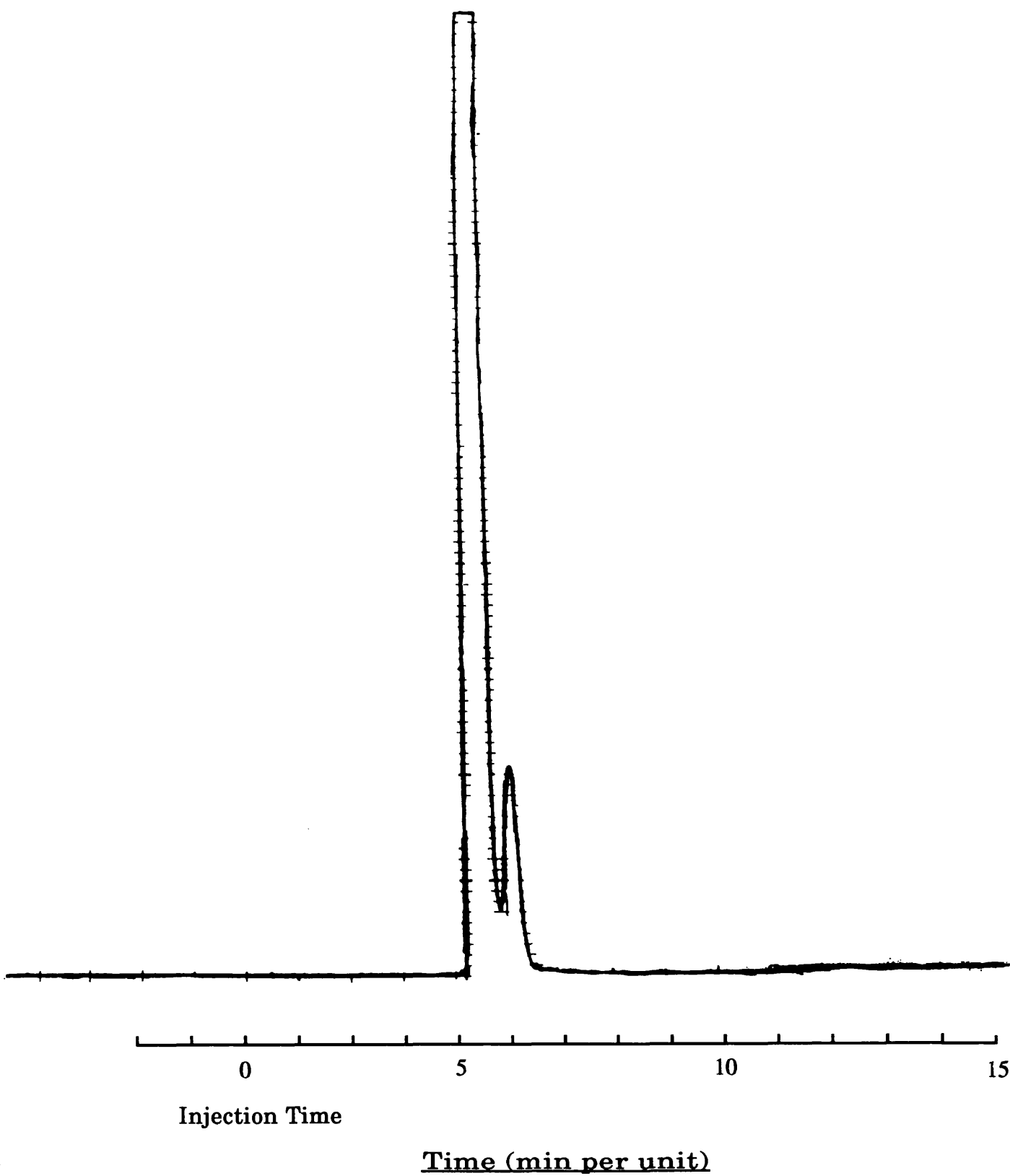


Fig 4.9 Benzene sample is placed in the gas column and its signal is observed adjacent to the large solvent peak of CH_2Cl_2 .

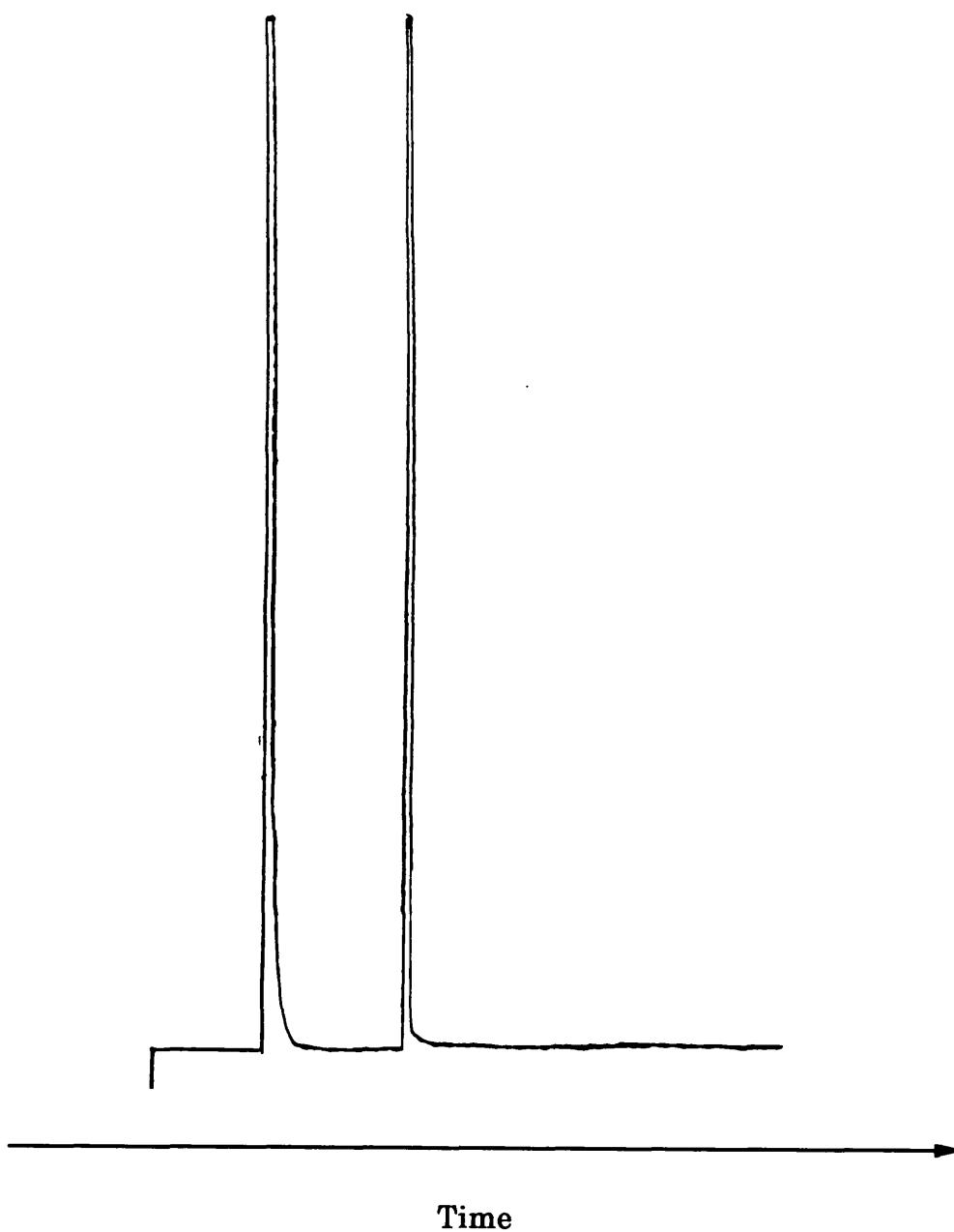


Fig 4.10 The nitrobenzene sample is placed into the gas column and observed are two saturated peaks associated with the solvent and sample.

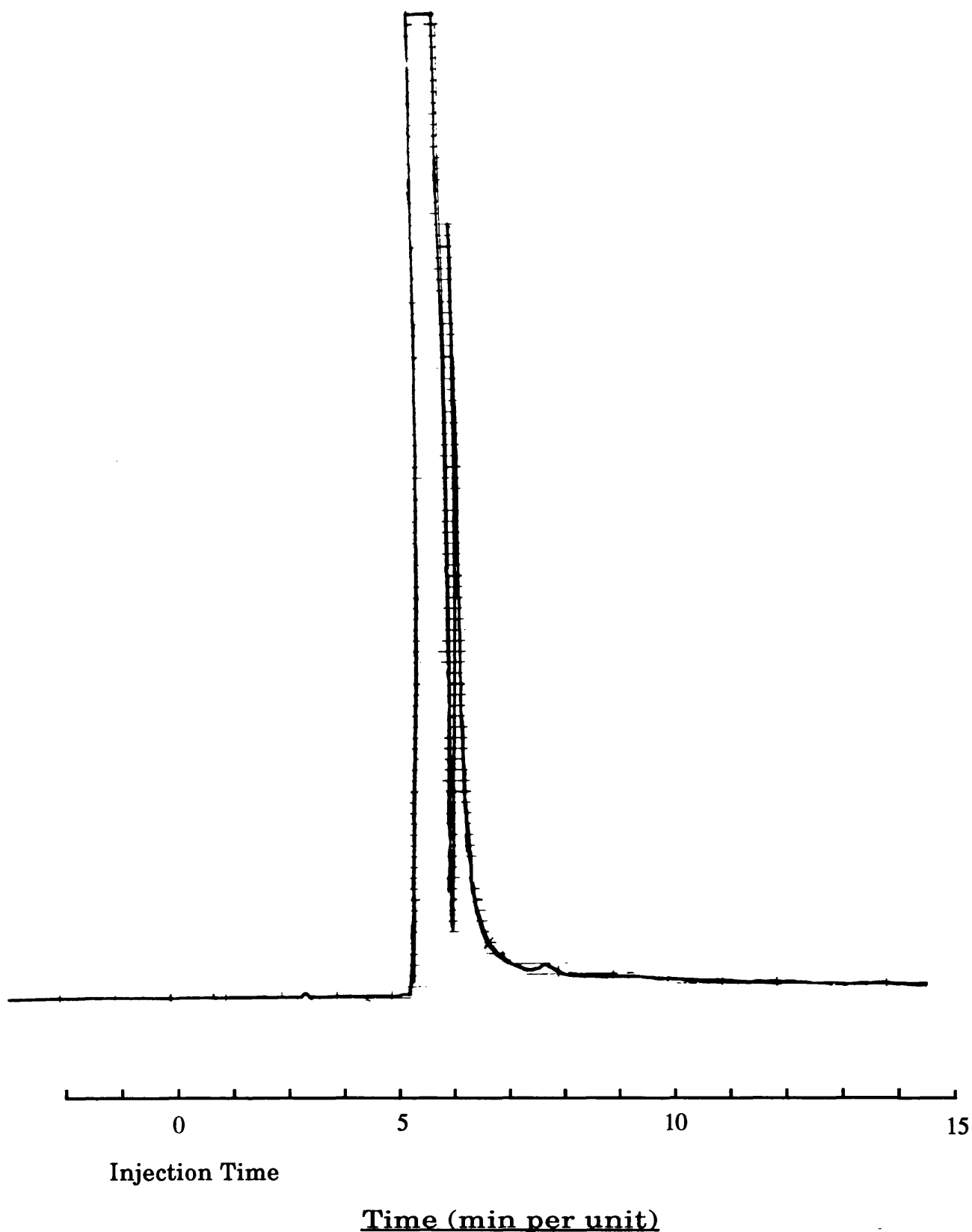


Fig 4.11 The spectrum shows in detail the region round the solvent peak from the sample of nitrobenzene. The peak adjacent to the solvent peak is a consequence of increasing the gain, during the run.

To obtain more accurate calculations of the times of arrival of the heavier ions, a computer program was developed using two reference peaks for calibration which could subsequently establish more precise arrival times.

This least squares program was used to predict the times of the various peaks, but this program was still not of sufficient accuracy to eliminate the ambiguities associated with the data. It became clear that the program could give reasonable estimates for the times of arrival for the small masses up to C₄ and C₅ groups but thereafter the squared relationship between the mass and time started to break down.

c)

A careful analysis by gas chromatography-mass spectrometry was also carried out using a Hewlett-Packard 5971 mass selective detector interfaced to a 5890 series gas chromatography. This analysis revealed a complete absence of impurities.

This experiment was carried out in the Chemistry Department by first placing benzene in the gas column and gauging the region in which the signal of benzene would be expected Fig 4.9. The graph shows a large solvent peak, with an adjacent peak associated with the benzene signal. Thereafter, the sample of nitrobenzene was introduced into the system and the spectrum showed no peak in the region where the benzene was originally detected, Fig 4.10. Because of the higher mass of nitrobenzene its signal was detected at the longer retention time. At this point the region adjacent to the solvent peak was magnified in order to show the presence of any benzene contamination which may exist Fig 4.11. The fact that the solvent peak was so close to the benzene signal made detection of any small traces of benzene more difficult. Nevertheless, careful examination of the spectrum showed no sign of the benzene when the gain of the system was increased.

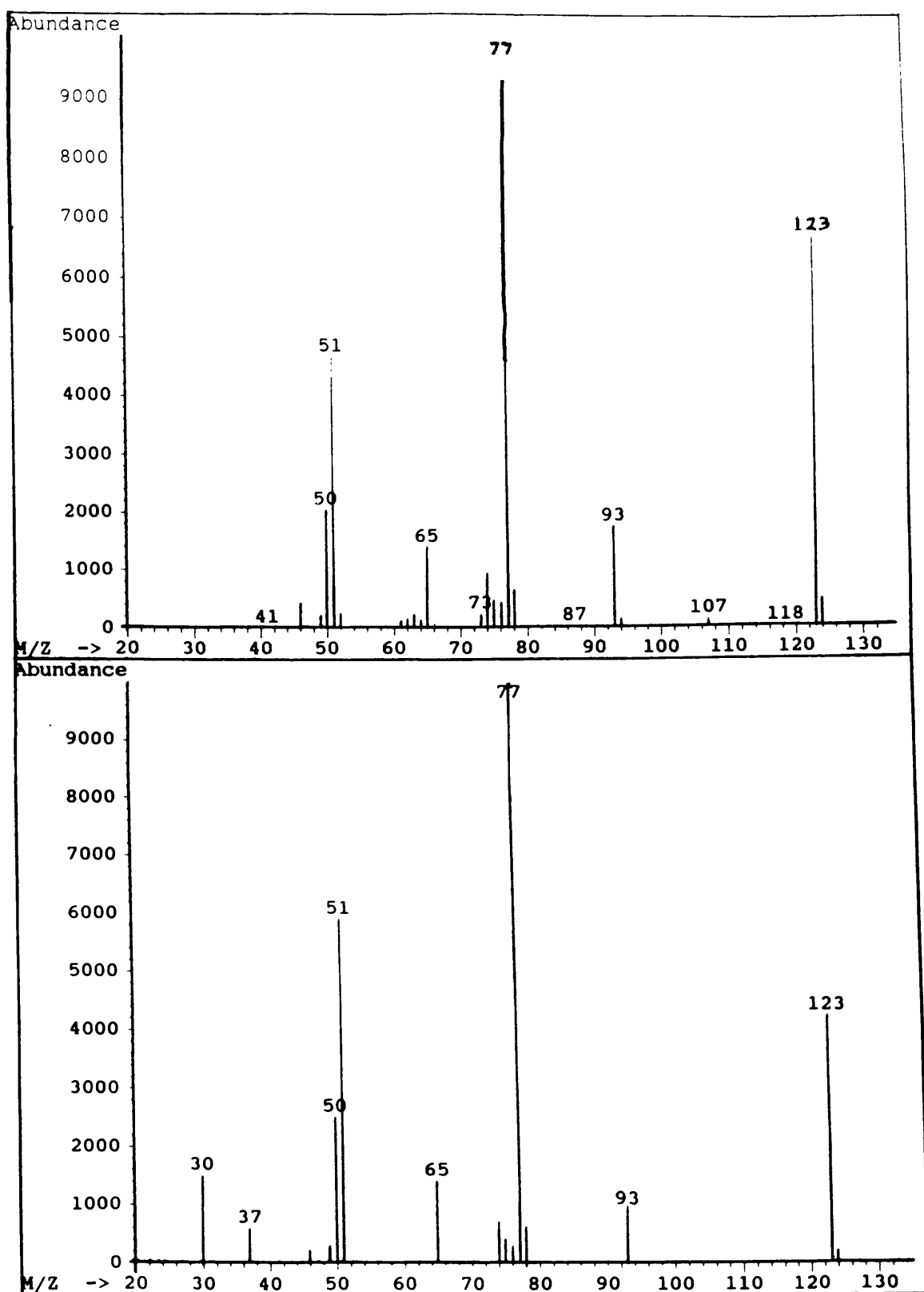


Fig 4.12 The upper electron impact spectrum is that from the chemistry library data base of pure nitrobenzene and the bottom one is that from our sample of nitrobenzene.

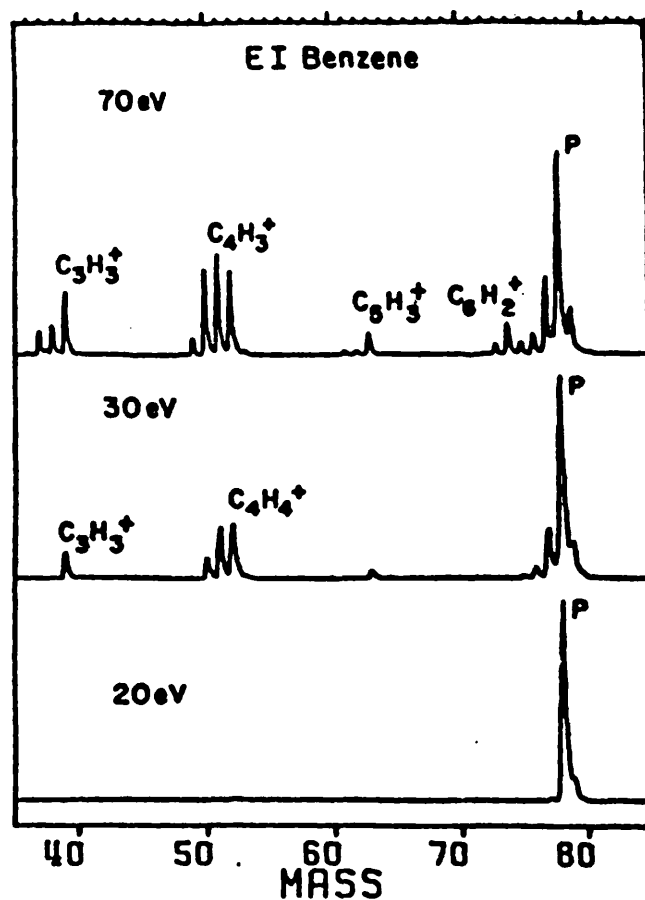


Fig 4.13 The Electron Impact mass spectrum of benzene at various energies shows that the dominant ion which remains is the parent one.

d)

The nitrobenzene signal was then analysed using electron impact mass spectrometry, with the parent molecule being ionised and fragmented using an electron beam of approximately 70eV.(39) A comparison was made with the mass spectra obtained from a library catalogue of pure nitrobenzene which showed marked similarities Fig 4.12. The disparity in the spectra was observed at the lower mass regions at 30 and 37amu which could be indicative of impurities present in the nitrobenzene sample. It is expected that a small concentration of impurities would exist but their identity cannot be gleaned from the information available. Electron impact mass studies of benzene shows a prominent parent peak for various ion energies used up to the energy used in the nitrobenzene analysis Fig 4.13. Therefore it would be expected if any benzene contaminant was present it should reveal itself in the mass spectra as a strong signal at mass 78. Because both the library spectra and our nitrobenzene sample show equal heights for the mass 77 peak it is unlikely that the benzene contaminant exists. In the library and sample spectra of nitrobenzene a small signal at mass 78 does exist in both spectra with equal heights but this could be attributed to a protonation type process, whereby a proton has attached itself to the phenyl ion produced in the break-up, resulting in a small signal at mass 78.

e)

The most convincing test to verify the existence of benzene contamination in our nitrobenzene sample was to carry out the following experiment. This involved using the laser system and recording the mass spectra of benzene at the same excitation wavelength as for the nitrobenzene spectra whilst maintaining the same laser intensity, focusing conditions etc.

This experiment has been carried out by first placing a sample of nitrobenzene in the system and recording the mass spectra. Attention was paid to the C₆ group, as the time of the peak from this group could not unambiguously verify its mass as being 77(C₆H₅) or 78(C₆H₆) .

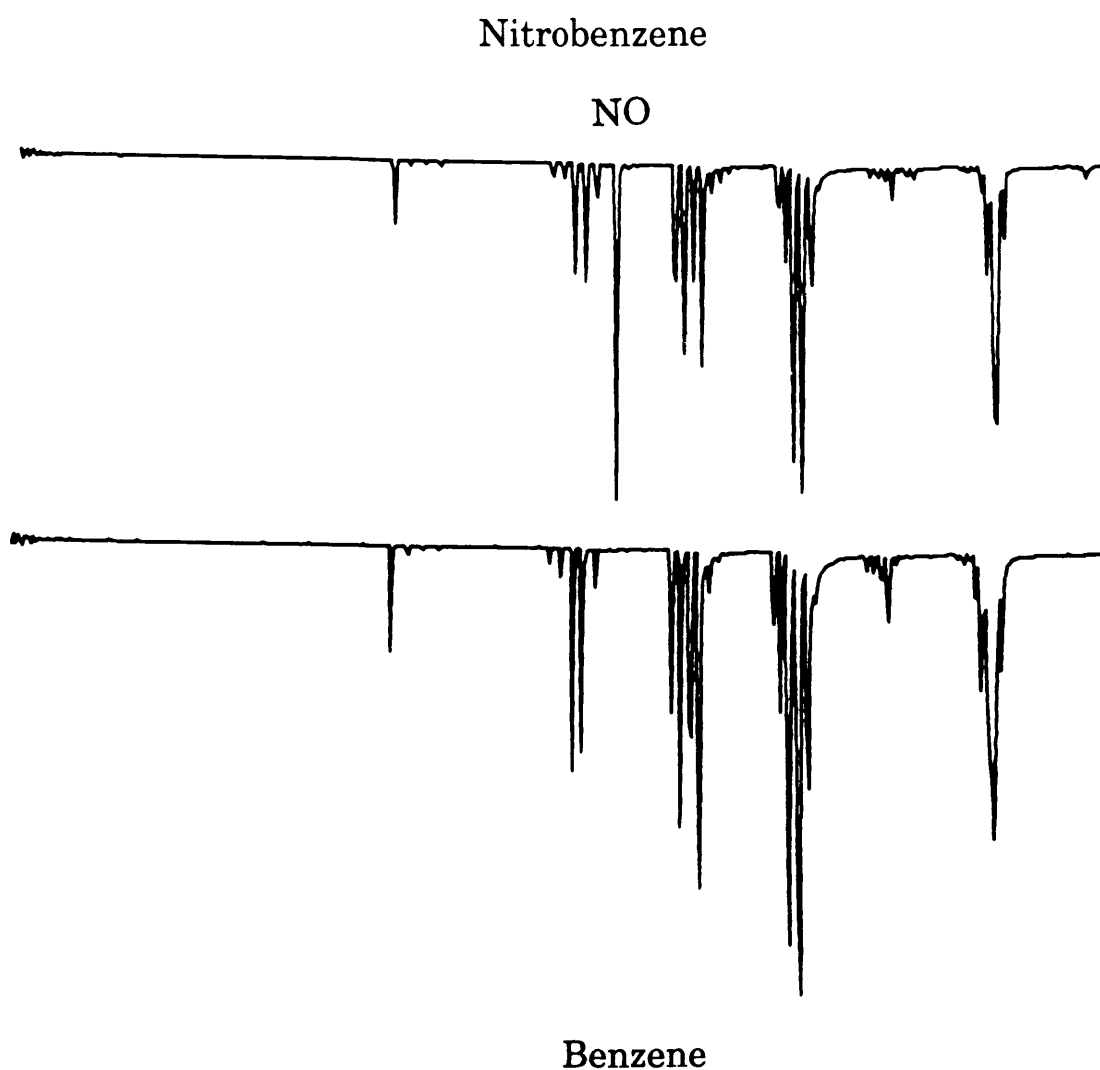


Fig 4.14 A comparison is made between nitrobenzene (top) and benzene (bottom) mass spectra. They have both been taken under identical experimental conditions i.e wavelength, power, and position. One clear distinction between the two is the presence of the strong NO ion in the nitrobenzene spectrum.

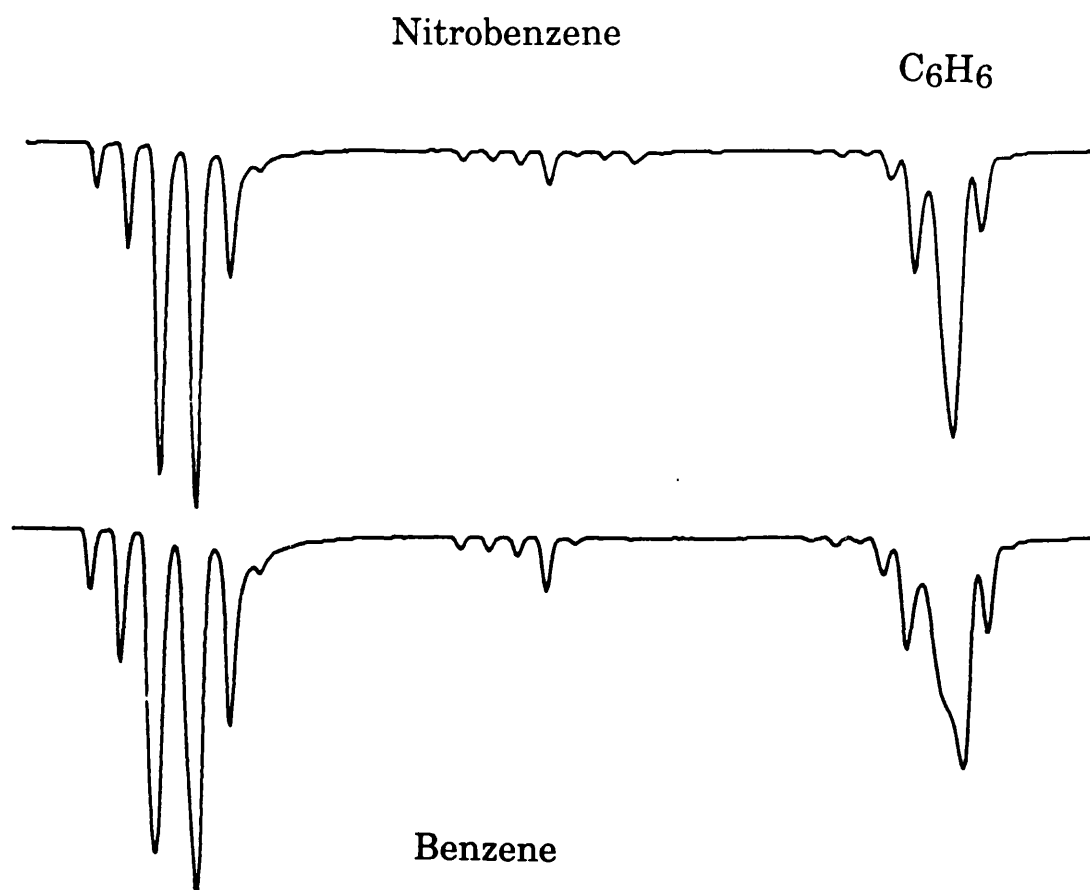


Fig 4.15 The most important region of study is the C_6 group which has been expanded for convenience. The C_6H_6 ion is observed to be present in both spectra thus justifying our assumption that the nitrobenzene sample has an unspecified benzene component.

The vacuum chamber was then baked out at high temperature to eliminate the presence of the nitrobenzene signal and thereafter a sample of benzene was introduced. Its mass spectra was also recorded under identical conditions. By careful comparison of these two mass spectra it can be shown that the peak in the C_6 group of nitrobenzene is in fact positioned at exactly the position of the mass 78(C_6H_6) peak of benzene Fig 4.14 & 4.15. This gives compelling evidence that the BDH sample of nitrobenzene has benzene contamination to an unknown level.

On heating the sample phial which contains the nitrobenzene sample, the size of the C_6H_6 ion is noted to increase in size initially and then to diminish in size and eventually disappear. This is explained because of the difference in boiling points of the two compounds i.e. nitrobenzene bpt. $210.8^{\circ}C$, benzene bpt $80.1^{\circ}C$. As the sample is heated the benzene component is evaporated off in preference to the nitrobenzene resulting in the decrease in the size of the benzene ion as the absolute numbers of benzene molecules decreases.

In order to allay any fears that the contamination may be produced by the system, samples from different manufacturers have been investigated. The sample in which contamination was present was that from BDH. A sample from nitrobenzene produced from Aldrich was also analysed which at no point in the investigation yielded any evidence of contamination, with wavelength scans giving structureless behaviour as expected from comparisons with the UV spectra.

(5) Interpretation of Results

The purity of the sample quoted by BDH is 99%. It is not clear as to what level of contamination is present. If one considers the boiling points of nitrobenzene ($210.8^{\circ}C$) and benzene ($80.1^{\circ}C$) it seems unlikely that any contamination should exist if a fractional distillation type process is deployed for purification.

The fact that no benzene UV signal was detected superimposed on the nitrobenzene signal could be explained by assuming that the nitrobenzene signal swamps all traces of the benzene signal. This could be a viable explanation if the vapour pressure of the two compounds are the same. But at room temperature, the vapour pressure of benzene is approximately two orders of magnitude larger than that of nitrobenzene. Therefore it would be expected that a greater number of benzene molecules are present in the vapour giving rise to a detectable signal.

The partial pressure of benzene gas in a gas mixture is the same as would be the actual pressure of that component alone if it occupied the same volume as does the mixture, a fact known as Dalton's law of partial pressures. That is, each of the gases of a gas mixture behaves independently of the others. The fact no observation of any benzene signal was made remains puzzling, but it could be that not enough absolute quantity of benzene exists in the cell and the partial pressure does not exceed the threshold detection level of the instrument as is the case for the gas chromatography analysis.

The null result obtained from gas chromatography could be explained by the fact that the sample was heated to 90°C before injection into the gas column. This would lead to the evaporation of most of the benzene impurity in the sample prior to its injection into the gas column. Also the absolute quantity of benzene in the sample could be below the detection threshold, and this instrument is unable to show its presence.

(6) Conclusions

The fact remains that the above techniques are unable to distinguish and show the presence of a trace impurity. On the other hand the laser system picked up the presence of the impurity with consummate ease. The importance of wavelength dependencies have been realised to supplement the mass spectral information. The wavelength dependence of the hydrocarbon ions from nitrobenzene reflect the UV absorption

Chapter 4

profile of benzene, which with hindsight gives us an instrument capable of detecting trace quantities of impurities at a level undetectable by the above described techniques. This example illustrates the enormous potential this technique has to offer as a very sensitive and selective detector.

(5) Nitrobenzene & Nitrotoluene

(1) Introduction

In the past few years, in the field of analytical and forensic science the importance of explosive identification and detection has taken on a more serious role. The problems associated with explosives detection have been exacerbated by new, more powerful and easily available supplies of plastic explosives, which have been deployed by terrorists in recent times to carry out violent actions. The present investigations for detection of these explosives has been carried out by looking at the characteristics of the vapours given off by such explosives by establishing unambiguous wavelength dependent identification of particular fragments.

The importance of studying these particular compounds in depth is realised since nitrotoluene may be placed as a taggant in all types of conventional explosives both in industrial and military use (40). Consequently any system capable of detecting nitrotoluene sensitively will have the inherent property of detecting explosives but could be fooled by non-explosive molecules which contain nitrotoluene. Nitrobenzene and nitrotoluene are among the simplest of the explosive molecules available, so were considered prudent choices for initial investigation. The primary reason for using nitrotoluene as a taggant is due to its relatively high vapour pressure compared with common types of explosives thereby enhancing detection ability.

The commonly used explosives such as 2,4,6-trinitrotoluene (2,4,6-TNT), 2,4-dinitrotoluene (2,4-DNT), pentaerythritol tetranitrate (PETN), 1,3,5-trinitro-1,3,5-triazacyclohexane (RDX) and 1,3,5,7-tetranitro-1,3,5,7-tetraazacyclooctane (HMX) have very low vapour pressures associated with them at room temperatures, therefore any detection system must have an inherently high detection sensitivity capability.

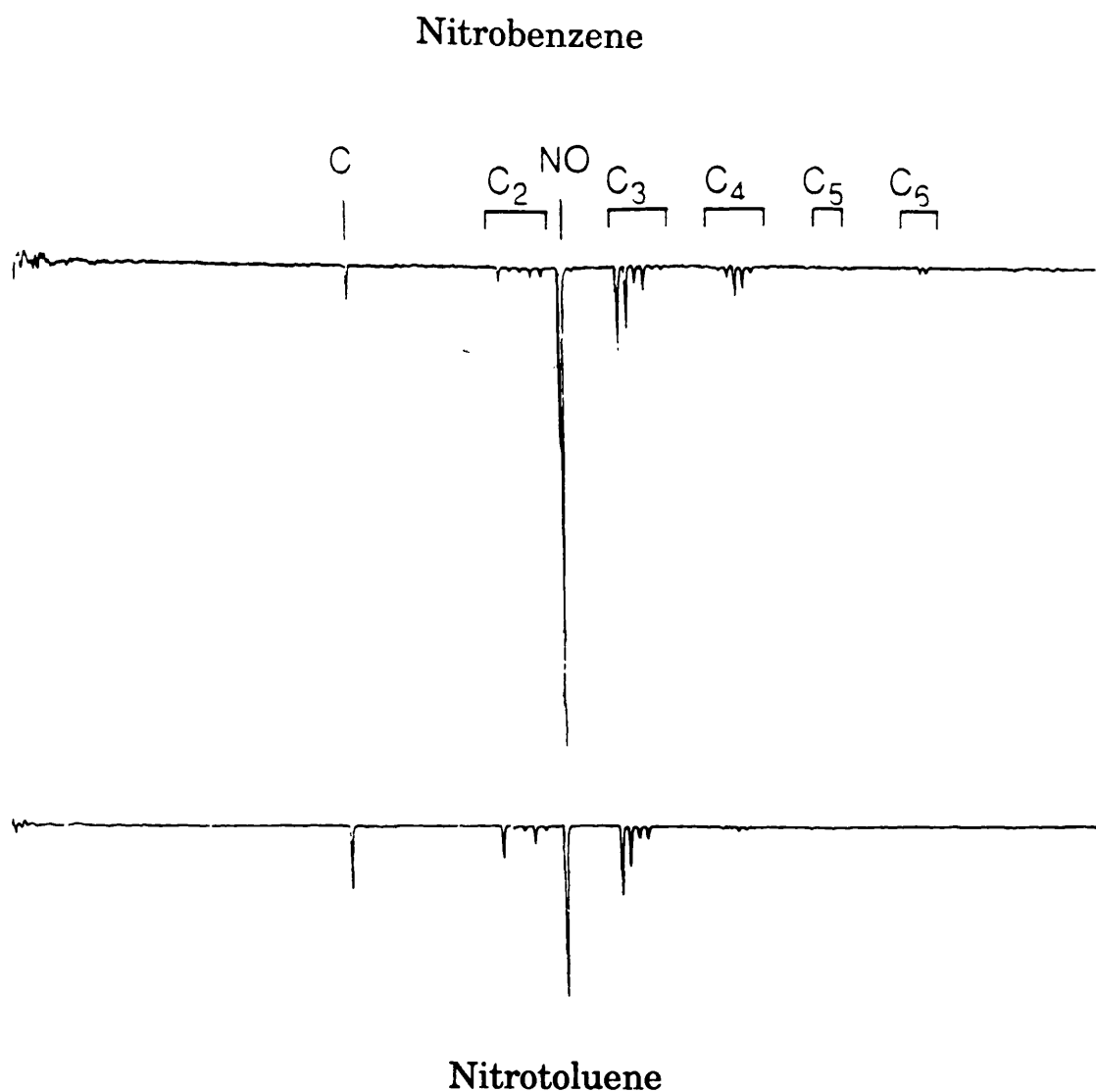


Fig 5.1 The Time Of Flight mass spectra of nitrobenzene at 247.3nm and o-nitrotoluene at 247.5 are shown, top and below respectively. Both spectrum show the presence of hydrocarbon fragments as well as a prominent NO ion peak.

Selectivity is also an important asset in order to distinguish between innocent vapours, thus reducing the number of false alarms to an acceptable level of performance. It has to be appreciated that a variety of other nitroaromatic substances exist which are in everyday use, such as perfumes & musks. These compounds must be easily discriminated while at the same time not compromising on the sensitivity ability of the technique.

(2) Results Obtained

Studies carried out have revealed that when UV laser radiation is incident on nitroaromatic molecules at wavelengths less than 260nm a range of hydrocarbon fragments (C_nH_m) are produced. (Fig 5.1)

Along with the hydrocarbons the parent ion has been observed for the first time, as well as the phenoxy (C_6H_5O), NO_2 and atomic ions such as hydrogen, carbon and oxygen.

In this chapter a detailed account of the observation of the NO ion will be given. Both nitrobenzene and o-nitrotoluene produce a very characteristic NO ion fragment which has strong wavelength dependent features. Wavelength dependent experiments on the NO ion fragment from nitrobenzene and o-nitrotoluene show strong resonance signals which correspond to rotational band structures observed in the ionisation spectra of the neutral NO molecule.(41)

In order to gain more insight into the behaviour of the NO ion, studies of NO and NO_2 neutral gas have been carried out.

In the wavelength region of study 224-238nm the NO^+ spectra from nitrobenzene and o-nitrotoluene differ significantly in their rotational intensities, these disparities will be discussed and used to distinguish between individual nitroaromatics.

(3) Nitrobenzene and O-Nitrotoluene Investigation

Nitrobenzene and o-nitrotoluene vapour pressures at room temperature are 0.477mbar and 0.315mbar respectively at 300K. Both nitrobenzene and nitrotoluene vapours have been studied in the deep UV region ($<260\text{nm}$) in vacuum conditions using the TOF mass spectrometer. Both the wavelength dependence of the fragment ion production and laser induced mass spectra have been recorded using the data acquisition system and the Lecroy oscilloscope. By deploying the REMPI technique in conjunction with mass spectrometry a very sensitive and selective procedure for the detection of nitrobenzene and o-nitrotoluene vapours at room temperatures is obtained, along with the possibility of extending this technique to other compounds. This technique has been used extensively in the past for research into the spectroscopy of organic molecules (42-46, 37)

The importance of studying nitrobenzene is that it is one of the simplest of the explosive nitroaromatics and one of the few nitro-compounds whose decompositional pathway have been the subject of ab initio molecular orbital calculations (47).

(4) Laser Induced Fragmentation In Nitroaromatics

Extensive studies of laser interaction with nitrobenzene have shown the fragments to have wavelength dependent characteristics (29,35). The most important fragment to date has been the NO ion with its very striking wavelength dependent behaviour (32,41). Both nitrobenzene and o-nitrotoluene have shown this prominent signal, the presence of which will be used in the future as a means for the identification of nitroaromatic species in general.

The hydrocarbon wavelength dependencies from nitrobenzene manufactured by BDH showed broad resonance structures but as Chapter 4 explains this has been due to an impurity of benzene within our sample. After the discovery that our BDH sample of

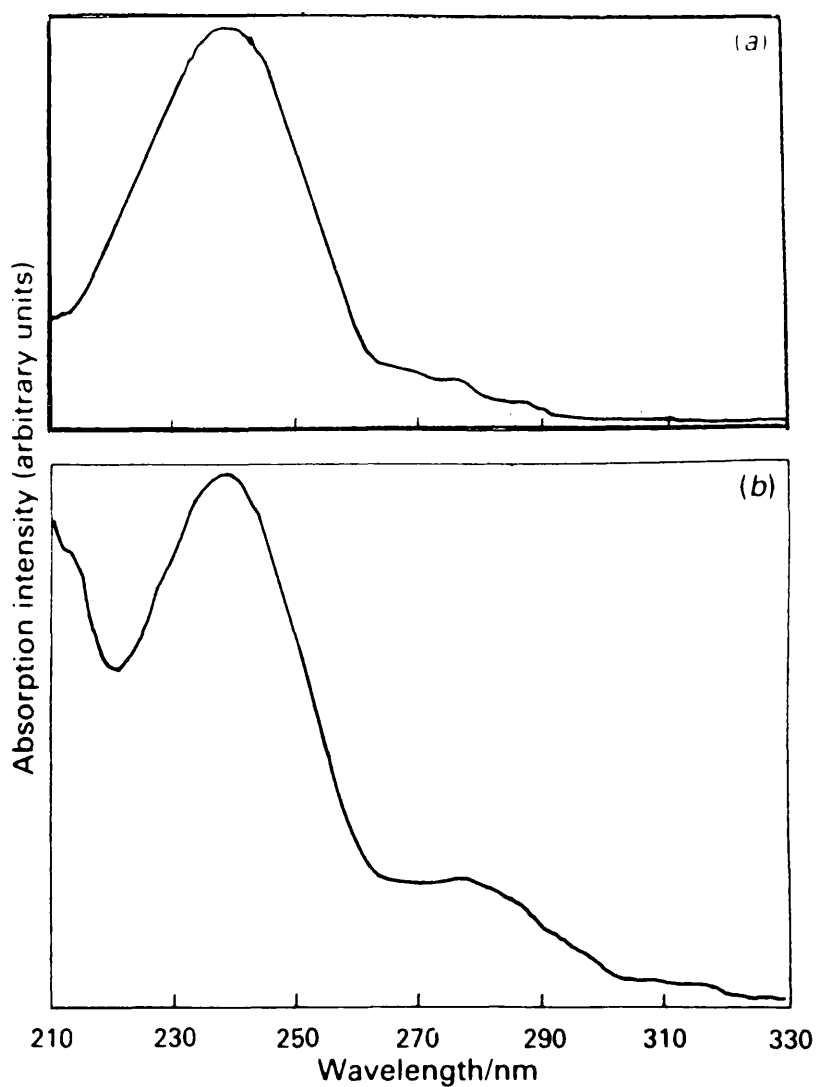


Fig 5.2 The single photon absorption spectra of a) nitrobenzene vapour and b) o-nitrotoluene vapour are shown. They have been recorded using the Beckman UV 5270 spectrophotometer with a resolution of 0.1nm.

nitrobenzene was contaminated it was possible to eliminate the benzene component by heating the sample. When observing the mass spectra on the screen, the C_6H_6 component was initially large, upon heating for approximately 5 minutes its size was seen to diminish as the benzene started to evaporate away. So it is possible to use this supply and obtain valid results, if this fractional distillation type procedure is carried out prior to obtaining data. Nevertheless, our experiments were carried out with nitrobenzene samples manufactured by Aldrich; these samples showed no benzene impurity even before heating.

Thereafter experiments have been carried out with Aldrich samples whose fragmentation patterns showed little structure which is indicative of samples with broad featureless UV absorption spectra. (Fig 5.2) O-nitrotoluene's hydrocarbon fragment ions also showed little or no structure, unfortunately it is a characteristic feature of most nitro-compounds that little structural information is available from the hydrocarbon fragments which is reflected by the broad structureless UV absorption profiles of these compounds. Without characteristic features in the wavelength dependencies of the hydrocarbon ions produced from both nitrobenzene and o-nitrotoluene it becomes more difficult to identify the individual samples and may lead to an increase in false alarms initiated by innocent vapours. As far as wavelength dependent features are concerned there exists differences in the behaviour of the NO ion, which are indicative of the original parent from which it is fragmented and thus can be used for selectivity purposes.

The fragmentation yields from nitrobenzene differed from o-nitrotoluene in that higher mass fragments (phenoxy, parent etc.) are produced from nitrobenzene which have so far not been recorded from o-nitrotoluene. A number of significant fragments have been found as well as the parent ion, which will be examined in order to give insight to the possible fragmentation processes allowed. The appearance of this ion is wavelength dependent, although due to its small size it is not easily seen

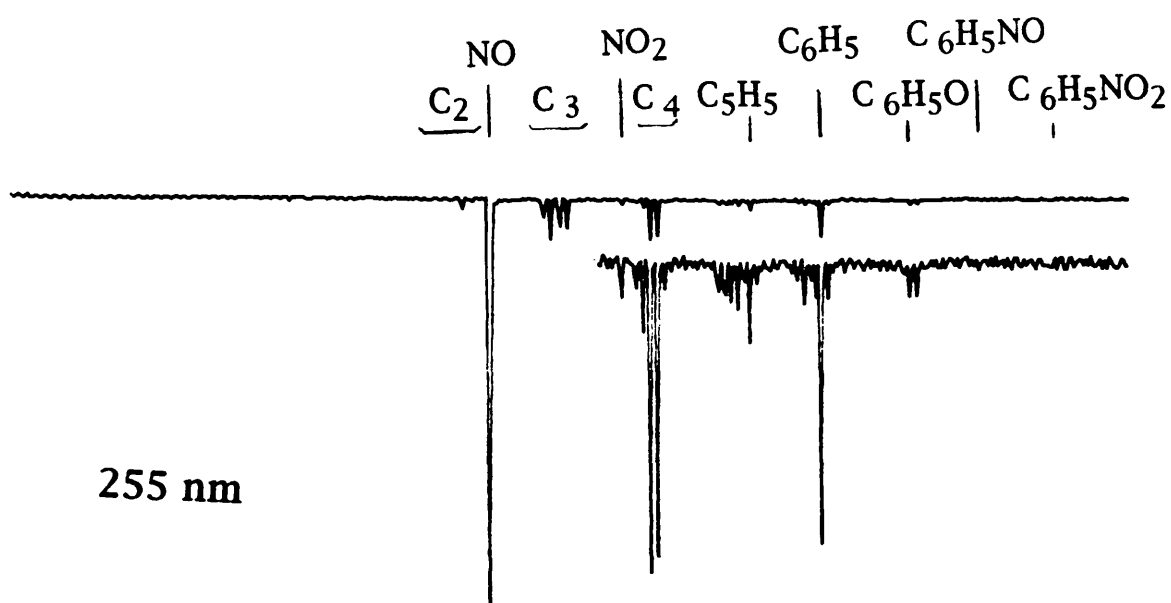


Fig 5.3 The laser induced Time Of Flight mass spectra of nitrobenzene recorded at 255nm is shown. The high mass fragment region has been magnified x8 to make clear the presence of the NO_2 ion and other small higher mass fragments. The laser pulse energy was constant for the spectra at $17\mu\text{J}$.

using the data acquisition system. Nevertheless mass spectra have shown the existence of this ion when averaging over a large number of shots (1000-2000).

Also of interest is the peak of mass 93 expected to be that of the $\text{C}_6\text{H}_5\text{O}$ ion. This ion has been found by Apel + Nogar at 248nm and was the highest mass fragment observed in previous experiments carried out using the laser ionisation method (38). The first interpretation by Nogar for this ion was that it is due to an impurity such as aniline. Also in evidence are NO_2 and atomic peaks which will be discussed in detail later. The NO_2 peak had first been observed at the higher wavelengths of 245.9nm, but at this stage its signal to noise ratio was very low, approx. 2. At the lower wavelength regions a relatively prominent NO_2 signal has been observed and recorded. It seems likely that the NO_2 production rate is also a function of wavelength, but again because of its small size it is difficult to record the wavelength dependent spectrum. The very presence of this ion verifies the possibility of alternate fragmentation paths. (Fig 5.3)

(5) Significance of NO ion

Due to the prominent nature of the NO ion signal obtained from nitrobenzene and nitrotoluene a detailed investigation has been carried out because of its strategic importance as a marker for explosive detection. In order to undertake this comprehensively a brief summary of the theory describing the transitions involved in diatomic molecules is presented.

Theory Of the NO Spectrum (49)

The bands observed in the ultra-violet regions cannot be interpreted as simple rotation or rotation-vibration spectra. In transitions between rotational and vibrational states alone a more complicated spectral output is predicted, unlike that observed in our spectra. By considering the transitions in the ultra-violet band region as due to electronic transitions within

the molecules then this interpretation does indeed account for all of the observed features of these spectra.

When considering the total energy of an electron in a molecule the Born-Oppenheimer approximation can be used to decouple the total energy into the following categories which greatly simplifies our ability to analyse the theory.

$$E = E_e + E_{vib} + E_{rot}$$

The vibrational energy is given by

$$E_{vib} = hf(v + 1/2) \{1 - \chi_e(v + 1/2)\}$$

Where χ_e the anharmonic constant and v the vibrational quantum number.

In general the rotational energy is given by:

$$E_{rot} = BJ(J + 1)$$

In this equation the Born-Oppenheimer approximation is not quite valid and the rotational constant is a function of the vibration

$$B_v = B_e - \alpha_e(v + 1/2)$$

J is the rotational quantum number, B_e and α_e are constants of the molecule.

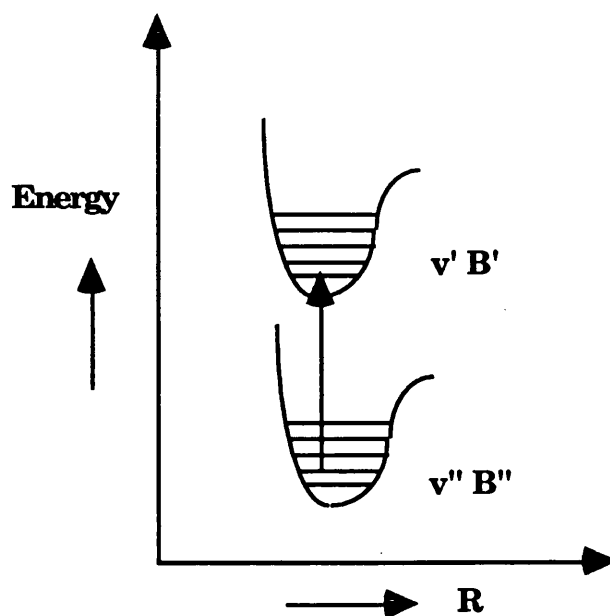


Fig 5.4 Schematic diagram showing the notation involved in the analyses.

When considering the selection rules $\Delta J = 0, \pm 1$ for transitions between two electronic states this leads to the formation of P, Q, R branches. By considering their transition energies in terms of frequency, the following equations are valid.

The three branches are defined as follows;

$\Delta J = 0$ denotes the Q branch,

$\Delta J = 1$ the R branch and

$\Delta J = -1$ the P branch.

$$\Delta E_{TOTAL} = \Delta(E_{elec} + E_{vib}) + \Delta\{BJ(J+1)\}$$

$$\bar{\nu}_{spect} = \nu_{(v', v'')} + B'J'(J'+1) - B''J''(J''+1)$$

For the Q-branch where $\Delta J = 0$ i.e. $J'' = J'$

$$\bar{\nu}_{spect} = \nu_{(v', v'')} + (B' - B'')J' + (B' - B'')J'^2 \quad (1)$$

The values of the quantum number varies as $J'' = 1, 2, 3, \dots$

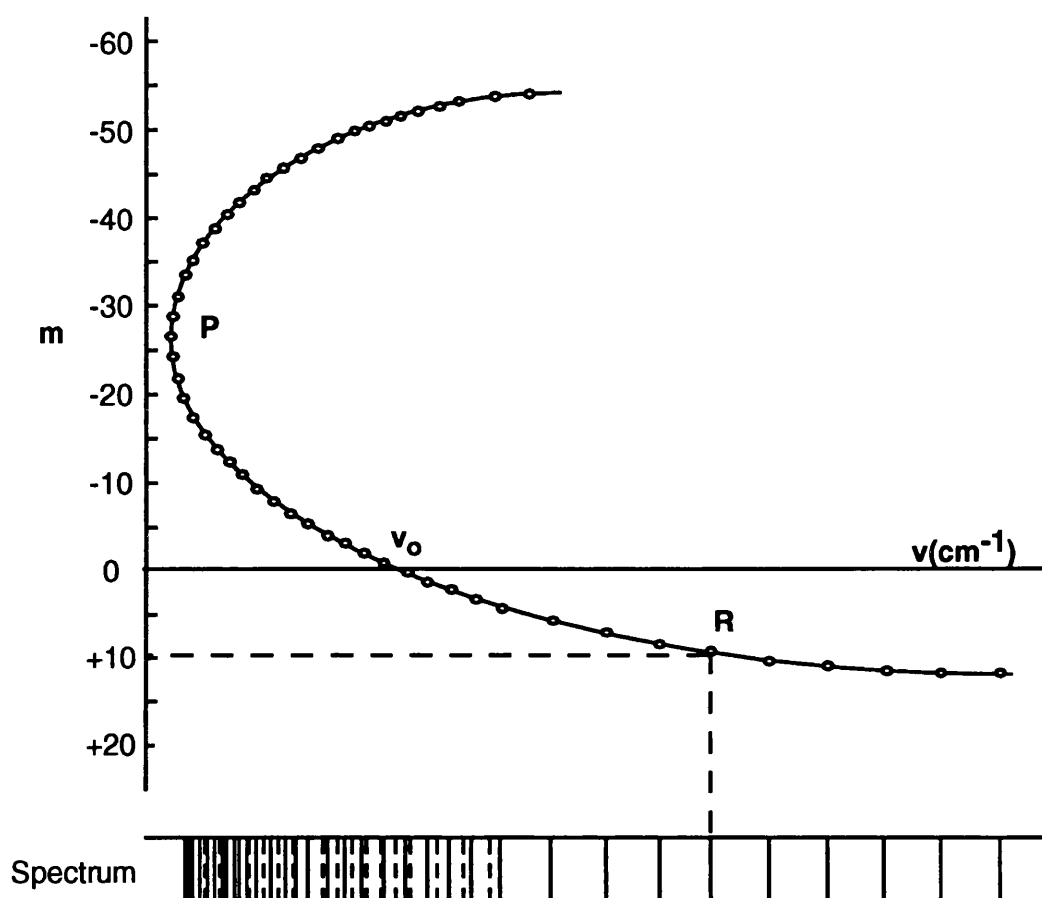


Fig 5.5 The Schematic spectrum below is drawn to scale as the Fortrat parabola above. The relation between the curve and the spectrum is indicated by the broken line for the point $m=+10$.

P-branch: $\Delta J = -1$, i.e. $J'' = J' + 1$

$$\bar{\nu}_{spect} = \nu_{(\nu', \nu'')} + (B' + B'')(J' + 1) + (B' - B'')(J' + 1)^2 \quad (2)$$

here the quantum number varies as $J'' = 0, 1, 2, \dots$

R-branch: $\Delta J = +1$, $J'' = J' - 1$

$$\bar{\nu}_{spect} = \nu_{(\nu', \nu'')} + (B' + B'')(J'' + 1) + (B' - B'')(J'' + 1)^2 \quad (3)$$

quantum number again varies as $J'' = 0, 1, 2, \dots$

The above two equations can be represented in the form

$$\bar{\nu}_{spect} = \nu_{(\nu', \nu'')} + (B' + B'')m + (B' - B'')m^2 \quad (4)$$

The series of lines corresponding to the positive values of m is called the R branch; that corresponding to the negative values is called the P branch.

The equation above(4) is that of a parabola. It is represented graphically, with ν as the abscissa and m as the ordinate Fig 5.5. This representation was first used by Fortrat, and the parabola is accordingly called a Fortrat parabola. In the figure, the intersection of the horizontal lines, having $m=0, 1, 2, \dots$, with the parabola are indicated by small circles. The abscissa of these intersections give the wave numbers of the lines. It is seen from this method of representation how the head of the band is formed: The nearer one comes to the vertex of the parabola, the more the lines crowd together. The vertex itself corresponds to the band head. As the band head is approached the close density of lines would give the impression that a continuous spectrum arises, but in actual fact it is composed of a finite number of very close transitions.

**Graph of Experimental Data compared with
Computer generated Data.**

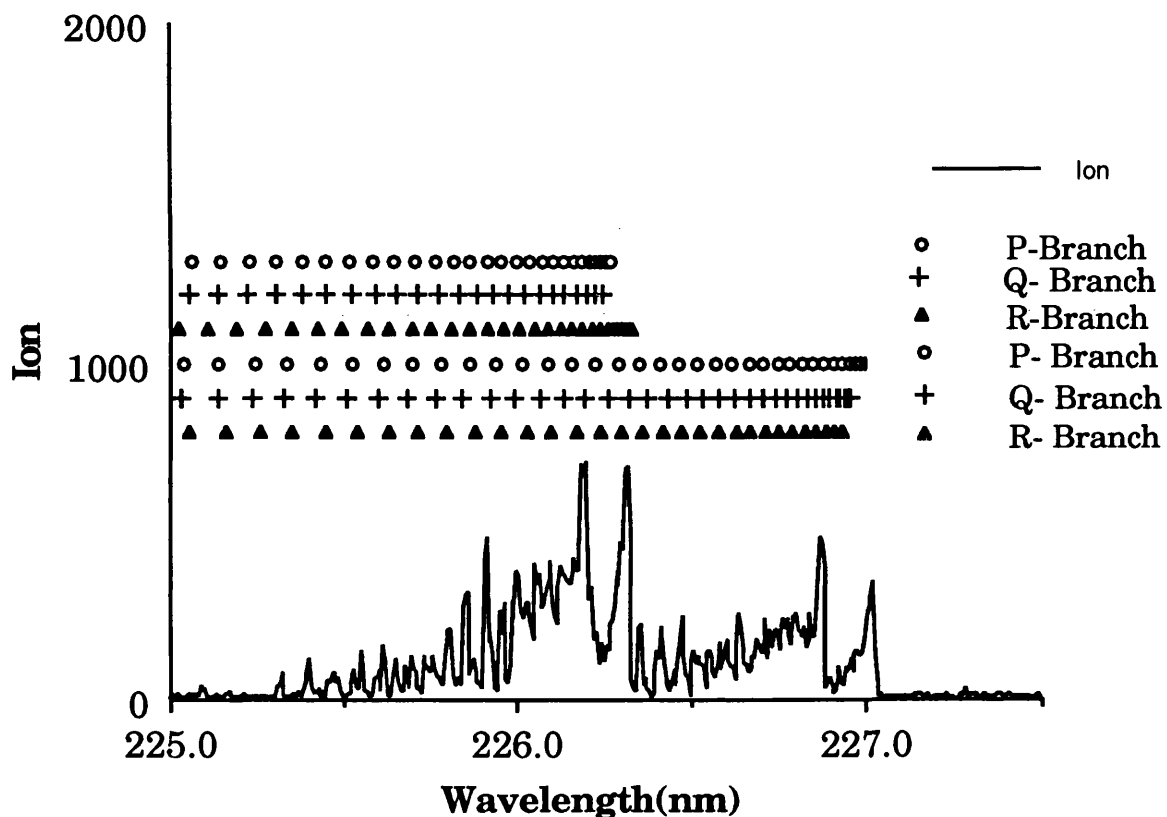


Fig 5.6) The P, Q and R branches from both the spin orbit split ground states to the first excited state have been calculated for the NO molecule. These are represented by the geometrical symbols and bear close resemblances to the positioning of the band heads in the experimental data.

A third branch appears known as the Q-branch or zero branch which is governed by the selection rule $\Delta J = 0$.

If the Fortrat parabola vertex is approached from the higher frequency side as in the example, then this is termed shading to the red and is determined by the fact that the rotational constant for the ground state is greater than that of the upper excited state i.e. $B' < B''$. This can be physically interpreted as the spacing of the rotational lines in the lower state being more widely spaced out than the upper state.

(6) Comparison Using Computational Analysis

A computer program was set-up to evaluate the wavelengths of the transitions possible in the NO diatomic molecule. The number of possibilities has been restricted by using the boundary conditions that $\Delta J = 0 \pm 1$. This subsequently means that P, Q and R branches have been evaluated only. The theoretical values were calculated by first of all evaluating the energy levels of the individual vibrational and rotational states in both the ground and excited state manifolds. Thereafter, the difference in energy between the ground and excited state was evaluated according to the selection rules with the energy of the transition expressed as a wavelength. Because of the splitting in the ground state due to the spin orbit interaction, two sets of P, Q and R values are calculated, one for each split state. The electronic energy between the ground and excited states was known to be $\sim 44,000\text{cm}^{-1}$, with the vibrational and rotational energies calculated using equation 4.

The calculated points were compared with Los Alamos Tables (50) and the experimental data with a reasonable comparison obtained. The program used a maximum rotational quantum number of 50 for both the ground and excited states. The P, Q and R points have been plotted separately for clarity but it can be seen that the band heads match closely with the experimental values. (Fig 5.6)

(7) Interpretation Of Data

Fig 5.6, NO ion spectrum shows a series of narrow rotational resonances with the most striking feature of the NO ion wavelength dependence being the two band heads. This feature of the spectra arise because of transitions originating from both members of the ground electronic state, $A^2\Sigma \leftarrow X^2\Pi_{\frac{1}{2},\frac{3}{2}}$, which is split owing to the spin-orbit interaction. The spin-orbit effect is due to the interaction between the electrons spin magnetic dipole moment interacting with the internal magnetic field of the molecule. Since the internal magnetic field is related to the electron's orbital angular momentum, this is called the spin-orbit effect.

Also to note is that the rotational structure lies to the blue side of the band head position. From the theory this would indicate that the rotational levels of the $v=0$ upper electronic state are more widely spaced out than those of the $v=0$ level of the lower ground state.

The various peaks have been associated as arising from the numerous excited rovibrational states in the electronic ground state manifold.

The band head features observed in the wavelength dependence have been identified as originating from the $A^2\Sigma \leftarrow X^2\Pi_{\frac{1}{2},\frac{3}{2}}$ electronic transitions in the neutral nitric oxide (NO) molecule. It has been identified that the NO^+ ion signal in the range 225-250nm arises from resonant two-photon ionisation, one photon to excite and one to ionise the neutral nitrogen monoxide molecule.

(8) Determining The Origins Of The NO Signal

The wavelength dependence of the NO ion arising from NO, NO_2 , nitrobenzene and o-nitrotoluene gas has been studied in the region from 224-237nm. (Fig 5.7) Neutral NO and NO_2 gas has been studied in order to give a better understanding of the

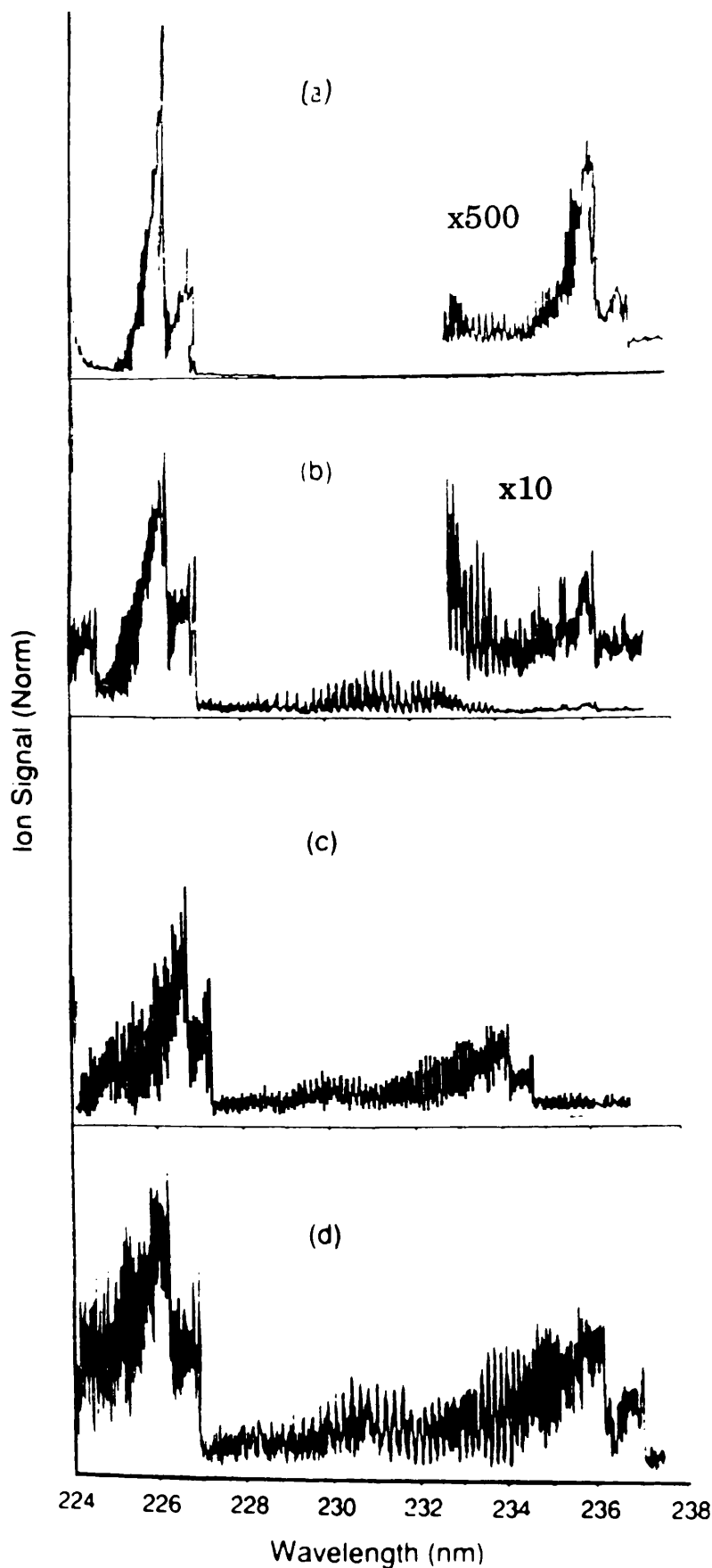


Fig 5.7 The NO ion spectra from (a) NO gas, (b) NO₂ gas, (c) nitrobenzene and (d) o-nitrotoluene is shown for the wavelength range 224-238nm. Comparisons can be easily made between the spectra highlighting the main similarities and differences.

possible route taken in forming the NO ion. All of the spectra show the double band head features described earlier. In the spectrum from the NO gas, the ratio of the two band intensities at 226nm and 235nm are in good agreement with that predicted by the UV absorption spectrum of neutral NO gas, thereby indicating that the ionising photon cross-section does not vary significantly with wavelength (Fig 5.8).

The band heads associated with the 226nm and 235nm transitions are via the A(0)--X(0) and A(0)--X(1) bands respectively. Observation of the NO ion wavelength dependence from NO₂ and nitrobenzene show similarities. Comparing the ratio of the two band heads at 226nm and 235nm from NO₂ and nitrobenzene it is found they are at a ratio of 30:1 and 3:1 respectively. The first interpretation of these results would indicate that a non-thermal type process predominates which results in a higher distribution of population in the upper vibrational levels. A thermal distribution of the populations in these vibrational states would follow a Boltzmann distribution, which would predict a ratio of 1000:1. The occupation of these higher vibrational levels can be accounted for by the excess energy gained from the photodissociation process.

Careful inspection of the spectra from NO₂ and nitrobenzene do reveal differences in the rotational intensities of the NO ion. The biggest disparity arises at ~232nm where the NO₂ sample shows rotational lines whereas the nitrobenzene has none.

(9) Sensitivity Measurements

Due to the very distinctive structure and large intensity of the NO ion a detailed investigation was carried out in order to find the optimum region in which to detect it.

For this reason a UV absorption spectrum of high purity NO gas was investigated to determine the position of the strongest

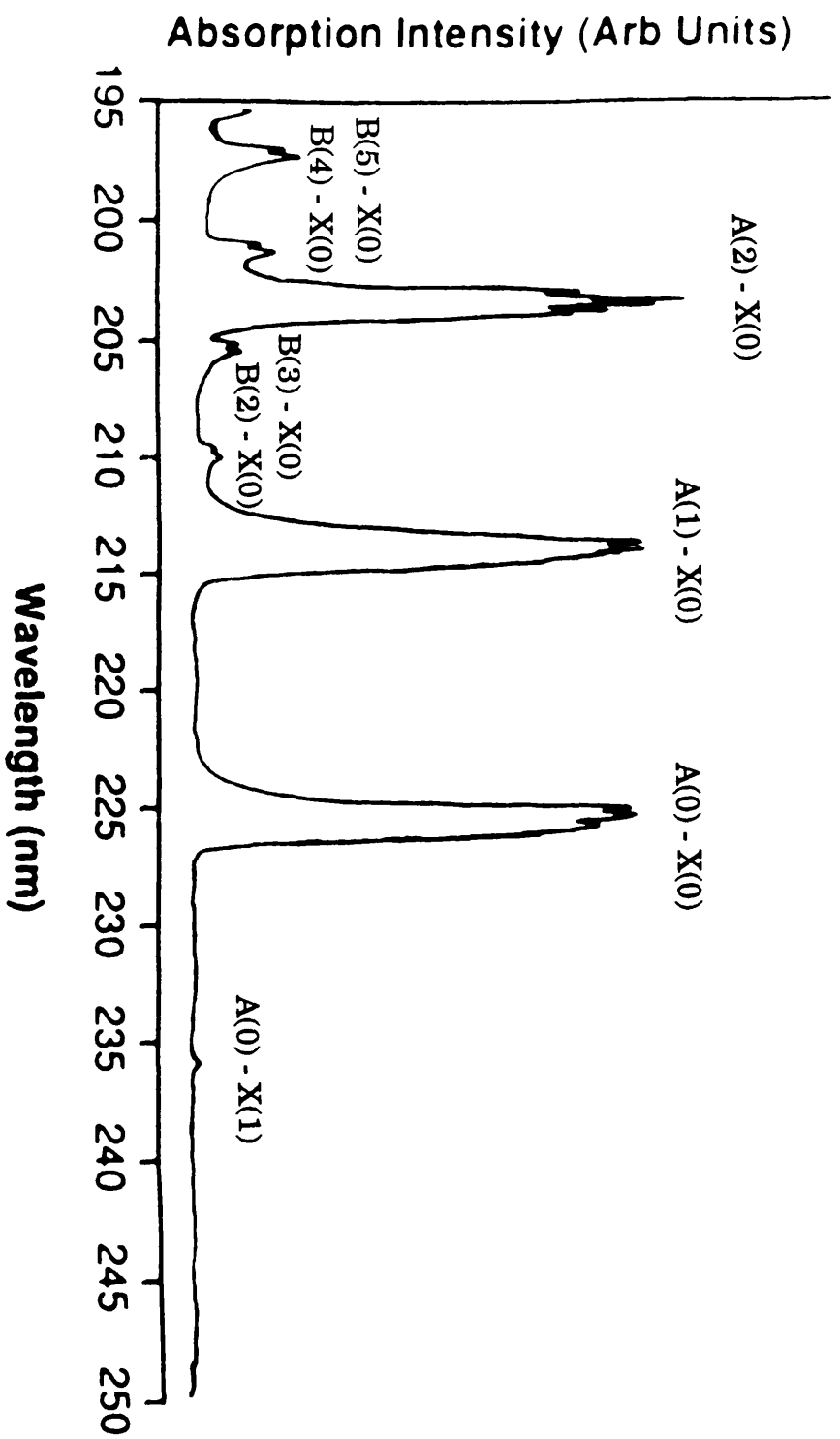


Fig 5.8 The single photon absorption spectrum of high purity NO gas between 195 and 250nm is recorded with a Perkin-Elmer Lambda 9 spectrophotometer, with a resolution of 0.5nm. Also indicated are the various absorption bands associated with each of the peaks.

absorption bands of the NO molecule thereby making it possible to be more selective in the wavelength region of study Fig 5.8.

The spectrum was recorded with the NO gas in the cell at atmospheric pressure, using a Perkin-Elmer Lambda Spectrophotometer. Operating at atmospheric pressures however leads to pressure broadening of the rovibrational absorption lines, which subsequently degrades the resolution. The resolution of the system is such that it is difficult to resolve the spin orbit splitting in the absorption band from the $A^2\Sigma \leftarrow X^2\Pi_{\frac{1}{2},\frac{3}{2}}$ transitions at 226.2 and 226.8nm. Shown on the UV spectrum are peaks which correspond to the 0-1 vibrational resonance at 236nm which compared with the 0-0 transition at 226nm is much weaker. Other intense absorption bands have been identified at 214nm and 204nm, which arise from $A^2\Sigma(v=1 \text{ or } 2) \leftarrow X^2\Pi_{\frac{1}{2},\frac{3}{2}}(v=0)$ transitions. (v is the vibrational level of the particular electronic state under consideration). Taking into account the large intensity of these absorption peaks it would suggest a dramatic increase in the photoionisation yield of the NO ion at these wavelengths. The transition originating from the $v=0$ level of the ground state is more intense by a factor of ~ 1000 than the absorption from the $v=1$ level. This ratio is expected with a Boltzmann population distribution verifying that the population of the states are governed by a thermal distribution type process.

As far as detection sensitivity is concerned the optimum region in which to work is deeper in the UV where strong absorption bands are in evidence. This strategy applies not only to NO gas but to all samples which may release or form NO molecules at some stage during laser fragmentation. The NO ion wavelength dependence from nitrobenzene is shown over the range 224-248nm Fig 5.9. This scan is a composite of 2 scans as one dye does not have the ability to extend over the requisite range. The graph has been redrawn with the y-axis drawn on a logarithmic scale to disclose more clearly the band head features at the higher wavelengths Fig 5.10. But the most important aspect of

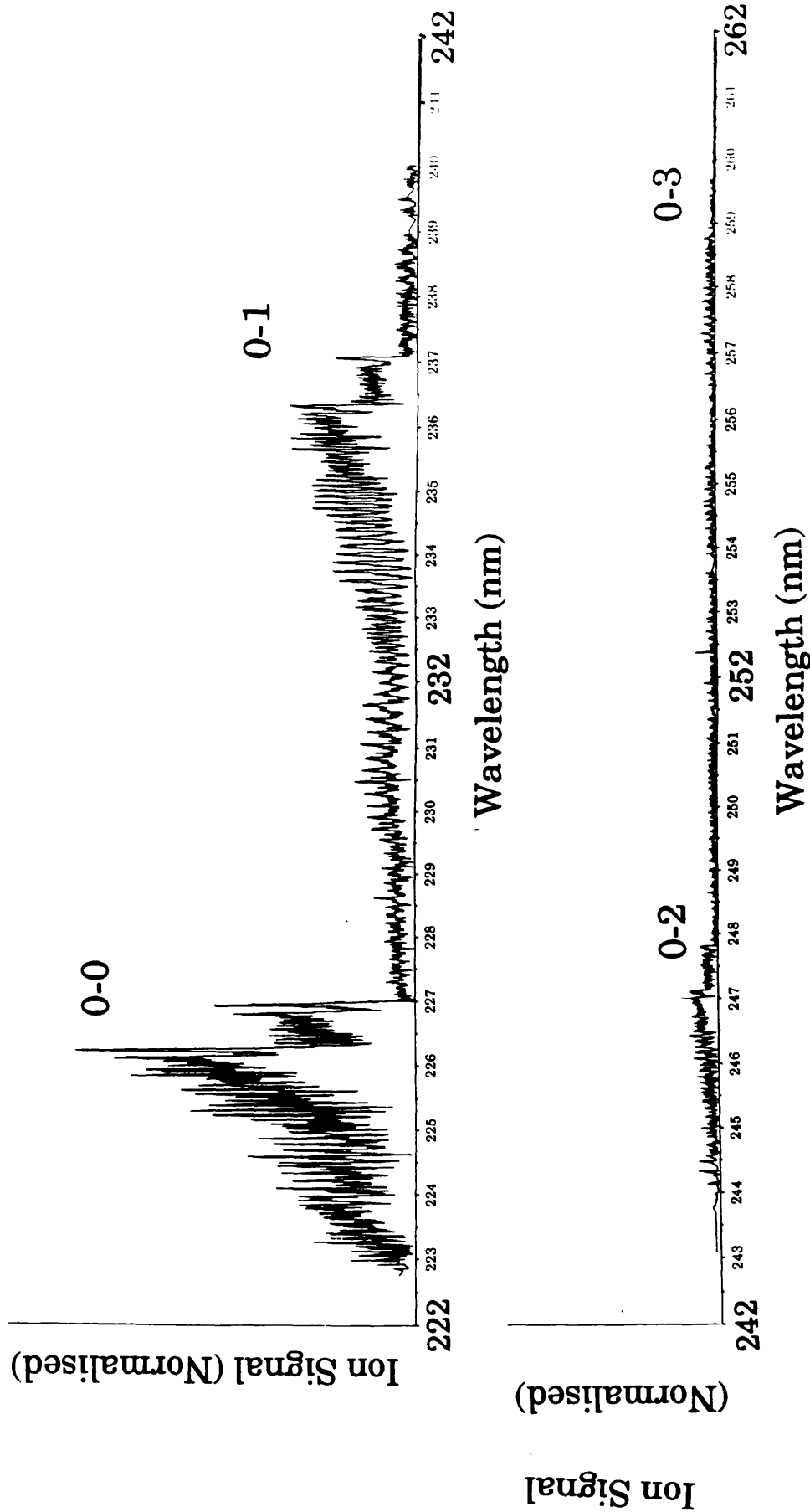


Fig 5.9 The relative intensities of the band heads from the NO ion produced by nitrobenzene in the range 222-262nm is shown.

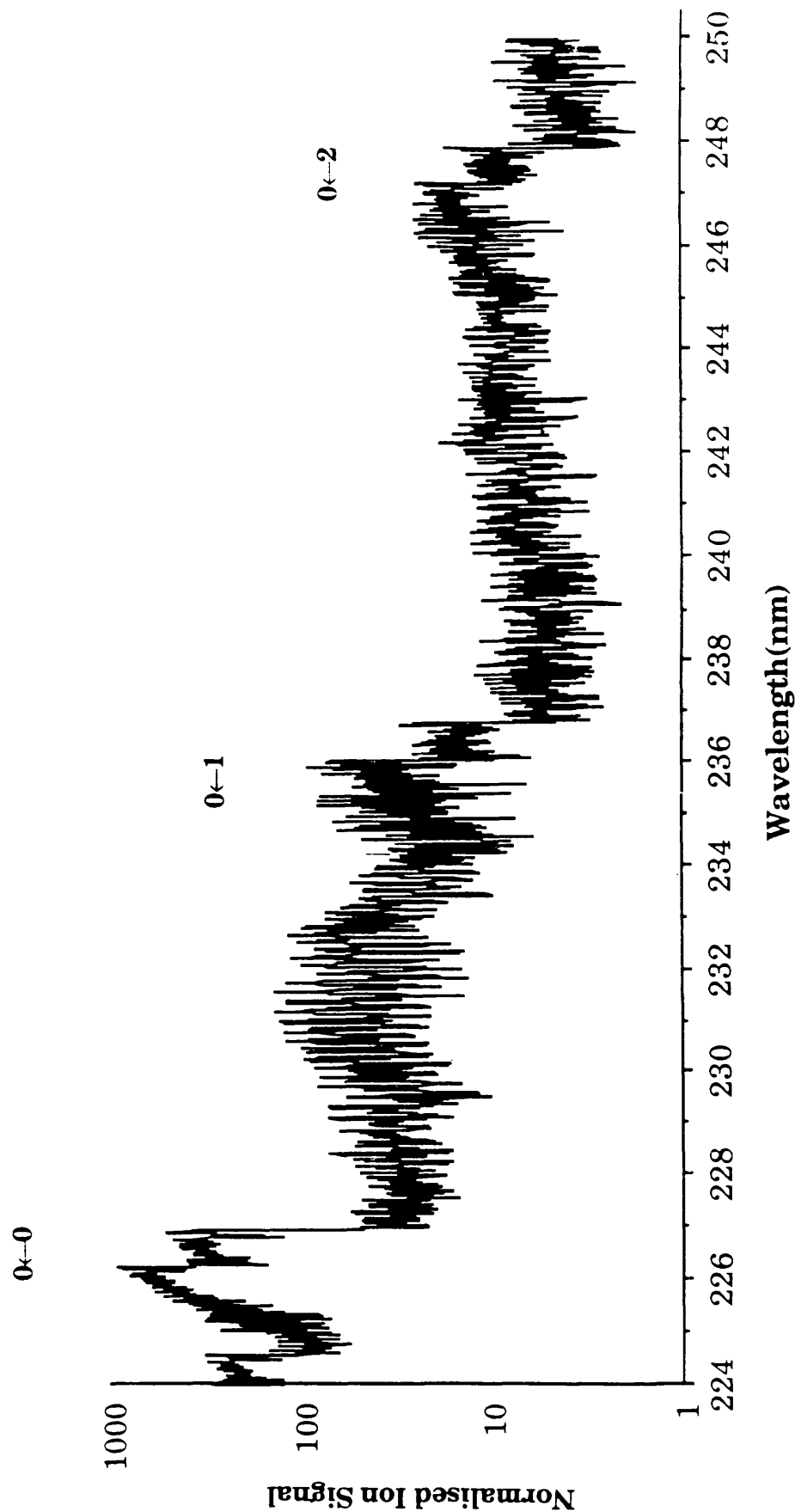


Fig 5.10 The wavelength dependence of the NO ion from nitrobenzene is recorded, showing the relative signal strengths of the $0 \leftarrow 0$, $0 \leftarrow 1$, and $0 \leftarrow 2$ transitions. The ion yield is plotted on a logarithmic scale with the ionisation intensity normalised linearly to laser fluences in order for a comparison of band intensities to be made.

these spectra are that they clearly demonstrate that the optimum region for detection sensitivity lies at 226nm.

At this stage sensitivity measurements were carried out by first obtaining the maximum signal at which the NO ion signal could be detected. The laser was scanned over the 0-0 vibrational resonance at 226nm and scanning stopped when the maximum signal intensity is reached. The dye laser was fixed at this wavelength and sensitivity measurements of nitrobenzene vapour in a TOF system using the following technique were carried out.

At first the system was baked out for a couple of days by wrapping the system with a heating tape which is set to 200°C in order to eliminate any background contamination. The turbo molecular pump takes the system down to a base pressure of 2×10^{-8} mbar (2×10^{-6} Pa).

The dye laser was operated at 226.3nm with no ionisation signal being observed. Thereafter a small controlled amount of nitrobenzene vapour was admitted into the chamber via the stainless steel tube controlled by the leak valve. A sufficient amount of nitrobenzene was admitted until a signal/noise ratio of 2:1 could be established. After which the needle valve was closed off and a pressure reading of 6×10^{-8} mbar (6×10^{-6} Pa) was measured. The digital oscilloscope was used to record the signal by averaging over 750 laser shots. Prior knowledge of the dimensions of the ionising beam allowed a value for the ionising volume to be evaluated to 6.3×10^{-5} cm³.

From the kinetic theory of gases the number of molecules per ml at normal temperature and pressure is 2.69×10^{19} . By multiplying this number by the volume and pressure at the interaction region an estimate of the number of ions created in the interaction region is evaluated to be approx. 100,000. By recording a signal with the above mentioned

statistics the ability of the apparatus to reach sub-attomole ($< 10^{-18}$ mol) detection limits has been demonstrated.

Therefore a highly sensitive laser based approach for the detection of simple nitroaromatic molecules which have attached a single NO₂ group per molecule has been shown. Taking into account the structure of the four most commonly used explosives, i.e. TNT, DNT, RDX & HMX it is clear that these compounds have attached a number of NO₂ groups per molecule. By taking advantage of this fact by looking for an increase in the intensity of the NO ion signal generated, this would prove of great importance as far as sensitive detection of the more important di- and tri- nitroaromatic compounds are concerned.

(10) Conclusions

A number of important fragments have been found in the dissociation of nitrobenzene and o-nitrotoluene. The most significant observation to date has been of the NO ion with large enhancements in signal intensity at the 226nm region. These observations show the importance of the NO⁺ ion in both detection and identification of nitroaromatics. Of strategic importance is the differences in the NO⁺ rotational spectra for the two nitroaromatics studied, from the point of view of selectivity. Most common types of explosive molecules have a number of NO₂ groups associated with them, therefore using the fact that there is very efficient ionisation of NO in this wavelength region, a potentially very sensitive as well as selective method of detection is likely using this approach. The selectivity aspect depends on factors which have caused the distinction between nitrobenzene and nitrotoluene. If the differences in the structure of the parent molecules are responsible for the disparity in the NO ion signals, then an important approach to detecting and identifying these materials has been achieved.

6. Analysis Of Oxygen & Hydrogen Ions & Photodissociation Pathways.

(1) Spectroscopy of Oxygen & Hydrogen

In the course of multiphoton studies on molecular species it has been observed that in addition to the ionised molecular fragments, a number of neutral atomic species are generated.

These are identified by tuning the laser wavelength to resonant transitions of the various atomic species. This approach can lead to the determination of whether atoms are produced in their ground or excited states. The realisation that neutral atomic species are liberated in photodissociation of molecules is not a new phenomenon and has been reported extensively in the past (30,51-55). Most previous studies have dealt with the production of atomic species from small parent molecules such as CO₂, O₂, NO₂ etc. With studies on the photodissociation dynamics of carbonyl and organometallic compounds, the production of transition metal atoms has been observed to occur readily.

In the work presented here, the laser induced photodissociation of nitrobenzene has been investigated in particular in the wavelength region 225-247nm. Carbon atomic transitions in the region 245-260nm from nitrobenzene and nitrotoluene have also been reported. The transitions have been identified as originating from both ground and excited states (30).

The availability of laser wavelengths in the region 225-245nm have allowed the production of neutral atomic hydrogen and atomic oxygen to be observed via resonant ionisation processes.

These signals were recorded both in the form of mass spectra at fixed wavelengths and in wavelength dependent spectra where the atomic ionisation yield is monitored as the wavelength is scanned through the resonances. In both cases the signals have

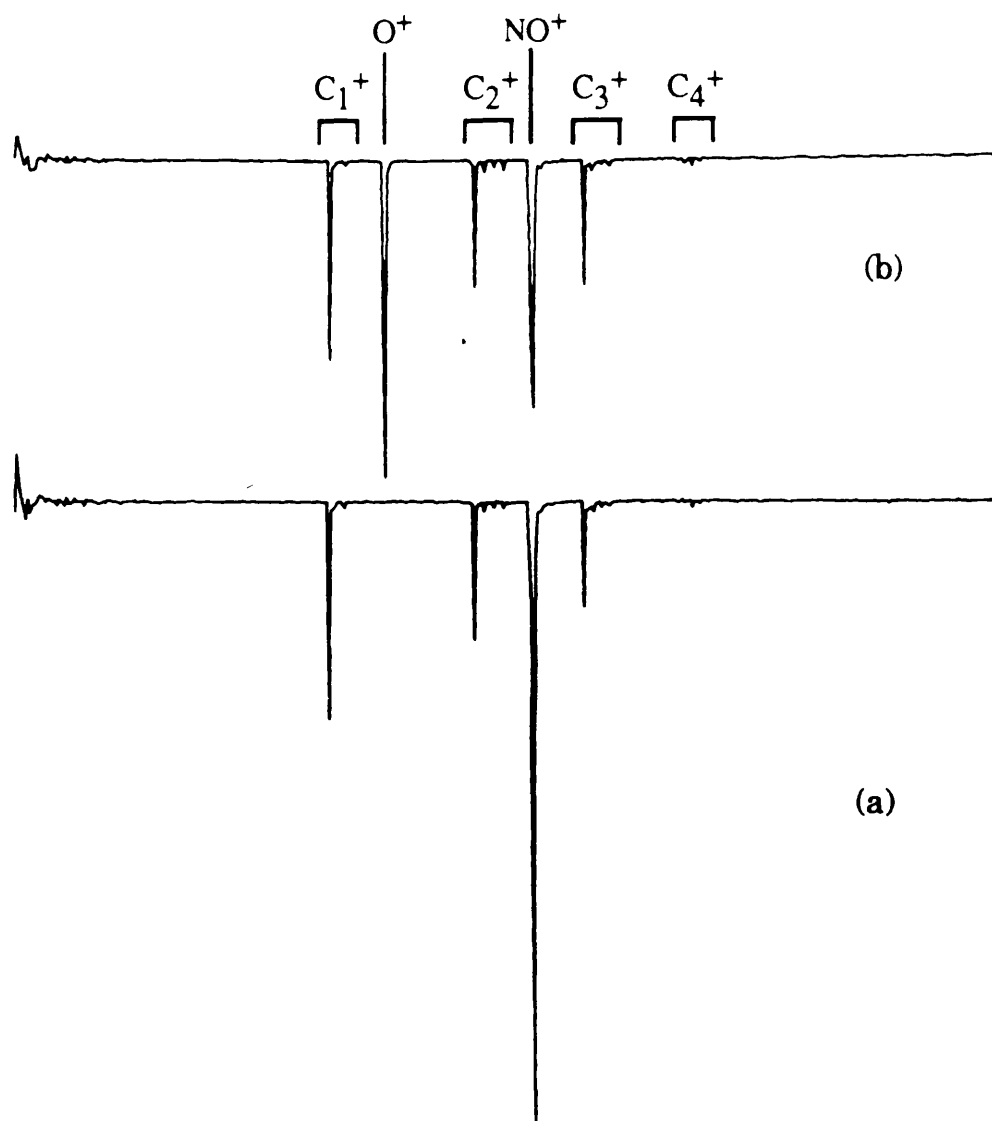


Fig 6.1 The Time-of-flight mass spectra of nitrobenzene have been recorded at a laser fluence of 4.6mJmm^{-2} .

a) This corresponds to a resonance of the NO^+ ion at a wavelength of 225.68nm .

b) The two photon resonance in atomic oxygen is observed at a wavelength of 225.65nm .

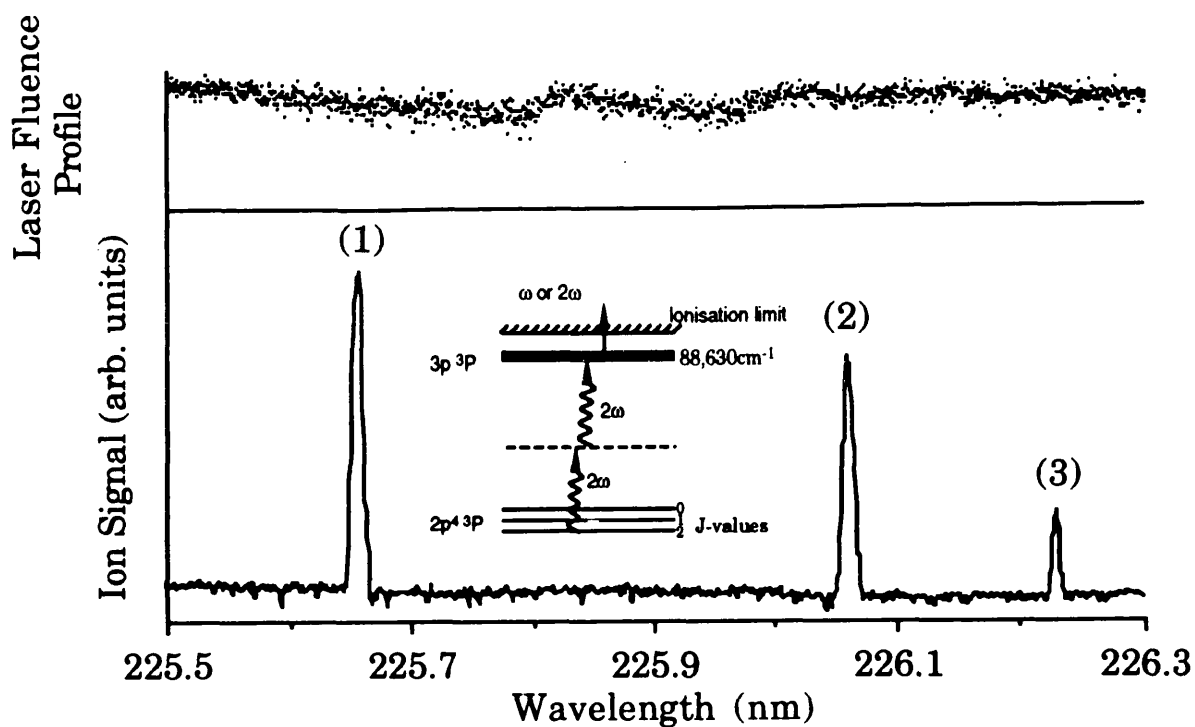


Fig 6.2 The ionisation spectrum of the oxygen ion signal from nitrobenzene sample is shown as well as the laser fluence profile during the run, with the maximum fluence being 5mJmm^{-2} . The resonant ionisation scheme for oxygen ion production is shown in the inset.

been recorded using a time of flight mass spectrometer with samples introduced into the system in the vapour phase and subsequently ionised using the doubled dye laser beam. Both the oxygen and hydrogen ion signals show large enhancements when the resonance condition is satisfied. This indicates that a large number of neutral hydrogen and oxygen atoms are produced in the fragmentation of the parent nitroaromatic compounds so far studied.

(2) Oxygen Data

In the course of studies on the NO^+ ion intensity in the 226nm region, the presence of sharp resonance enhancements at the $m/z = 16$ position in the spectrum was found. These mass spectra clearly show the presence of the on-resonance oxygen ion signal with slight de-tuning of the resonance condition leading to the complete absence of the ion Fig 6.1. This behaviour is expected of atomic transitions as they are in general of narrow bandwidth. In the mass spectra recorded the most intense oxygen signal at $m/z = 16$ is observed at 225.65nm. The mass spectra have hydrocarbon fragments which show little or no variation as would be expected for non-resonant ionisation for small wavelength changes. The NO^+ ion peak is present in both spectra at differing intensities. This can be readily explained by the very strong wavelength dependence of the neutral NO absorption spectrum.

After recording the mass spectra the timing gate was positioned on the $m/z = 16$ ion peak and a wavelength scan of the region between 225.5nm to 226.3nm was carried out. During the scan a total of three atomic peaks were recorded which differ in intensity, with the strongest peak at 225.65nm and weakest at 226.23nm Fig 6.2. The three peaks observed have been identified as originating from the ground state excitation of the oxygen atoms via the resonant excitation step $2p^4\ ^3P \rightarrow 2p^33p\ ^3P$. The ionisation of the atom corresponds to a 2+1 scheme with two UV

Peak Number	2ω Wavelength (nm)	Initial State	Final State	Initial J value	Final J value	Initial State Energy (cm^{-1})	Final State Energy (cm^{-1})	Excitation Photons	Ionisation Photon
	225.655	$2p^4\ ^3P$	$2p^33p\ ^3P$	2	2	0	88,630.84	$2\omega + 2\omega$	ω
1	225.656	2	1	0	88,630.30	$2\omega + 2\omega$	ω
	225.655	2	0	0	88,631.0	$2\omega + 2\omega$	ω
	226.059	1	2	158.5	88,630.84	$2\omega + 2\omega$	ω
2	226.061	1	1	158.5	88,630.30	$2\omega + 2\omega$	ω
	226.059	1	0	158.5	88,631.0	$2\omega + 2\omega$	ω
	226.233	0	2	226.5	88,630.84	$2\omega + 2\omega$	ω
3	226.235	0	1	226.5	88,630.30	$2\omega + 2\omega$	ω
	226.233	0	0	226.5	88,631.0	$2\omega + 2\omega$	ω

Fig 6.3 The assignments for the three peaks observed in Fig 6.2 & Fig 6.4 are given for the oxygen atom in the table.

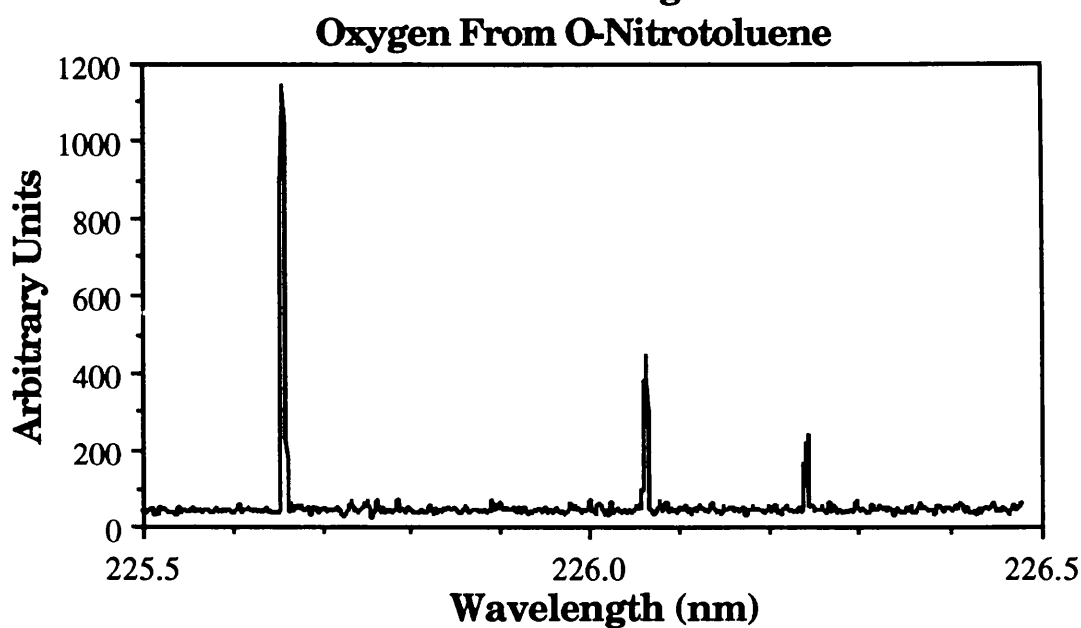
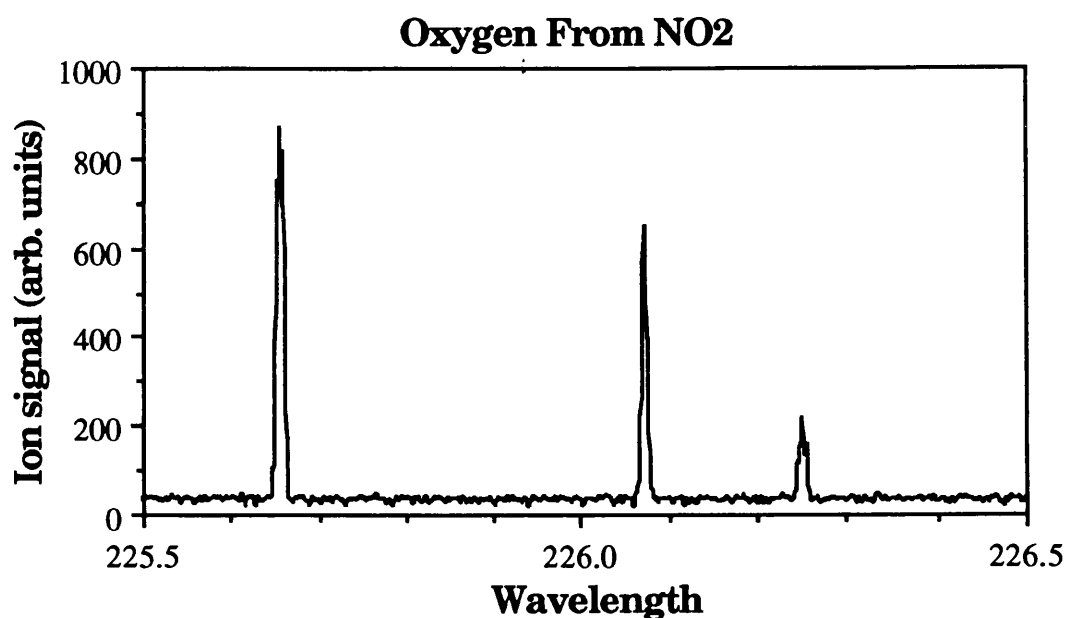
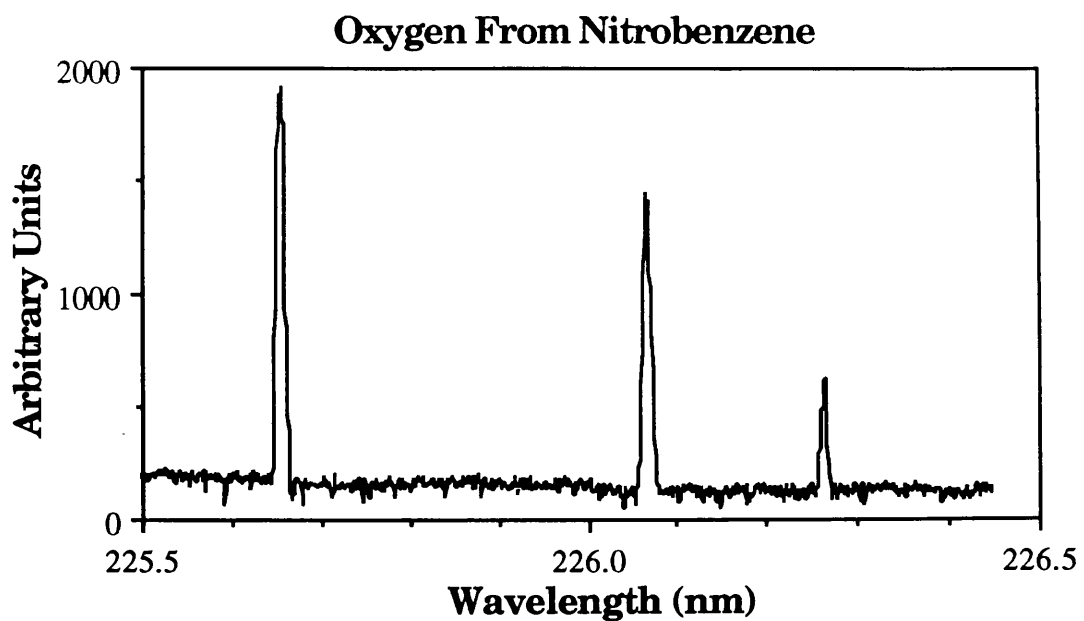


Fig 6.4 The oxygen atomic resonances have been recorded from nitrobenzene, o-nitrotoluene and NO₂.

photons for excitation with subsequent ionisation brought about by either a fundamental or UV photon Fig 6.3.

Of the total of nine peaks expected from a triplet to triplet transition involving the $2p^4\ ^3P_J \rightarrow 2p^33p^3P_J'$ states, only three peaks have been resolved Fig 6.3. It is expected that due to the fine structure in the ground state with energy levels of 0, 158.5 and 226.5 cm^{-1} the experimental resolution of the system is insufficient to distinguish all of the transition peaks with some overlapping taking place. As well as observing oxygen resonances from nitrobenzene, experiments have been carried out on nitrotoluene and high purity NO_2 gas. In both of these compounds the three resonances peaks observed with nitrobenzene were also recorded Fig 6.4.

(i) Analysis

The FWHM for each of the three atomic transitions in all compounds studied were equal in size. This would indicate that the different electronic transitions producing the lines do not influence the magnitude of the bandwidth of the atomic transitions.

Possible sources of line broadening include Doppler broadening. However, it is predicted that any differences in the translational energy of the oxygen atoms liberated would contribute in a negligible way to the total broadening of the peak. Collisions are another source of broadening but when considering the low pressures at which the measurements were carried out (10^{-5} mbar) it seems unlikely any significant contribution will be made by this process either.

Measurements taken of the oxygen power dependence from nitrobenzene showed a gradient of three, which can be used to account for the oxygen signal assuming a saturation of one of the levels has taken place. The resultant process would entail one photon to liberate a neutral ground state oxygen atom which subsequently undergoes ionisation via a 2+1 scheme Fig 6.5.

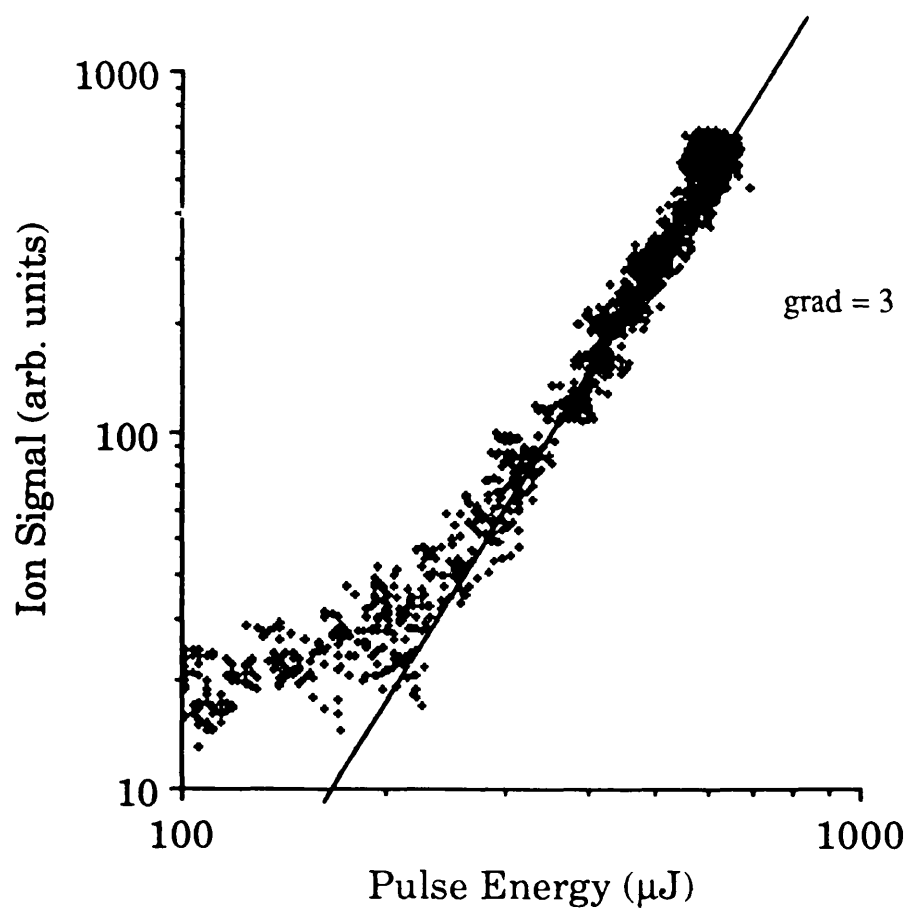


Fig 6.5 The variation of the oxygen ion signal with laser fluence from nitrobenzene at 225.65nm is shown. The oxygen ion signal shows a gradient of three indicating a cubic power dependence.

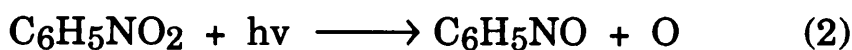
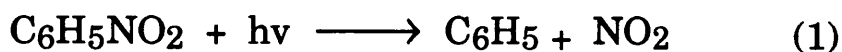
Work carried out on resonant enhanced multiphoton studies of atomic oxygen by S.N Dixit et al(56) have used ab initio calculations for three photon ionisation with 2 photon resonance via the $2p^3np$ and $2p^3nf$ levels. Their calculations showed that transitions via these levels had the most efficient ionisation path. Although even this scheme requires a few GW/cm^2 for a 5nsec pulse to achieve about 50% ionisation.

In the present experiment both the UV and fundamental (FM) beams are focused into the chamber producing a typical energy density of $20\text{mJ}/\text{mm}^2$.

So it seems likely that the dissociation of the oxygen atom from the nitrobenzene molecule on the interaction of the first photon is the step which is saturated.

(ii) Origin Of The Oxygen Ion Signal

The possible paths predicted for the oxygen ion arising from nitrobenzene on absorption of a UV photon are (29,30,31,33,):



Our experiments with NO_2 gas indicate that path (1) results in oxygen via



According to Slanger et al the production of atomic oxygen in the ^3P ground state from ground state NO_2 molecules is possible for wavelengths less than 397nm (57). But as more energetic photons are used it becomes possible to open a second channel

with the release of oxygen atoms in the metastable 1D state. This route becomes possible for wavelengths $<243.9\text{nm}$.

The resonant ionisation of 1D oxygen atoms can take place via the $^1D^0$ state. This involves 3+1 absorption scheme with one UV and two FM photons for excitation at wavelengths of 230.43nm and 460.86nm respectively. Thereafter either UV or FM photon can initiate the ionisation step. (Fig 6.5a)

An intensive investigation was carried out to detect the presence of an oxygen resonance at 230.43nm which would confirm the presence of the 1D excited oxygen atoms. All of the experimental data showed a null result. This in itself does not dismiss the possibility of $^1D^0$ oxygen atoms being produced. Because ionisation involves a three-photon process the total cross-section is very low consequently the power of the lasers may be insufficient to initiate this step. The fluence levels used in this experiment of 5mJmm^{-2} may not be of sufficient strength to allow the process to proceed. In light of this fact the production of oxygen atoms in the 1D state cannot be discounted or confirmed.

(3) Hydrogen Atom Production

In the course of laser ionisation studies on nitrobenzene, a very intense ion peak at $m/z = 1$, corresponding to hydrogen ion, was observed as the laser wavelength was scanned through the wavelength 243.13nm . This resonance was first reported by Spinelli et al (1987) when he carried out work on benzene in the gas phase (58). Other studies which have cited the production of hydrogen atoms include work recently reported by Hass et al (1993) in the 243nm dissociation of ammonia and by Mordaunt et al (1993) in the 121.6nm photodissociation of methane (59,60). The present studies have recorded the presence of hydrogen ions produced from the UV photodissociation of nitrobenzene vapour. Both wavelength dependence and mass spectral data have been used to show the presence of the on resonance hydrogen ions as the wavelength is tuned to a resonant excitation of the hydrogen

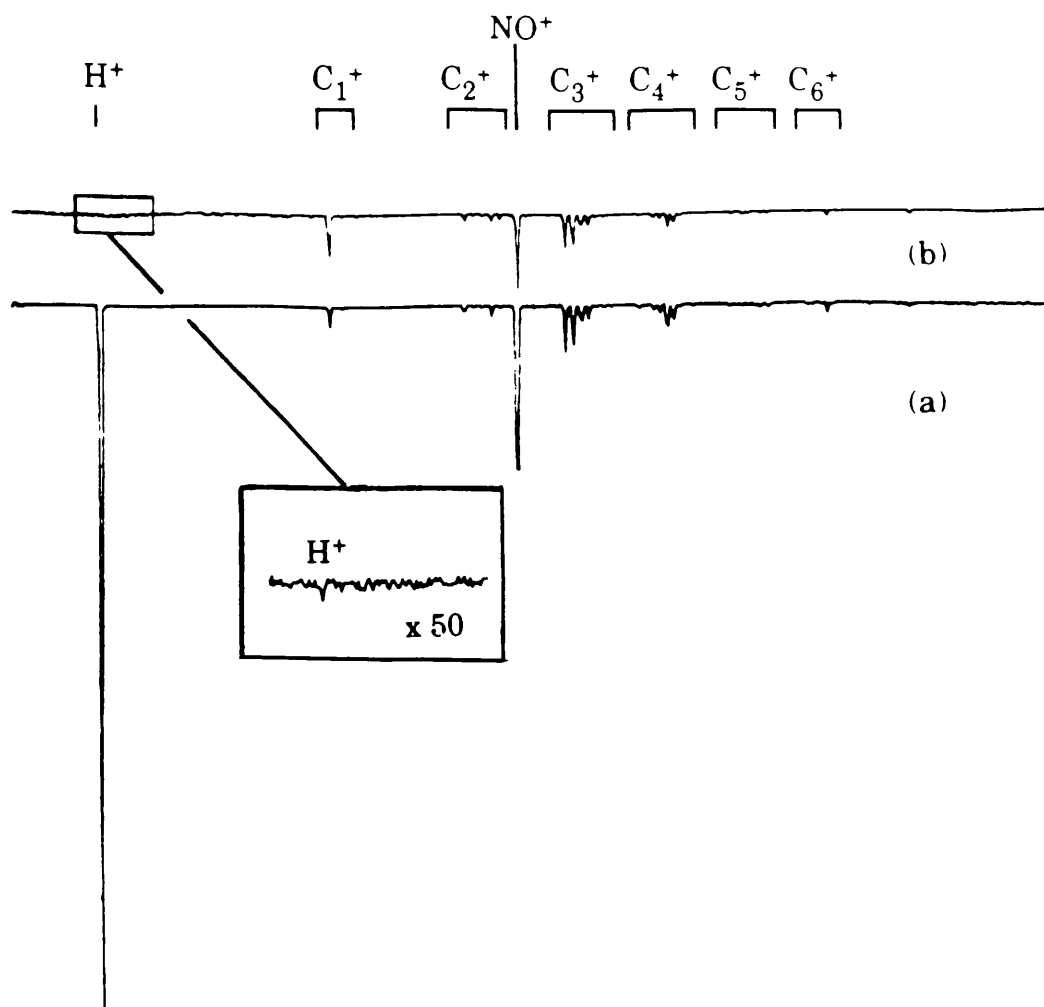


Fig 6.6 The on-resonance and off-resonance hydrogen ion resonance from the nitrobenzene sample are shown on the time-of-flight mass spectra at a laser fluence of 1mJmm^{-2} .
a) The spectrum of the hydrogen ion resonance at 243.13nm is shown.
b) The off resonance case shows a very small hydrogen ion peak. The inset is of the hydrogen ion region at $\times 50$ gain.

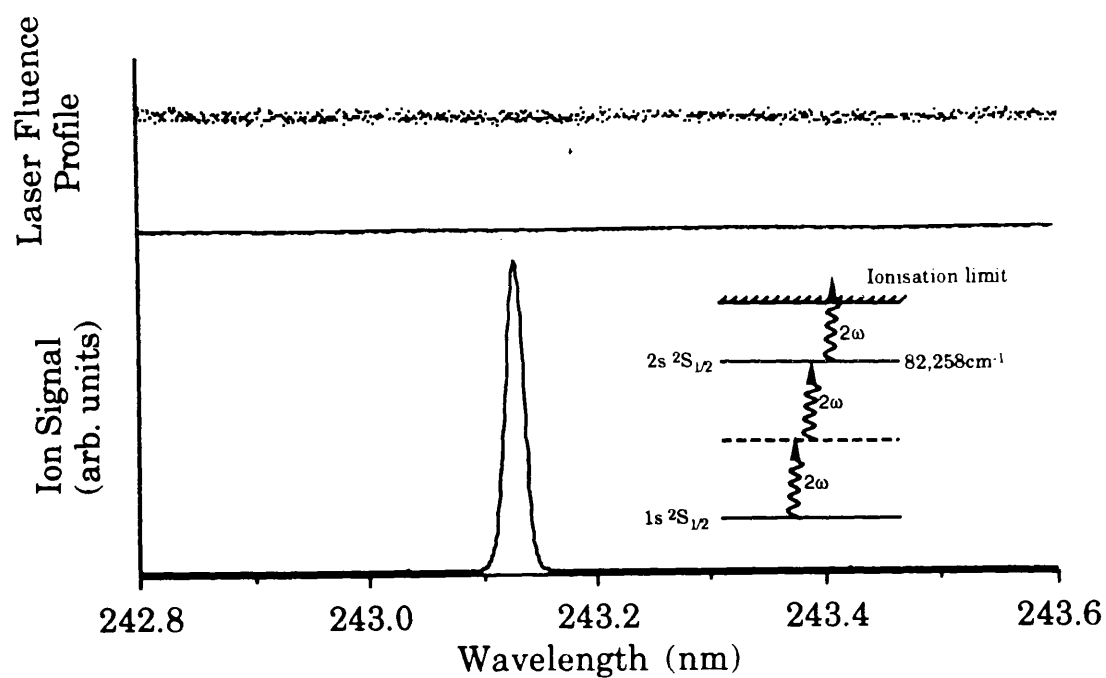


Fig 6.7 The hydrogen ion signal as a function of the laser wavelength from nitrobenzene is shown. The laser fluence profile above is also recorded, with the maximum fluence being 4.6mJmm^{-2} . The hydrogen ion is formed through the ionisation scheme shown in the inset.

atom Fig 6.6 a&b. The ionisation process involves a 2+1 scheme with all three photons involved being in the UV range. The resonant excitation step is $1s^2S_{1/2} \rightarrow 2s^2S_{1/2}$ with two laser photons of wavelength 243.13nm able to induce this transition. Fig 6.7 shows the variation of laser fluence during the scan, showing a nearly constant value of 1mJmm^{-2} .

The time-of-flight mass spectra of the hydrogen ion signals are shown for the on and off resonance conditions at 243.13nm and 243.25nm respectively. In the off-resonance case the region of the hydrogen ion is expanded by a gain of 50 shown in the inset portion. This shows a small H^+ ion signal which can be accounted for by a non-resonant multiphoton ionisation process.

The on resonance signal shows a sharp peak indicative of an atomic transition, which from its large size would indicate that a large number of hydrogen atoms are produced in the photodissociation of nitrobenzene.

Here as in the oxygen ion mass spectra the hydrocarbon fragments remain virtually unchanged over the shift in the wavelength of 0.12nm. As before, the NO ion shows the biggest changes since, as in the case of the oxygen ion product this wavelength region lies within a rotational band of the NO molecule.

(4) Conclusions

After laser induced fragmentation of nitrobenzene vapour which has been carried out in a linear time-of flight mass spectrometer, there have been observed resonant ionisation of oxygen and hydrogen atoms. From the prominent size of these resonance signals it can be assumed that a large number of hydrogen and oxygen atoms are created as a result of multiphoton fragmentation of nitrobenzene.

(i) Future

One possible experimental set-up which may be used in order to monitor the production rate of molecular/atomic species liberated in the fragmentation yield as a function of wavelength is as follows. By operating two lasers one of which is used to scan over the appropriate region of investigation thus varying the energy for the dissociation process. The second laser is fixed on the resonance of the species whose production rate is to be measured as the wavelength is varied. By operating under this condition it is possible to ascertain the production yield of any species as the fragmentation process proceeds throughout the wavelength scan. In order to gain more insight into the dissociation pathways, more accurate information is required regarding the production rate of NO molecules, carbon, oxygen and hydrogen atoms as a function of wavelength, which can be attained using the above set-up.

(5) Photodissociation Pathways Of Nitrobenzene

In the light of benzene impurities in the BDH sample of nitrobenzene (Chapter 4), it was decided to re-investigate the fragmentation processes from the Aldrich sample over an extended wavelength region (225-275nm). Amplifiers were used to increase the signal sizes but due to the low signal to noise ratio it was not possible to record wavelength scans of the higher masses. Most of the data used in the interpretation of the analysis was in the form of mass spectra averaged over 1000-2000 laser shots. Large sampling numbers are used because of the small size of the signals observed which lead to difficulties when trying to record the wavelength spectra.

In the mass spectrum of nitrobenzene a number of higher mass fragment ions, most notably the parent ($\text{C}_6\text{H}_5\text{NO}_2^+$), nitrosobenzene ($\text{C}_6\text{H}_5\text{NO}^+$), phenoxy ($\text{C}_6\text{H}_5\text{O}^+$) and phenyl (C_6H_5^+) ions have been observed. The lighter fragment groups such as C_nH_m (with $m=0,1,2,\dots$, $n=1,2,3,4,5$) which are characteristic products of laser induced fragmentation of nitroaromatics in general were also observed. All previous mass spectra recorded of nitrobenzene did not show the presence of the higher mass fragments. After implementation of the heating mechanism, which has facilitated the flow of the sample under investigation into the interaction region, it has been possible to record the higher mass fragments observed from the nitrobenzene sample. Experiments were undertaken with the sample phial kept at approximately room temperature with the ceramic lining the path to the interaction region kept constant at 120°C. Specific details of the sample entry heating mechanism is given in chapter 7.

Because of the ease with which fragmentation occurs in nitroaromatic compounds, they are considered ideal candidates for dissociation pathway studies (61-64). Our interest in these compounds is governed primarily because of their association with high explosives. Nitrobenzene is considered to be one of the

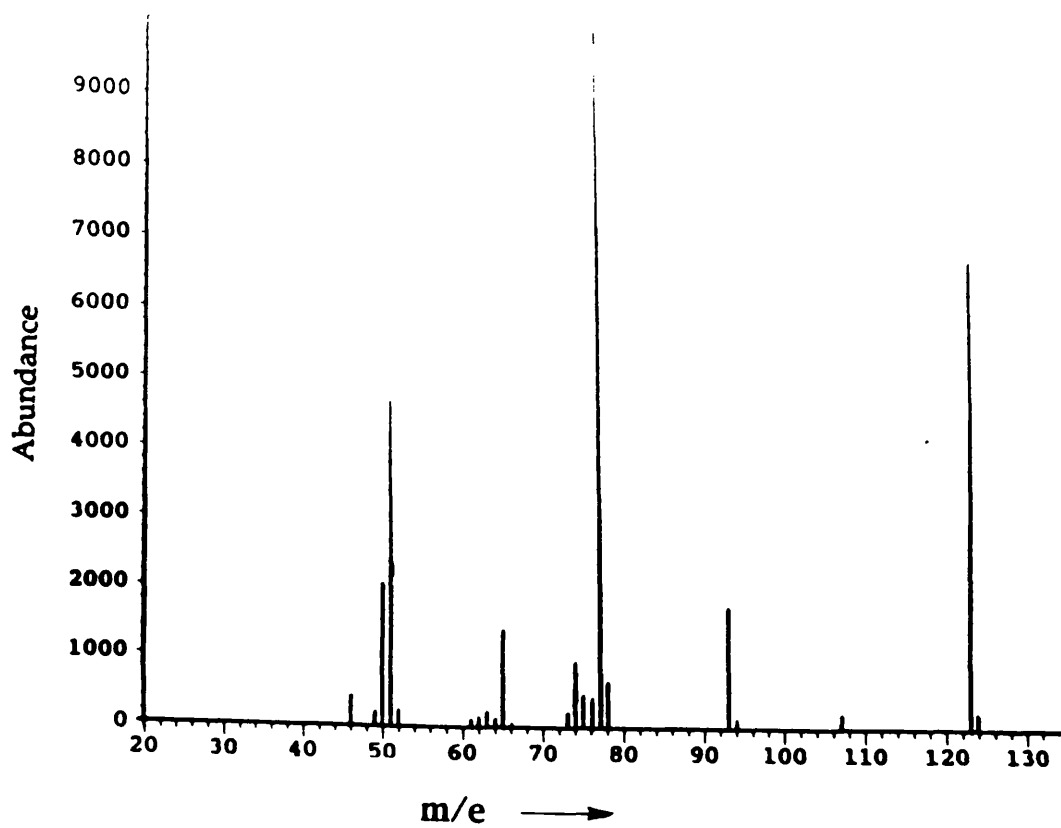


Fig 6.8 The Electron Impact spectrum of nitrobenzene at 70eV is given showing the presence of the higher mass fragments.

simplest explosives. A thorough investigation of this compound is considered prudent to ascertain the properties and an understanding of its photochemistry which may be utilised when dealing with more complex molecules.

By building a picture of the possible pathways taken after laser irradiation, the origin of the fragments formed may be elucidated. The fragmentation patterns may be used to aid the identification of the original parent, although the exact nature of the path leading to the fragments is still uncertain, as it is believed that a number of channels are open simultaneously.

(6) Resume of Possible Photodissociation Pathways.

a) Non- Laser Analysis

Early work on nitrobenzene was carried out by Schuler and Woeldike using a discharge lamp.(65) Their work suggested the following dissociation channel:



Also Hastings & Matsen (66), have observed the nitrosobenzene fragment as a dissociation product, consequently they have proposed the pathway



A library electron impact mass spectra of nitrobenzene using 70eV electron bombardment shows the presence of the products from the above reactions (67)(Fig 6.8). Other peaks also observed in the spectra can be explained by assuming the pathway



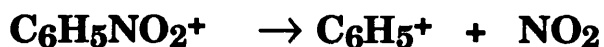
with subsequent dissociation of the phenoxy radical to give



b) Laser Analysis

The above three pathways described are predicted from processes which do not involve laser photolysis. In order for us to make reasonable comparisons with previous work consideration has to be given to work involving laser photolysis (29,31,35,48,68). Galloway et al (33), have used a UV laser for photolysis with ionisation of the neutrals brought about with a VUV laser. These studies have verified the existence of the above three pathways with evidence of the nitrosobenzene and phenyl ions.

From the work obtained by other studies on the fragmentation of nitrobenzene it can be safely assumed that the parent ion breaks into the following routes (69-75).

**(7) Technique And Application**

Experiments have involved working with gas phase nitrobenzene introduced into the system with the aid of a heating mechanism. Mass spectra have been recorded at finite wavelengths over the range 225-275nm. Typically experiments are carried out using both the FM and UV components passing through the system, but in this series of experiments an Inrad Harmonic Separator model 752-104 was used to allow only the second harmonic beam through which is focused into the high vacuum chamber using a 30cm quartz lens.

Nitrobenzene has an ionisation potential (IP) of 9.9eV (76) therefore allowing it to ionise the molecule using two UV photons with wavelengths < 251nm. This wavelength is of importance in

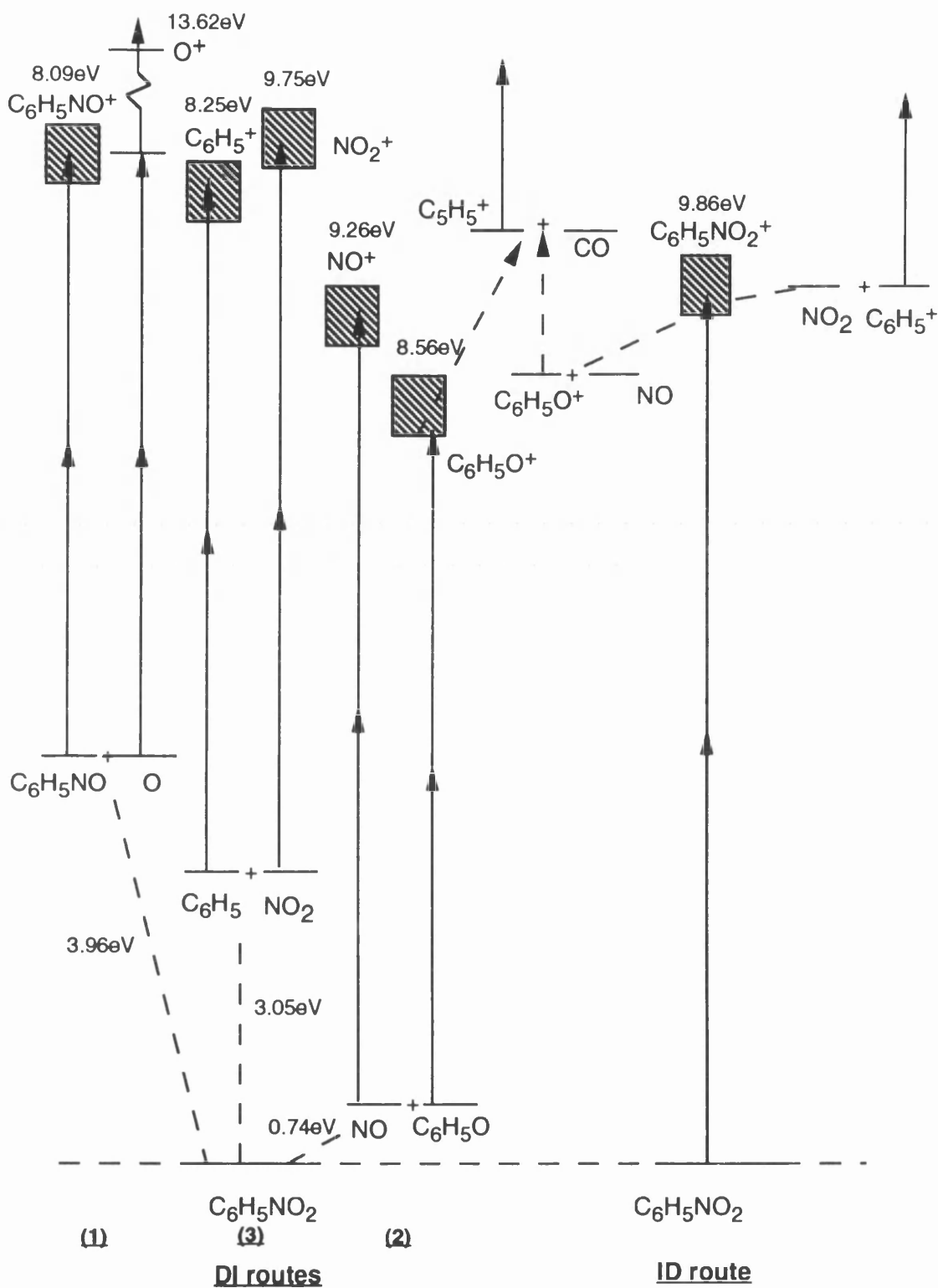


Fig 6.9 The various paths possible for the fragmentation process to follow.

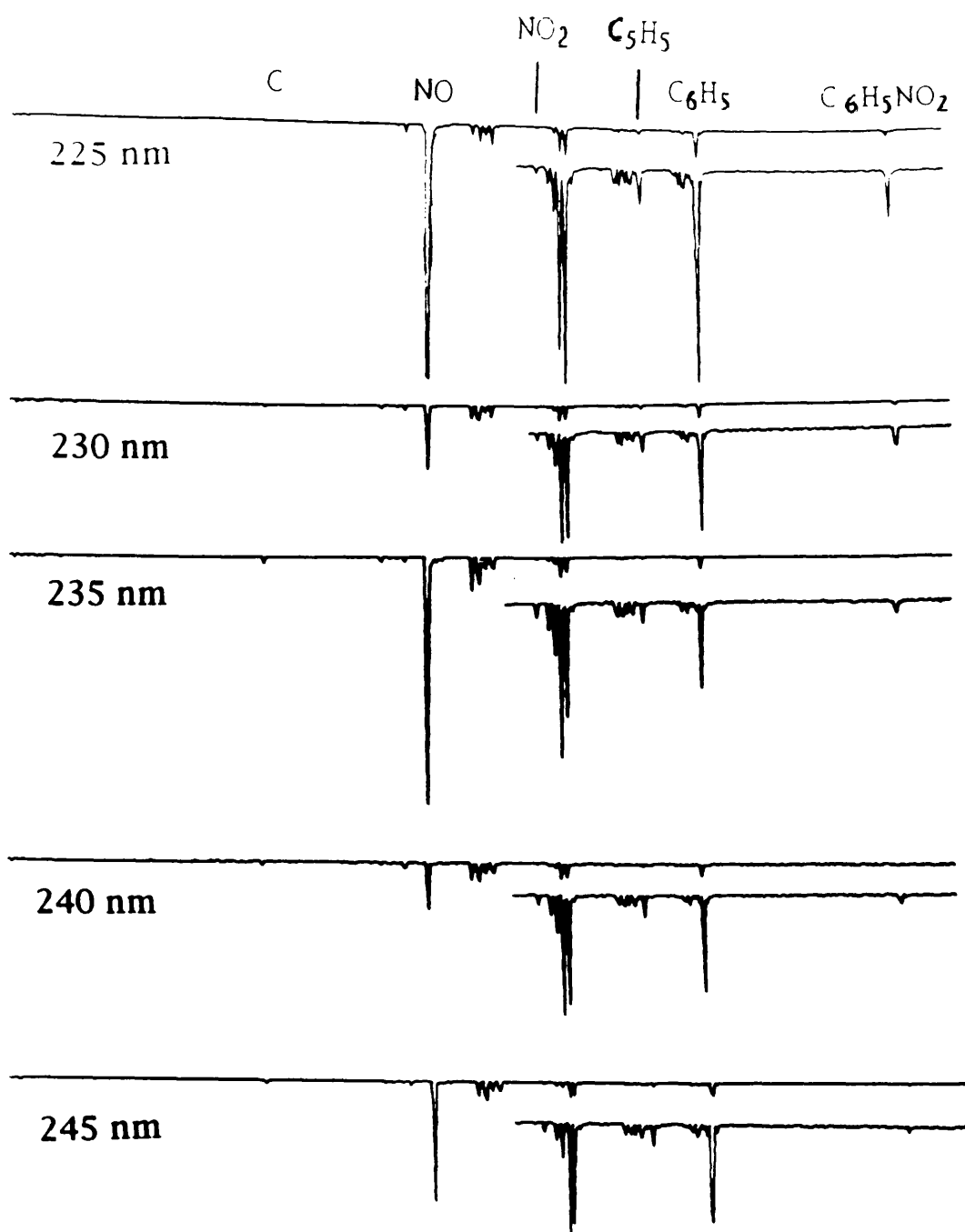


Fig 6.10 The time-of-flight mass spectra of nitrobenzene have been recorded at several laser wavelengths in the range 225-245nm. In order to highlight the higher mass fragments this region of the spectra has been magnified by x8. The laser focusing conditions and pulse energy was kept constant for each spectra at 8.5mJ/mm².

that it will determine whether or not ionisation or dissociation of the parent molecule is the dominant process.

Careful consideration has to be given to the initial absorption of a single photon leading to the intermediate state regarding the possible fragments formed thereafter. If absorption of another photon takes place from the intermediate state this results in the ionisation of the molecule which can then be followed by dissociation processes. Also the possibility exists depending on the lifetime of the intermediate state for its dissociation resulting in neutral fragments which are then ionised via multi-photon absorption.

In the analysis of our data the dissociation followed by ionisation process is denoted as **DI**, and **ID** will represent the ionisation followed by dissociation route. The various paths discussed are shown on Fig 6.9.

(8) Results and Discussions

On analysing the mass spectra, it is clear that when lasers are used for photolysis that the products depend on both the wavelength and power of the laser beam.

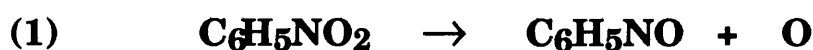
Clear evidence of the wavelength dependent nature of the fragmentation process is realised when comparing mass spectra taken at different discrete wavelengths as other parameters such as laser intensity and focusing conditions are kept constant Fig 6.10.

The most significant mass spectra are those involving the presence of the heavier masses, these include the parent, nitrosobenzene and phenoxy Fig 6.11. The parent ion to our knowledge, has never been reported before in two photon laser photolysis experiments. This ion along with the other heavier masses is only reproduced over a limited wavelength range, with the parent ion created only in the region when the two photon

energy exceeds the ionisation potential of the molecule. The fragmentation patterns observed for wavelengths greater than 251nm would be indicative of predissociation process either through absorption of one or two photons. When considering wavelengths <251nm the ID route becomes possible but nevertheless it does not discount the possibility of DI process taking place simultaneously.

A number of channels which may exist will be discussed by giving evidence to support our predictions. Firstly, consideration will be given to three possible dissociation ionisation routes.

(i) Dissociation Ionisation



The thermochemical threshold for the above reaction is 3.96eV, thereby allowing this path to exist at all of the wavelengths used in our experiment. The observation of the nitrosobenzene ion took place at wavelengths shorter than 257.5nm (Fig 6.11, Fig 6.12) in our set-up although it has been observed by Galloway (33) at less than 280nm which corresponds to an energy of 4.43eV still within the appearance potential of the ion. The difference in the wavelength at which the ion is first detected can be accounted for by the different excitation process involved. Galloway et al use a single VUV photon to ionise the neutrals formed whereas two photons are used in our experiment. The nitrosobenzene ion has been detected in the region 240-257.5nm, with the intensity of the ion varying with wavelength Fig 6.12.

In this pathway the oxygen atoms produced have energy such that they can only be produced in the ground state in the wavelength region 220-270nm. Assuming the oxygen to have arisen from the above pathway it is possible to make some inferences about the parent state by applying the conservation of spin. The neutral atomic oxygen released is in the triplet state whereas the ground state nitrobenzene is a singlet (77).

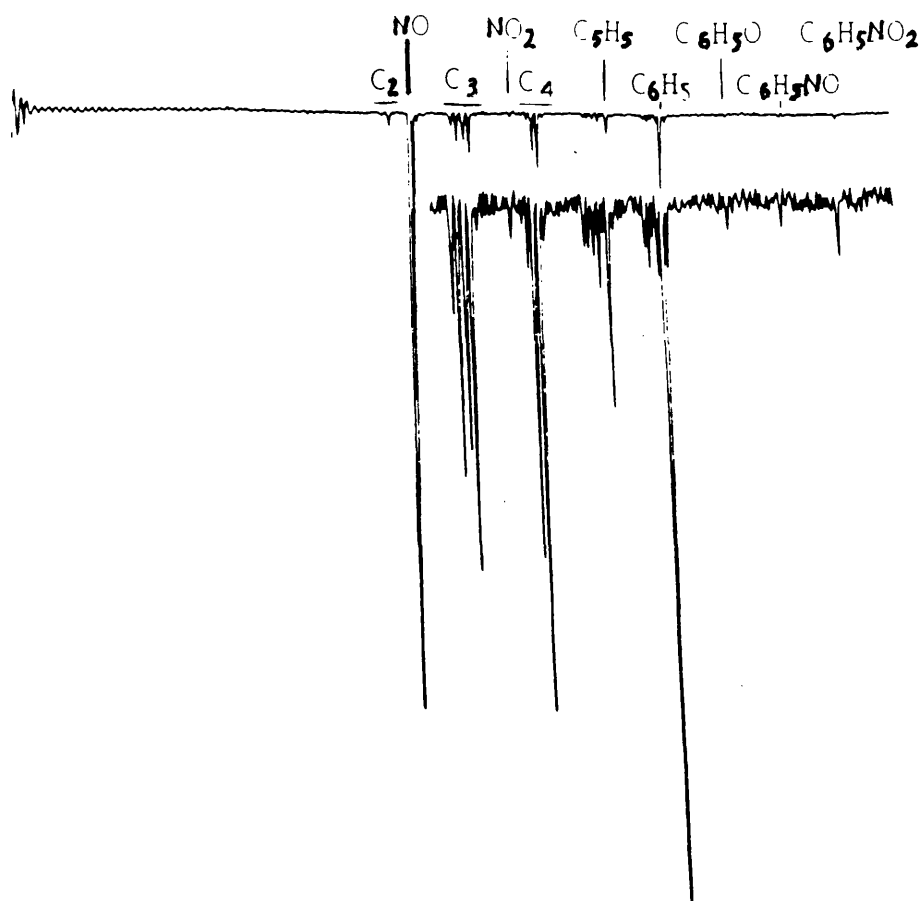


Fig 6.11 The nitrobenzene mass spectrum at 246nm averaged over 2000 laser shoots with pulse energy $12\mu\text{J}$ is shown. The spectrum has been magnified x10 again to highlight the higher mass fragments but in particular to show the presence of the parent ion.

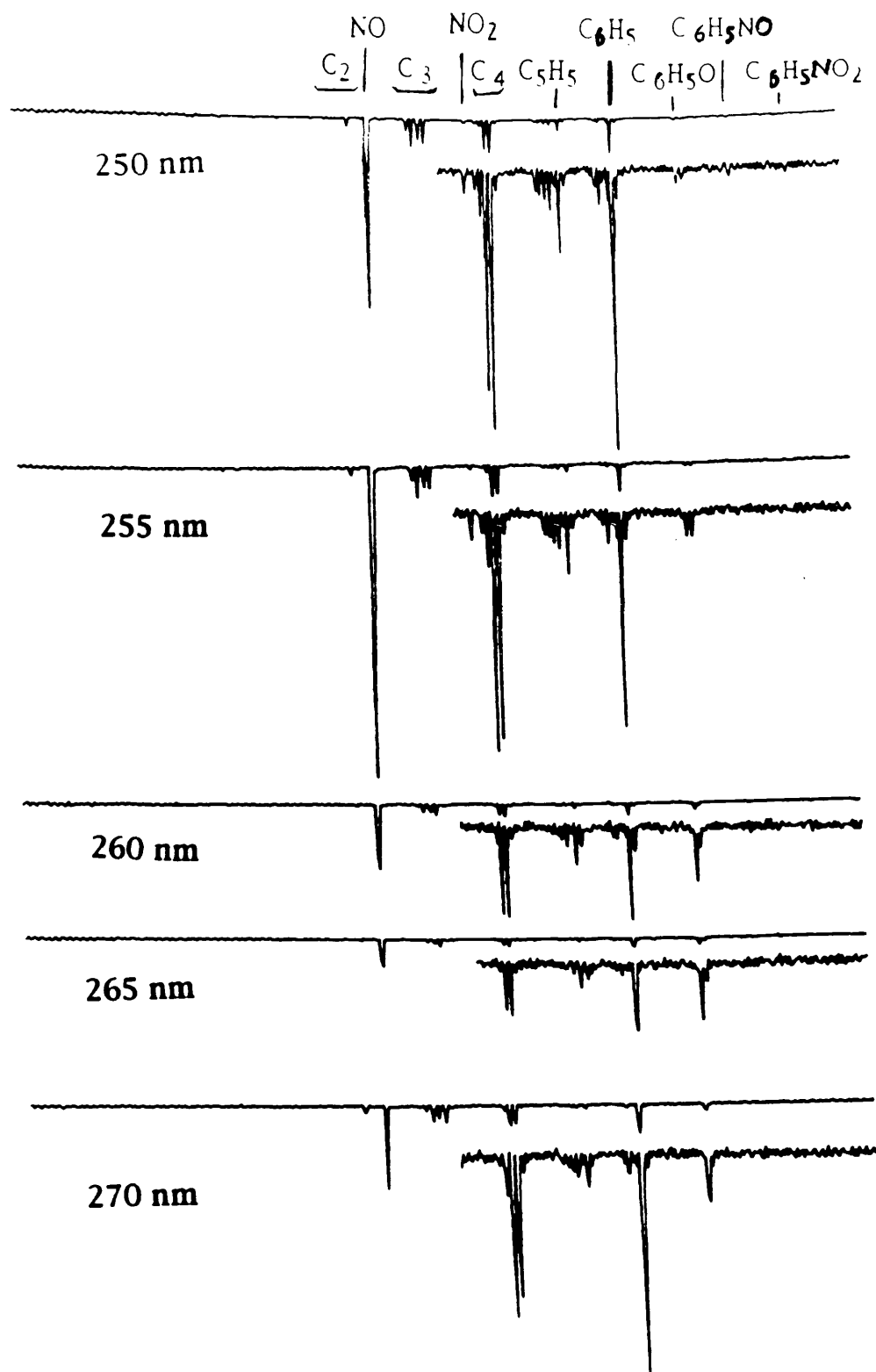
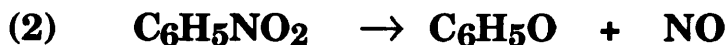


Fig 6.12 The time-of-flight mass spectra of nitrobenzene have been recorded at several laser wavelengths in the range 250-270nm. The higher mass fragments are highlighted for each spectrum by a magnification of x8. The laser focusing conditions were identical and the pulse energy was constant at 17 μ J.

Therefore in order to satisfy spin conservation it is probable that the parent after excitation to the intermediate state has undergone non-radiative de-excitation through intersystem crossing into a triplet manifold from which the dissociation has taken place.



The phenoxy ion was observed for a laser wavelength between 245-272.5nm. In previous experiments, the ion has been recorded by Apel and Nogar (48) although recently the absence of the ion in the mass spectra of Galloway et al has been explained by another fragmentation mechanism involving further dissociating of the phenoxy radical (78).



As well as noting that the phenoxy ion is generally present at the longer wavelengths Fig 6.12, the variation in intensity of the ion as a function of power was measured. The wavelength was fixed at 266nm and the mass spectra of nitrobenzene taken at different powers (Fig 6.13).

The spectra show that the various fragments increase in intensity at different rates, which would imply that the individual ions require different numbers of photons for ionisation. The phenoxy ion shows the least variation as the fluence is altered. Typically the number of phenoxy ions would be expected to increase with fluence. Since this is not observed it may be inferred that fragmentation of the phenoxy ion is taking place at higher fluences. Therefore as the fluence increases the rate at which they are produced from the parent increases but the total number is kept fairly constant because of the higher rate of fragmentation possibly into the C_5H_5 ion as described by the above equation.

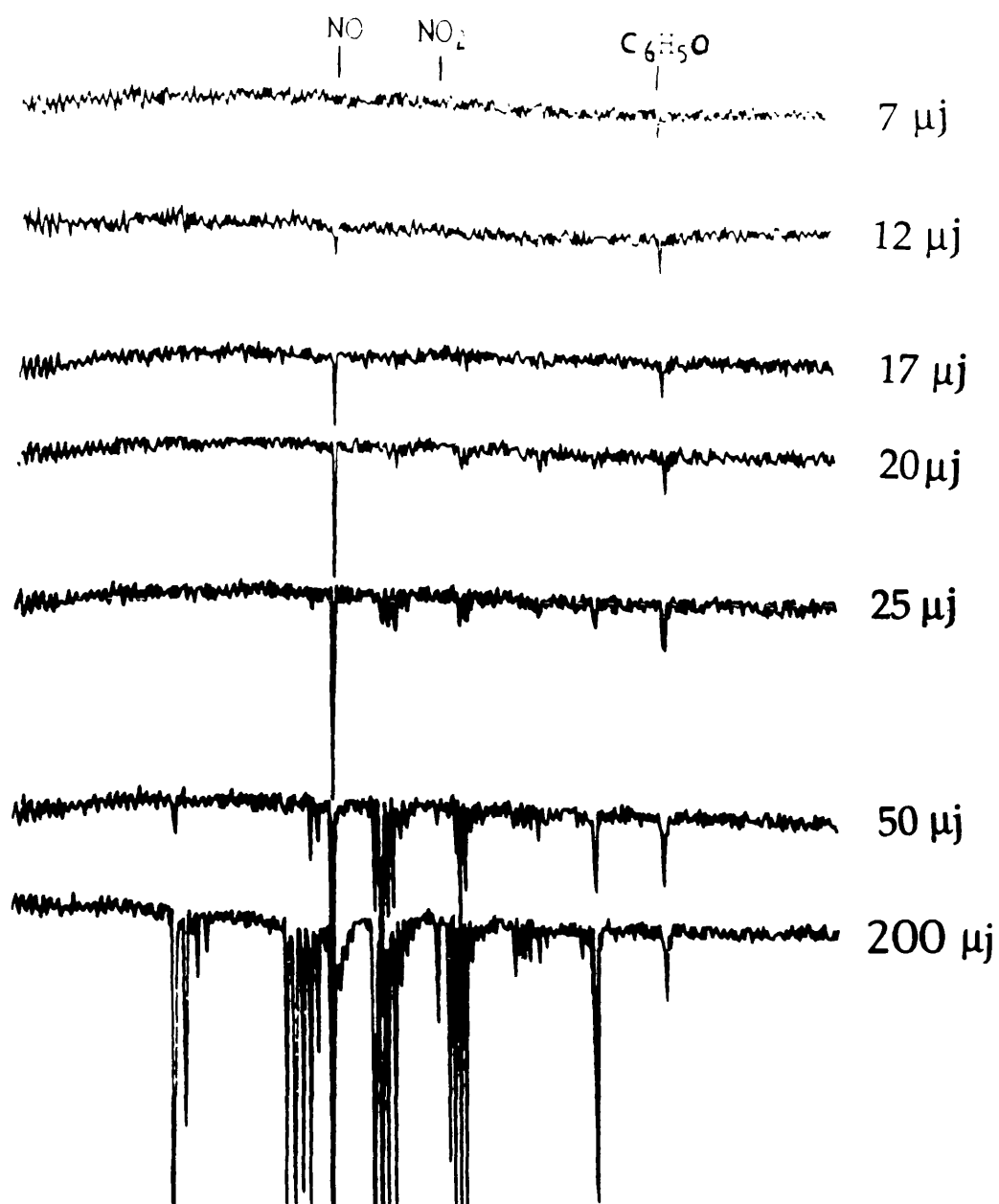


Fig 6.13 The mass spectra of nitrobenzene at 266nm and chamber pressure 10^{-5} mbar at various pulse energies is shown. The variation of the fragments intensity with power is demonstrated.

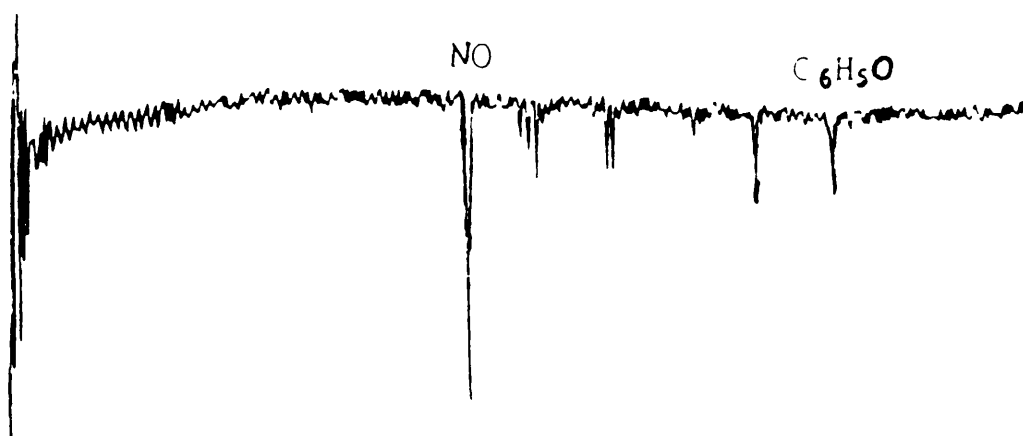


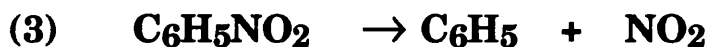
Fig 6.14 The mass spectrum of nitrobenzene recorded at 272.5nm is shown with a distinctive NO ion signal.

Of particular interest is the first three mass spectra of Fig 6.13 which show that only one of the many possible pathways is visible at the laser intensity and wavelength used. i.e pathway (2) only.

Mass spectra taken at 272.5nm shows the presence of a large NO⁺ ion Fig 6.14.

Since the IP of NO is 9.26eV, two photons at 272.5nm do not have enough energy to ionise ground state neutral molecules. Ionisation of this molecule at the present wavelength could only have taken place from excited or "hot" NO molecules released in fragmentation. The NO measured at 272.5nm could be accounted for by ionisation from vibrationally excited NO molecules. From the size of the signals observed this would indicate a significant excited state population, greatly exceeding that which would be predicted by a Boltzmann distribution.

The NO ion could also have originated from the NO₂ radical which is produced from the photolysis of nitrobenzene. NO produced in this process has been found to exhibit an inverted population with respect to the occupation numbers of the vibrational levels of the ground state neutral NO molecule at room temperature, which could account for its presence at 272.5nm (41,79-82). However, experiments with NO₂ gas lead to the conclusion that NO⁺ production from the photolysis of NO₂ is much less efficient (by two orders of magnitude (31,67,83) than direct production from NO gas within the present experimental conditions.



This pathway is considered to be the dominant one at the shorter wavelengths (33). In the wavelength range of study the energy available after dissociation is calculated to be between (1.5-2.1eV).

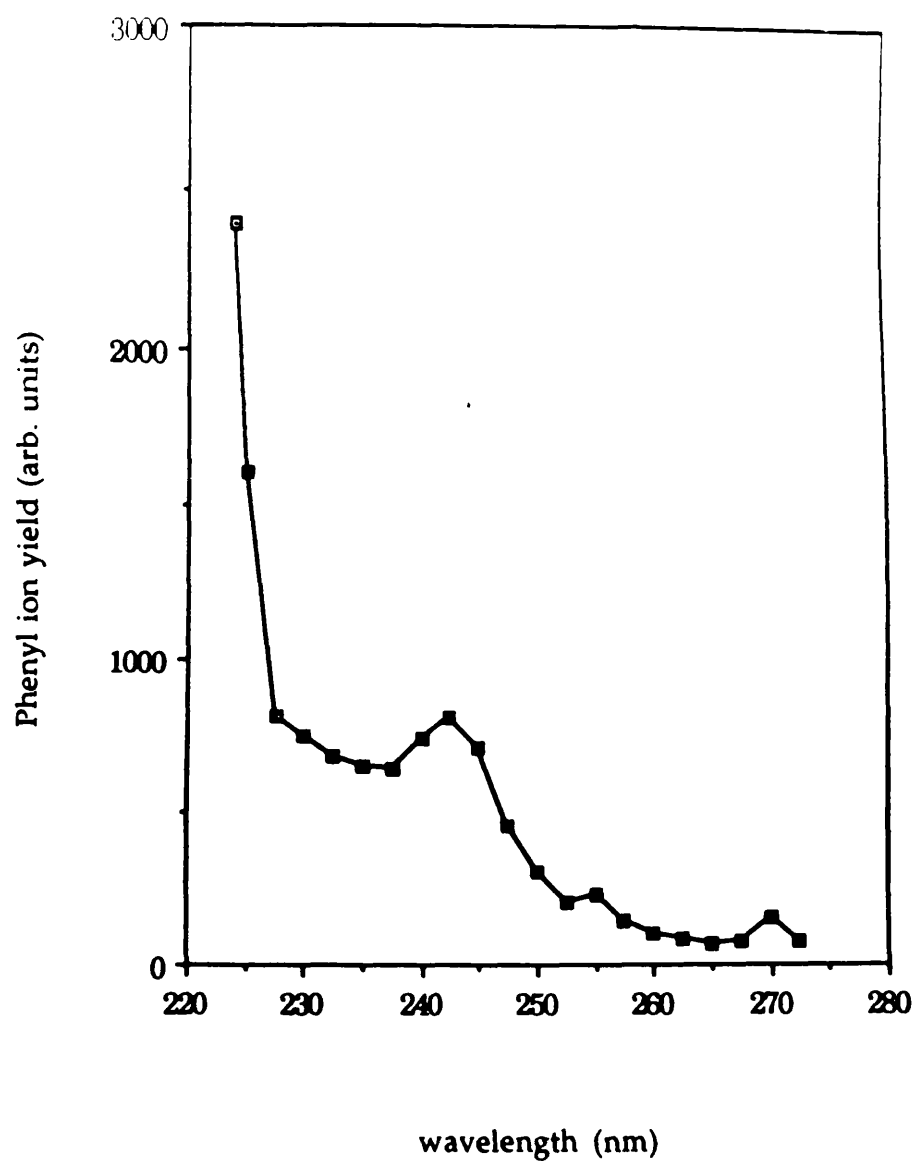


Fig 6.15 The variation of the phenyl ion yield at discrete laser wavelengths is presented.

Considering the scenario whereby all the energy after photolysis of the nitrobenzene is transferred as internal energy to the phenyl radical, it would still not be sufficient to cause excitation into the first electronic state although higher vibrational levels of the ground state may be populated.

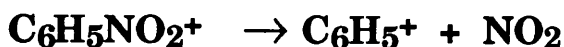
The phenyl radical also exhibits an absorption band at ~250nm corresponding to the $B_{2u} \rightarrow A_{1g}$ and $B_{1u} \rightarrow A_{1g}$ transitions of benzene (38). Therefore in this region any ground state phenyl radicals produced may be subsequently excited to a real intermediate state after the absorption of a second photon from the same laser pulse which induced dissociation of the parent. The phenyl radical has an IP of 8.25eV and ionisation can take place from the excited state with the absorption of a further photon. Making the assumption that the ionisation process is far from saturated and independent of wavelength, it is expected that the production rate of the phenyl ion mimics the absorption spectra of both nitrobenzene and phenyl which are both very similar Fig 4.7.

The phenyl ionisation yield was measured as a function of wavelength at discrete intervals with other parameters held constant Fig 6.15. The ionisation yield closely followed the profile of the absorption spectra for wavelengths >240nm, with the peak in the 240nm region being noticeable. Below this value a gradual decrease in the ion signal unlike the steep fall-off shown in the UV absorption spectrum was observed. In the lower wavelength region it becomes apparent that a marked difference in the behaviour of the phenoxy ion with respect to the absorption profile exists. This could be explained by the fact at higher photon energies another pathway is opened, in which ionisation followed by dissociation (**ID**) mechanism is activated.

(ii) Ionisation Dissociation

As has been stated earlier the production of the parent ion occurs for wavelengths below 250nm Fig 6.10. As the IP of nitrobenzene

is 9.86eV it requires two photon absorption to induce ionisation in this wavelength region.



The ionisation of the nitrobenzene molecule followed by dissociation into the phenyl ion could account for the dramatic increase of the yield of this ion Fig 6.15. The appearance potential of this fragmentation process has been estimated by a number of authors as 11.08 (75), 11.15 (63), 11.2 (71), 11.66 (70), 11.93 (62), 12.14eV (84). The observed increase in the C_6H_5^+ ion yield at 225nm (11.02eV) is consistent with the $11.08 \pm 0.16\text{eV}$ produced by Nishimura et al (75).

It is, therefore postulated that two photons at 225nm reach an excited state above the ionisation continuum, which on decomposition, results in the production of a large number of phenyl ions.

(9) Conclusions

Two main types of fragmentation routes have been used to explain the presence of the various fragments observed from the photodissociation of nitrobenzene in the gas phase. The dissociation ionisation pathway had associated with it three different routes. The evidence for the existence of such pathways is in the appearance of the higher mass fragments such as nitrosobenzene, phenoxy, phenyl as well as NO_2^+ . By taking mass spectra at several discrete wavelengths the wavelength dependent nature of these ions is elucidated. From the data collected it is probable that a number of channels discussed are open simultaneously over short wavelength ranges.

The second route involving an ionisation dissociation type process is carried out above the ionisation threshold of the molecule. It is this route which is used to understand the sudden increase in the phenyl ion intensity at shorter wavelengths.

7.Explosives

(1) Introduction

The primary objective of our experiments is to establish a procedure for the very sensitive and selective detection of explosive mixtures. In order to achieve this goal a series of experiments have been undertaken involving common, yet powerful, explosive compounds.

The explosive molecules dealt with so far include TNT(2,4,6-trinitrotoluene), DNT (2,4-dinitrotoluene), PETN (pentaerythritol tetranitrate), RDX (1,3,5-trinitro-1,3,5-triazacyclohexane), HMX (1,3,5,7-tetranitro-1,3,5,7-tetraazacyclooctane) and EGDN Fig 7.1. The analysis of these compounds has been carried out in the TOF system involving the modified sample entry system.

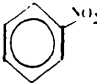
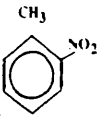
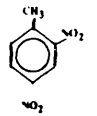
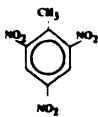
This series of experiments relies on the detection of the vapours given off, and thereafter depends on any characteristic properties which they may display on laser interaction. Because of the very low vapour pressure associated with these compounds high sensitivity is essential for their detection. In order to alleviate the problems associated with the low vapour pressures at room temperature a heating mechanism has been constructed to increase the sample yield in the interaction region.

Most of the information accumulated on the products is recorded in the form of mass spectra which have been averaged over typically 500 shots. It is our objective to identify any features from the mass spectra which allow us to make inferences as to the identity of the original parent molecules.

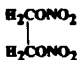
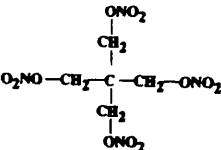
Previous experiments on simple explosive compounds such as nitrotoluene and nitrobenzene have demonstrated the importance of the NO^+ fragment as providing a large signal with a distinct wavelength dependence. The maximum ion signal from

SPECIES	FORMULA	FULL CHEMICAL NAME	STRUCTURE	M Pt (°C)	B Pt (°C)	MOL. WT
---------	---------	--------------------	-----------	-----------	-----------	---------

NITROAROMATICS

NB	$C_6H_5NO_2$	Nitrobenzene		57	210	123.11
NT (o-)	$C_7H_7NO_2$	Nitrotoluene		-9.5	221.7	137.14
2,4-DNT	$C_6H_3CH_3(NO_2)_2$	2,4-Dinitrotoluene		71	300	182.14
2,4,6-TNT	$C_6H_2CH_3(NO_2)_3$	2,4,6-Trinitrotoluene		82	240	227.13

NITRATE ESTERS

EGDN	$(CH_2ONO_2)_2$	Ethylene glycol dinitrate				152
PETN	$C(CH_2ONO_2)_4$	Pentaerythritol tetranitrate		141		316

NITRAMINES

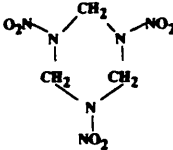
RDX	$(CH_2NNO_2)_3$	1,3,5-tri-nitro-1,3,5-triazacyclohexane		204		222
-----	-----------------	---	---	-----	--	-----

Fig 7.1 A table representing the facts and figures of the various compounds and assigning them into separate categories.

VAPOUR PRESSURES OF EXPLOSIVES

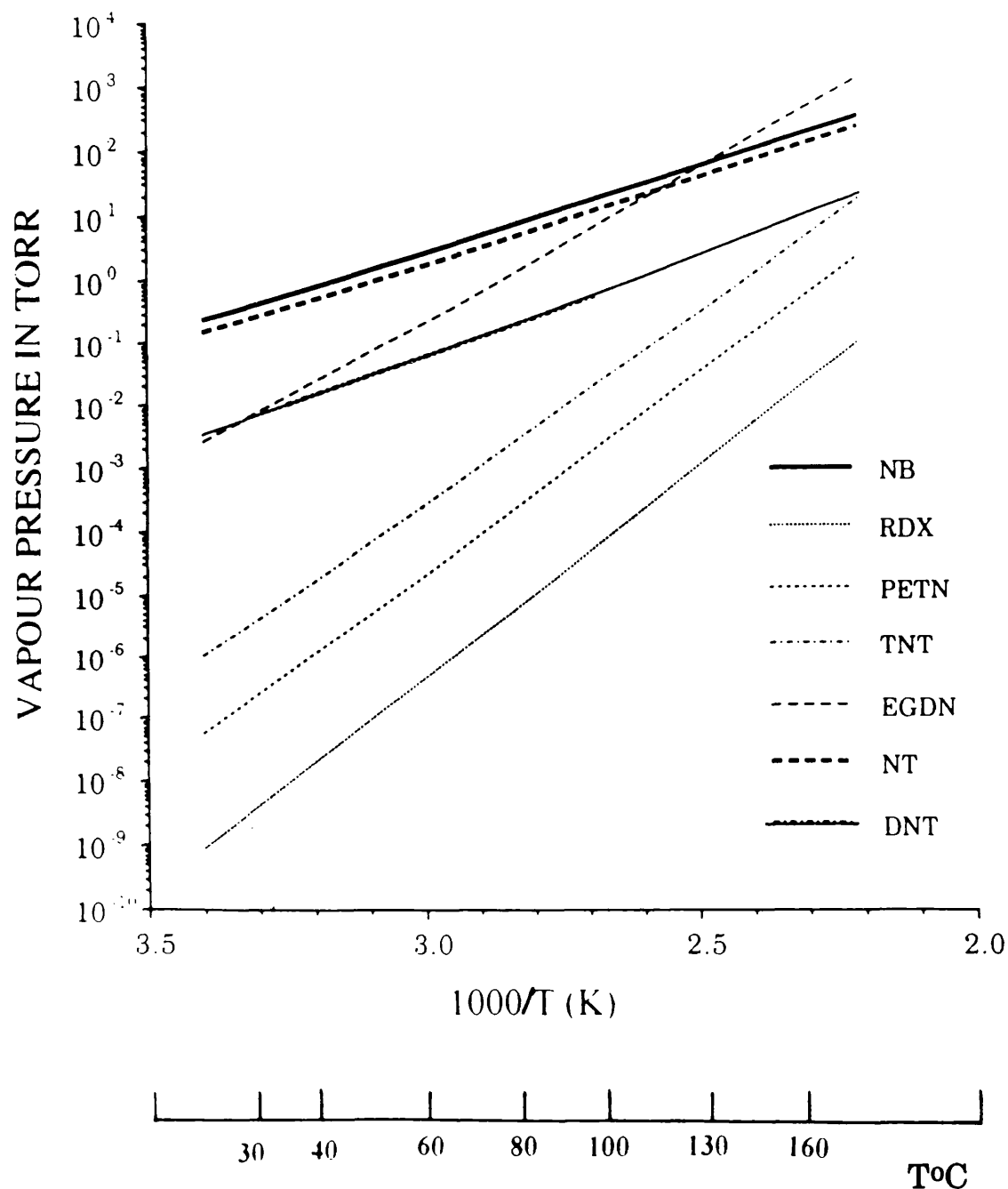


Fig 7.2 The vapour pressure as a function of temperature is shown for a number of explosive molecules.

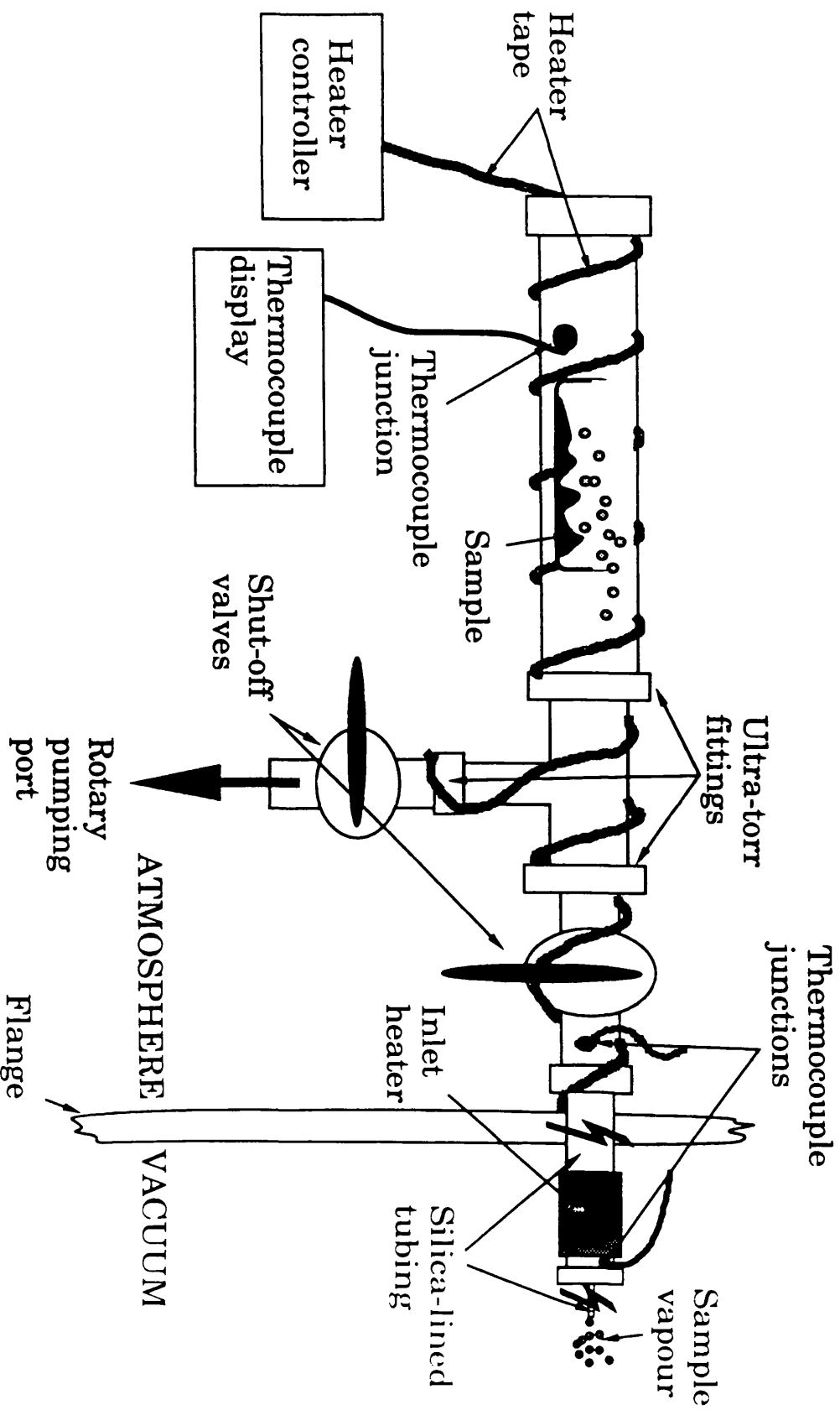


Fig 7.3 The modified sample introduction system is presented which caters for samples introduced in both solid and liquid form.

the $A^2\Sigma(v=0) \leftarrow X^2\Pi_{\frac{1}{2},\frac{3}{2}}(v=0)$ transition occurs at 226.3nm which corresponds to the greatest ionisation efficiency, and it is for this reason that all mass spectra have been studied at this wavelength.

Experiments carried out include taking mass spectra for type identification. The various fragments observed have been looked at in order to find any trends which are indicative of the groups to which they belong. Temperature dependencies have been taken to ascertain maximum sensitivity levels. The NO ion intensity has been plotted against different temperatures and comparisons made with the graphs of theoretical vapour pressure as a function of temperature.

One of the most important aspects of explosives analysis involves the sensitivities at which they can be detected. The various compound sensitivities have been measured at room temperature ($\sim 25^\circ\text{C}$) with the calculations relying on the minimum sample pressure at which the NO ion signal is recorded.

(2) Experimental Set-Up

The experimental set-up is as described in Chapter 2 with the following modifications. The impetus for these changes has been due to the characteristics of the compounds to be analysed; namely their low vapour pressures at room temperatures. From the vapour pressure graphs it is noted that a rapid increase in vapour pressure arises with small variations in the temperature Fig 7.2.

To cater for the low vapour pressure materials a heated silica-lined inlet system has been designed Fig 7.3. In order to facilitate the rapid and efficient changing of samples, swagelock ultra-torr fittings have been used. This set-up can be used with samples both in the liquid and solid states, with liquids being dealt by attaching a glass phial to the inlet system.

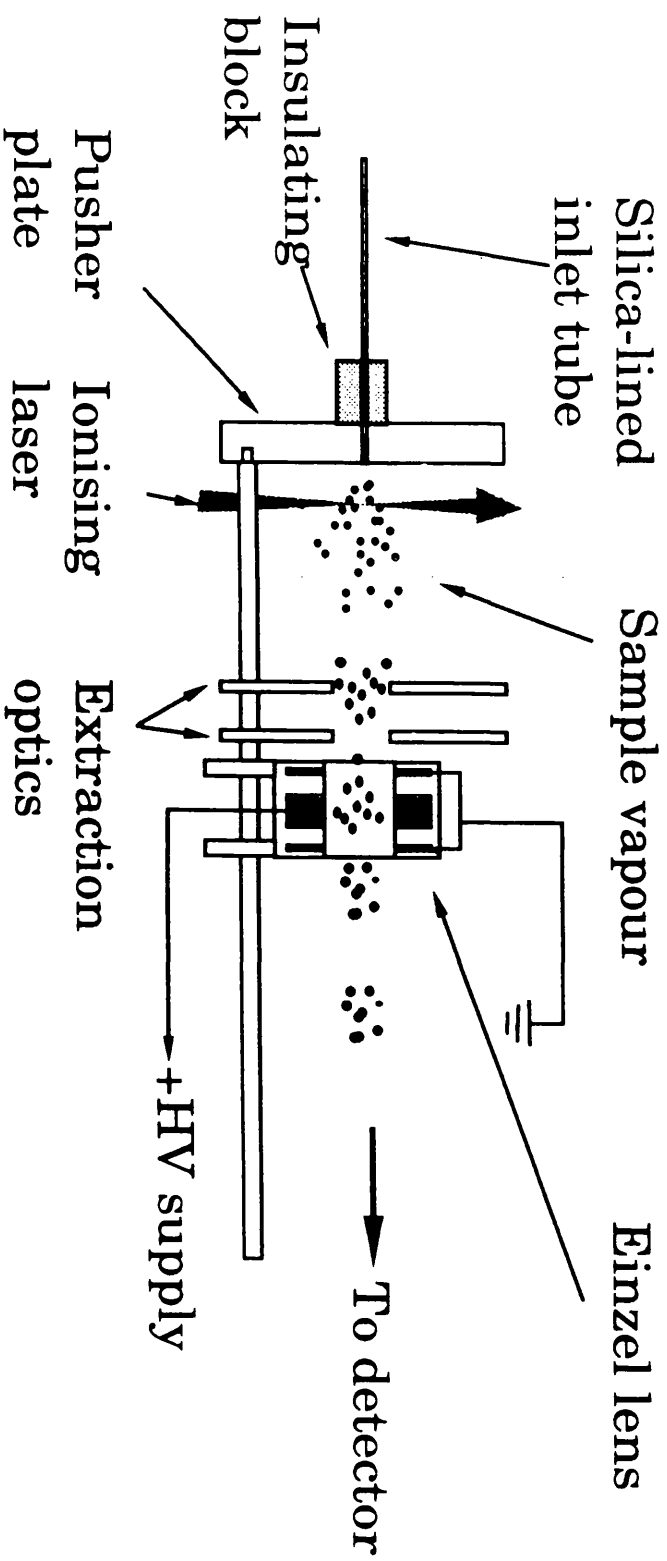


Fig 7.4 The positioning of the einzel lens is indicated within the ion optics assembly with the optimum voltage applied in order to attain electrostatic focusing of the ions down the TOF tube to the detector, thus improving transmission efficiency.

Most of the explosive compounds at Standard Temperature and Pressure (STP) are in solid form, and are studied by placing them into a pyrex "boat" which is subsequently inserted into the sample tube. After the sample introduction, this region is at atmospheric pressure and cannot be opened to the high vacuum of the chamber directly. A roughing pump is used to evacuate this region to a pressure of 10^{-3} torr and the shut-off valve is opened to allow admittance of the sample into the chamber.

The region between the inlet line from the shut-off valve to the high vacuum pump has a heating filament wound round it and is heated separately from the sample tube. The temperatures reached by the heating filament are measured using a thermocouple device, which throughout our experiments was maintained at a constant temperature of 120°C. However the temperature of the sample holder is the most important parameter as far as our measurements are concerned. The heating of this section involved using a constant power heater to supply energy to the heating tape wound round the sample region. This arrangement allows control of the temperature which is monitored by a second thermocouple.

A further modification to the apparatus involves the implementation of an einzel lens arrangement Fig 7.4. This has been positioned behind the earth plates of the ion optics as is demonstrated in the diagram. The primary aim of this device is to improve the existing poor transmission efficiency of the TOF system currently thought to be in the region of 10^{-5} . This is brought about by earthing the central electrode and optimising the voltages to the end plates such that electrostatic focusing of the diverging ions can be achieved in the extract region.

(3) Results and Discussions

Laser induced mass spectra taken at the NO resonance of 226.3nm are shown for all of the compounds Fig 7.5. Sensitivity measurements which rely on the presence of this peak will be

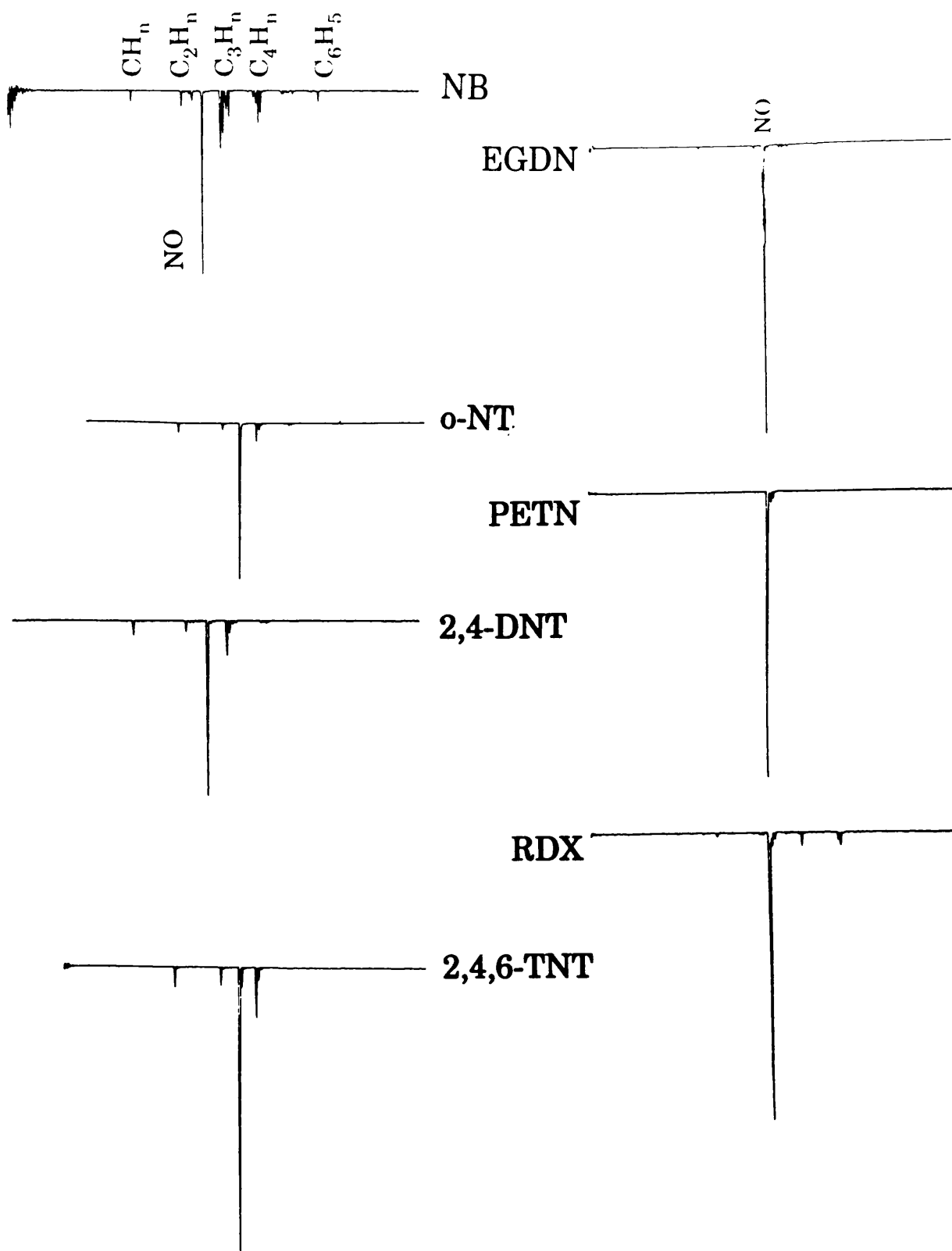


Fig 7.5 The TOF mass spectra for the various compounds studied are presented at 226.3nm.

discussed later. As expected, ultra violet laser interaction with the nitro-compounds leads to rapid predissociation and results in characteristic fragment ion spectra for the various compounds. Along with the hydrocarbons is observed the characteristic NO ion exhibiting a strong resonance at 226.3nm. In all of the materials analysed except in the case of PETN, other fragments apart from the NO ion have also been observed.

By looking at the hydrocarbon fragments formed and noting any characteristic trends, it is our intention to associate these features to the type of species under investigation. The classification of these compounds is divided as described in Fig 7.1. This assigns the samples into three distinct groups viz. nitroaromatics, nitrate esters and nitramine groups.

(4) Mass Spectra

For the nitroaromatics dealt with, namely nitrobenzene, o-nitrotoluene, 2,4 DNT and 2,4,6 TNT, there were some similarities in the hydrocarbon fragment distribution, with the compounds displaying characteristic hydrocarbon groupings (C_nH_m). Nitrobenzene shows the presence of all the hydrocarbon groups unlike the toluene based samples of o-nitrotoluene, DNT and TNT which appear to show very low intensity C_4 , C_5 and C_6 groups Fig 7.5. Nitrobenzene which has been extensively investigated previously gives the higher hydrocarbon components as well as displaying the parent ion Fig 6.10.

The nitrate ester group containing EGDN and PETN shows features which can distinguish it from the nitroaromatics so far studied. The difference in spectra which leads to this discrimination lies in the substantial reduction in the fragment yields from both compounds. This is particularly so in the case of PETN which appears to show a complete absence of any fragments. When examined at higher gain it is realised that some hydrocarbon fragment activity is present in the EGDN spectrum although PETN still does not show any of the

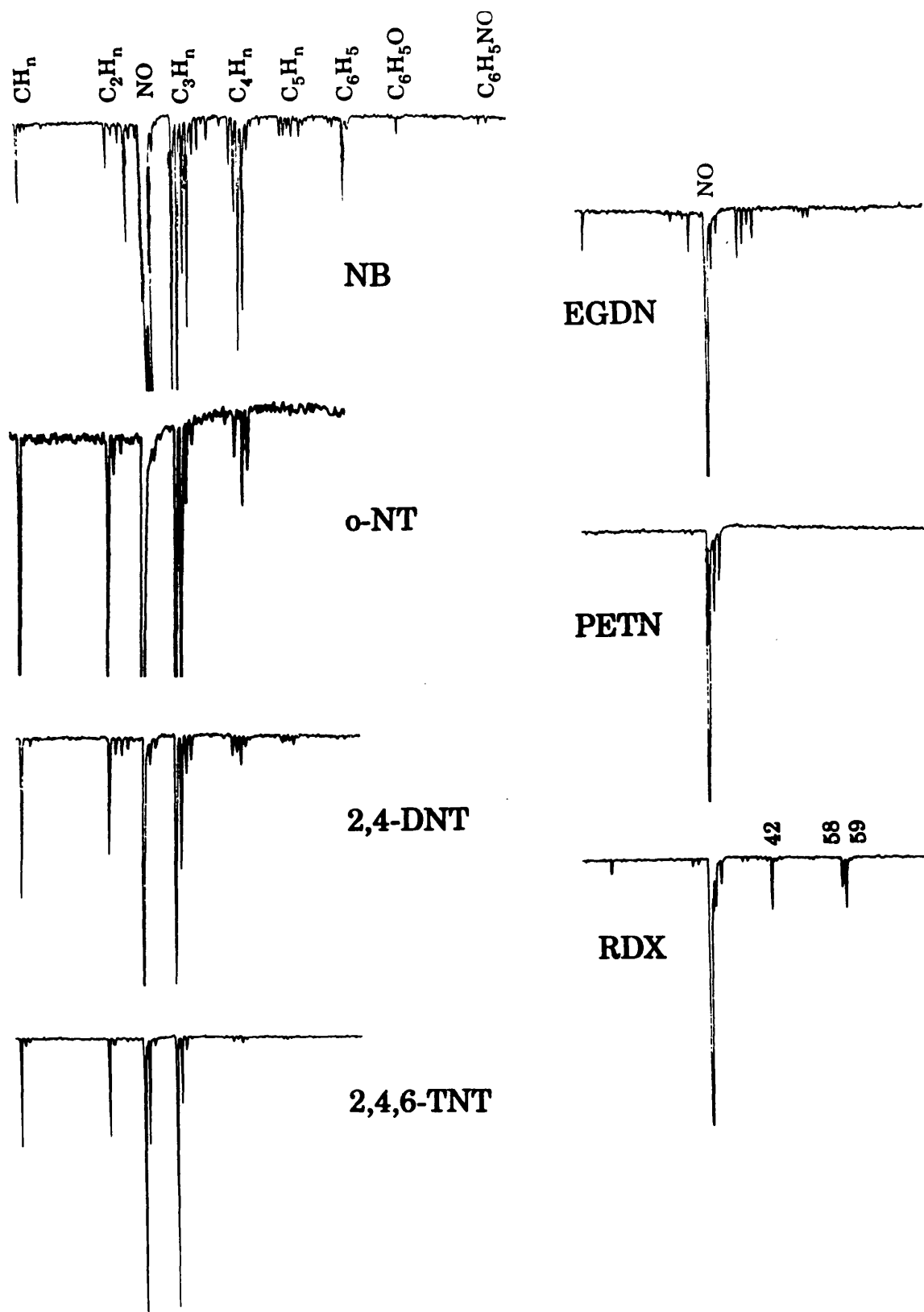


Fig 7.6 The same spectra presented in Fig 7.5 but with the y-gain set to a higher value in order allow easier inspection of the various hydrocarbon fragments.

fragments Fig 7.6. The hydrocarbon intensity from EGDN is significantly smaller than that obtained from the nitroaromatic species and may well be due to residual hydrocarbon contamination rather than arising from the EGDN sample. This preliminary set of data would indicate that nitroaromatic species more readily fragment to form the various hydrocarbon ion components than do members of the nitrate ester group.

These observations raise the question as to the pathways followed by the rest of the molecular fragments which, especially for the PETN case, are undetected. One possibility is that the residual fragments do not absorb laser radiation at these wavelengths and so are not ionised.

The final explosive investigated comes from the nitramines group and is called RDX. From the mass spectra taken of this compound so far, this would seem to be the one which can most readily be identified using mass spectral information alone. This is based on the observation of masses at 42, 58 and 59amu which are unique to this particular compound. The component at 42amu has been observed in electron impact studies and has been identified as the $(\text{CH}_2\text{NCH}_2^+)$ fragment (85). Electron impact studies of this compound did not show prominent peaks at 58 and 59amu although it is speculated that they may be an arrangement of the $\text{N}_2\text{C}(\text{CH}_2)_2\text{H}_{2,3}$ radical.

The mass spectra have revealed some promising signs for the discrimination of the various compounds studied. But the viability of using this approach in the presence of innocuous compounds has yet to be justified.

(5) Temperature Dependencies

A series of experiments implementing the sample inlet line heating mechanism was carried out on TNT, EGDN, PETN and RDX samples. Because of the low vapour pressure of these compounds at room temperature no signals could be recorded.

EGDN

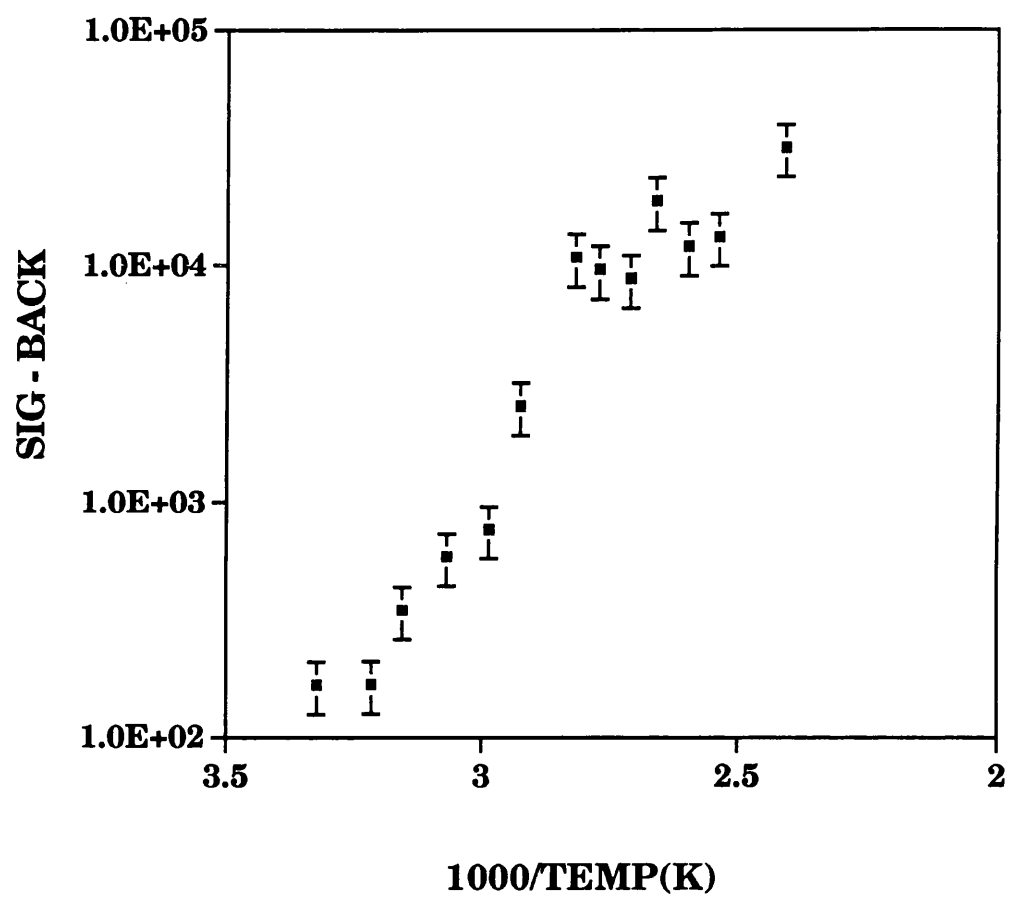


Fig 7.7 The variation of the NO ion from EGDN as a function of temperature, with fractional errors of 20% on the y-axis.

TNT

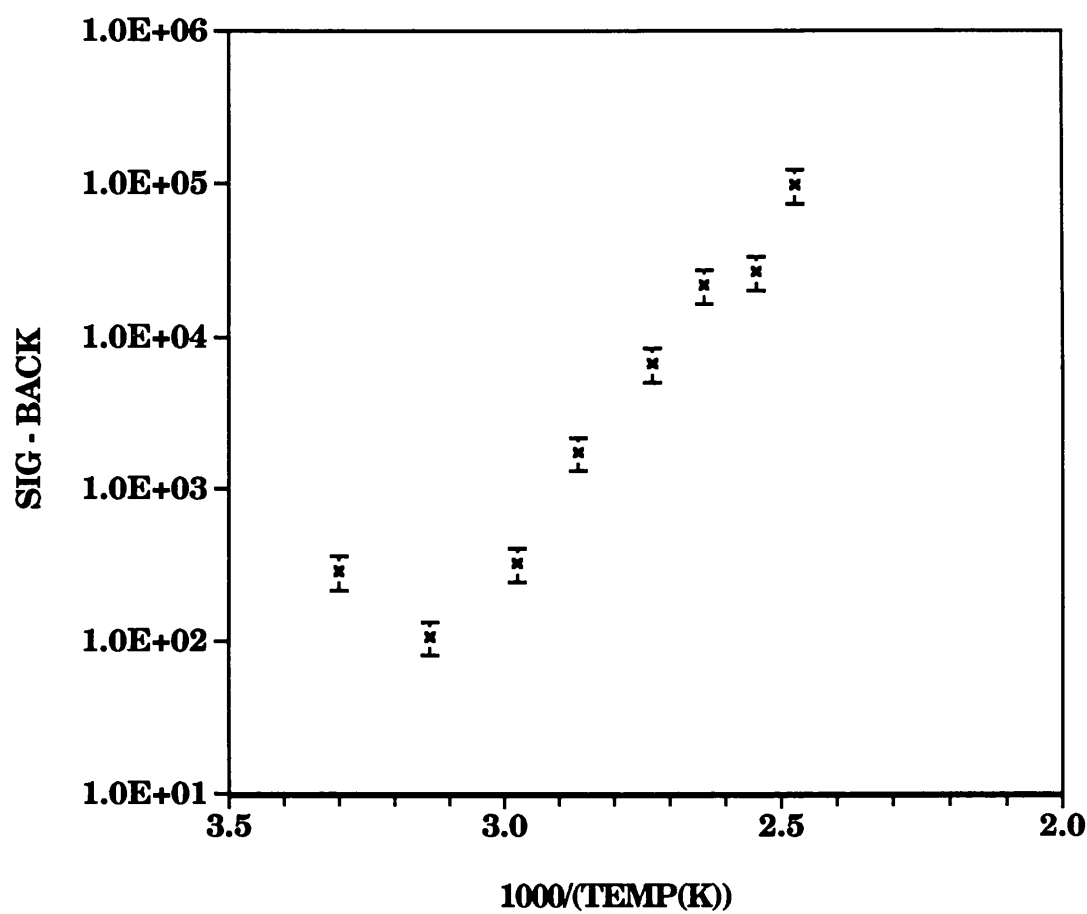


Fig 7.8 The variation of the NO ion signal from TNT as a function of wavelength. With the data points having a fractional error.

RDX

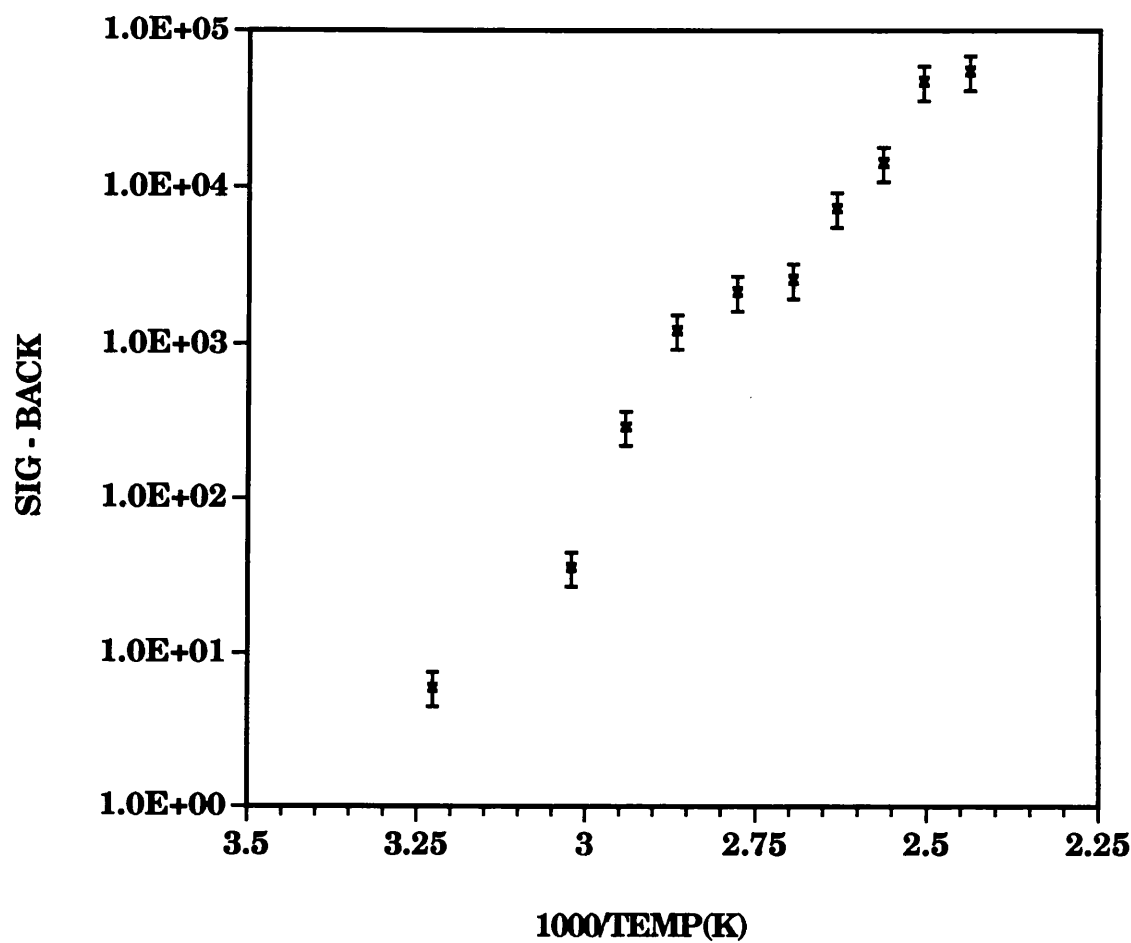


Fig 7.9 The variation in the signal from RDX as a function of wavelength is presented. With the data points showing 20% fractional error bars.

PETN

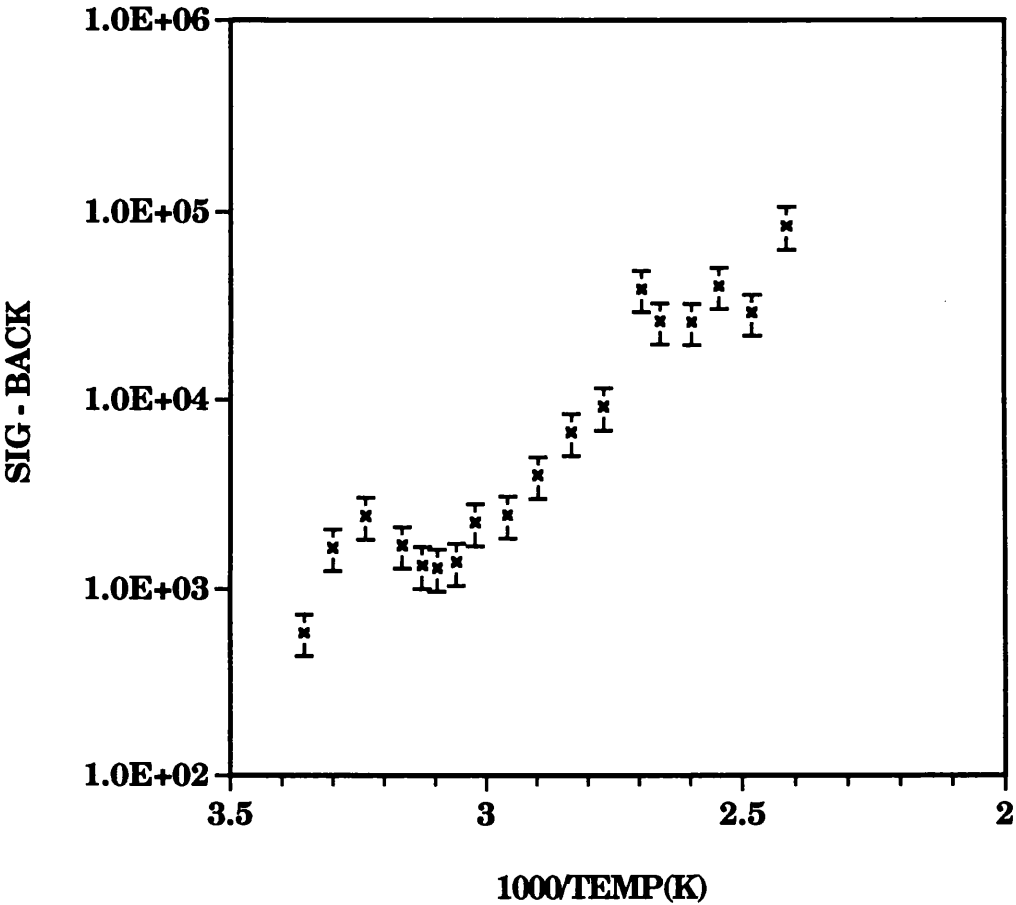


Fig 7.10 The variation in the NO ion signal recorded from PETN as a function of wavelength is shown. Each data point is shown with a fractional error.

The aim of our experiment is to compare the variation of the NO ion signal with temperature to the graphs of vapour pressure as well as determining the lowest temperature at which it is possible to detect the presence of the NO peak from a particular species.

The graphs of the 4 compounds studied in this fashion are shown Fig 7.7-7.10. The data for the graphs were recorded using the following technique. The sample inlet holder was heated to a set temperature and held at this temperature for approximately a minute to allow thermalisation. Thereafter the valve to the chamber line is opened and the sample sucked through. The mass spectra are averaged over 250 shots and the heights of the NO ion peak are measured. A plot of the NO⁺ intensity against 1000/T(°K) was constructed and compared with the vapour pressure versus 1000/T(°K).

Taking the RDX case for comparison purposes, it is clear that the theoretical prediction of the vapour pressure change over temperature range studied is approximately 4 orders of magnitude Fig 7.9. The NO ion signal over the same temperature range varies only by 2-3 orders. Although these values fall short of the predicted value it nevertheless signifies an important point as far as sensitivity is concerned. The temperature range covered in order to get 2-3 orders of magnitude increase in signal is ~100°C, therefore a marked increase in the sensitivity of our instrument can be achieved even with a single order of magnitude change in the temperature.

The difference in the comparison of the experimental and theoretical graphs can be put down to adsorption of the samples onto the walls of the inlet system. This might seem unlikely considering they are silica lined and constantly heated to ~120°C. However, when the sample inlet valve is closed an NO⁺ signal with a slow decay time is observed thereafter possibly arising from the outgassing of the sample from the walls of the inlet line. It is for this reason that when changing to different

samples the system is usually baked out for a couple of days in order to eliminate any residual signals, indicating that desorption is taking place from the walls of the system.

Another explanation for the disparity in the data could be that when the valve connecting the sample holder to the main chamber is opened, the saturated vapour pressure of the sample cannot be maintained. Although the saturated vapour pressure is a function of temperature alone, it would require a certain period of time before an equilibrium situation arises when exposed to a new volume. Therefore after opening the valve the vapour pressure in the sample holder would take an unknown time to reach its predicted value.

Comparisons of the vapour pressure variation with the NO^+ ion signal from EGDN and PETN showed that the experimental data provided an underestimate for the predicted value. (Fig 7.7, Fig 7.10) From such a comparison it would be expected that the NO ion signal increases in size in accordance with the vapour pressure increase with temperature.

The NO ion variation from EGDN and PETN samples matched more closely the predicted vapour pressure dependencies than that obtained from the sample of RDX.

The graph of TNT showed the most marked similarity with that expected. In fact these values were slightly above that which is predicted from the Fig 7.8.

When changing samples it was noted that the signals from TNT could be most readily eliminated from the system, within the space of a couple of minutes. This contrasts markedly with the other samples analysed, especially RDX which remained in the system persistently. It is anticipated that this difference between the samples is down to the different sticking coefficients for the molecules.

SENSITIVITIES OF DIFFERENT EXPLOSIVES IN LASER TIME-OF-FLIGHT MASS SPECTROMETER

EXPLOSIVES	TEMP (t) OF MEASURE- MENT °C	SAT. VAPOUR PRESSURE AT t °C (torr)	MINIMUM PRESSURE DETECTED torr	IDEAL GAS + MASS EQUIVALENT pg	EQUIVALENT CONCENTRATION	SAUSA et al
NB	20	0.04 unsaturated	$(1\pm0.6)\times10^{-6}$	65	1.3 ppb	2.4 ppm
DNT	26	0.005	$(4\pm2)\times10^{-6}$	400	5.3 ppb	
TNT	27	5×10^{-6}	$(0.4\pm0.2)\times10^{-6}$	50	0.5 ppb	1.7 ppm
EGDN	room temp.	permeation	tube	400		
PETN	25*	5×10^{-8}	$(0.05\pm0.04)\times10^{-6}$	8.4	65 ppt	
RDX	40*	5×10^{-8}	$(0.05\pm0.04)\times10^{-6}$	5.6	65 ppt	8 ppb

* Minimum detectable temperature † Calculated for a sample container of 10 ml volume.
The Glasgow measurements were all carried out with explosives in low pressure air (10^{-3} torr)
Sausa's measurements were all carried out with explosives in air/ argon at atmospheric pressure.

7.11) A table of sensitivities comparing the values obtained from Sausa's group with our own measurements.

The TNT molecules seem to show the least inclination to adhere to the surface and it is expected for this reason that the NO^+ ion signal variation resembles most closely the predicted vapour pressure dependency.

(7) Sensitivity Measurements

In the recorded mass spectra of explosive molecules, an averaging process is deployed in order to gauge the carbon containing fragment ion component. Consequently they are not considered to be the best signals to be used for sensitivity measurements. Conversely the dominant nature of the NO^+ ion at resonance wavelengths provides an ideal candidate as has previously been explained. Calculations involving evaluation of the sensitivities have been carried out at room temperature for nitrobenzene, 2,4-o-nitrotoluene, 2,4,6-TNT and PETN using the NO^+ ion intensity. By operating at this temperature it is possible to obtain the values of sensitivities achievable obviating the need to employ any heating apparatus. With the RDX sample an increase over the room temperature was required in order to get a measurable NO^+ ion signal. This involved heating the RDX sample to a temperature of 32°C . When considering the EGDN sample unlike the previous case it is provided in a permeation tube. The advantage of using a permeation tube is that the permeation rate is known, thereby giving us an accurate account of the quantity of sample released over a given time.

The table indicates the sensitivities predicted from temperature dependent measurements with the TOF mass spectrometer Fig 7.11. In these measurements the lowest temperatures at which an NO^+ ion signal could be recorded lead to the minimum vapour pressure for signal detection. Together with knowledge of the volume of the sample holder the number of sample molecules contained within the holder may be evaluated.

Volume of container 10ml at STP.

$$\frac{10}{22400} 6 \times 10^{23} = \text{No. of Molecules in 10ml}$$

Minimum pressure of detection Y torr.

Molecular weight of sample Z, therefore mass of sample available for detection

$$\frac{10}{22400} \cdot 6 \times 10^{23} \cdot \frac{Y}{760} \cdot Z \cdot U = \text{Mass of sample (grams)}$$

where U is the Atomic Weight in grams.

The equivalent concentration is calculated from the minimum pressure detectable divided by the atmospheric pressure.

The last column of the table is denoted to the results obtained by Sausa et al(78). In their experiments, a TOF spectrometer was used with the sample introduced in a cooled state via a supersonic jet of argon gas at atmospheric pressures.

At 10^{-6} torr, this corresponds to the detection of approximately picograms of explosive material in a container of volume 10ml. In order for us to make comparisons with other peoples work the equivalent explosives concentration at atmospheric pressure should be given. An explosives concentration of parts per billion is achieved when observation of a signal at 10^{-6} torr takes place, compared to atmospheric pressure. Sausa measurements indicate parts per million (ppm) concentrations of explosives at atmospheric pressures of argon and air. These two figures can be reconciled as being equivalent to each other when one takes into account the manner in which the sample is introduced into the TOF.

As the TOF is operated under high vacuum conditions in order to prevent molecular collisions and also for the efficient and long term operation of the ion detector, this means when introducing the sample from atmospheric conditions into a high vacuum environment typically 99.9% of the sample is lost.

For our sensitivity values of (ppb) to be realised for pure samples in real atmospheric samples the loss of three orders of magnitude must be made up.

(7) Conclusions

The possibility of sensitively detecting and identifying explosive materials using a laser ionisation technique has been investigated. This technique can reach parts per billion sensitivity levels with explosive mixtures when operated at the optimum wavelength of 226.3nm. Strong enhancements of the NO ion on resonance, as well as fragments which are characteristic of the type of species under investigation have been observed. These fragments provide a good indicator for the classification of the compounds under investigation and further promotes the selectivity aspect of the technique.

The NO ion intensity has been recorded as a function of temperature showing that the variation does not exactly correspond to the vapour pressure predictions, thus indicating an inefficiency in our sample introduction system.

It is noted that a substantial increase in the sensitivity can be attained by increasing the temperature of the sample.

One important point highlighted from the nitrobenzene impurity chapter is the possibility of contamination giving spurious results. This dilemma is also a feature of our investigation with the explosive compounds whose purity cannot be guaranteed. However it has to be appreciated that the samples dealt with in our analysis are the types most likely to be found in reality and in this respect provide realistic samples which would be encountered in normal practice.

8. Conclusions

The goal of explosive detection is of strategic importance from the point of view of both military and civil security. For this reason extensive research funding has been given to a variety of differing techniques and procedures as discussed in the introduction.

Resonance Enhanced Multiphoton Ionisation Mass Spectrometry is one such procedure which has been used to investigate the simplest nitroaromatic compounds, nitrobenzene and o-nitrotoluene. Subsequent studies have involved working with more complex explosives, for sensitive detection and identification purposes.

Chapter 4 described the situation in which a 'suspect' sample of nitrobenzene was analysed. The suspicion over its quality arose when the wavelength dependence of the hydrocarbon fragment yields showed a remarkable similarity to the UV absorption of benzene over this wavelength region. A series of experiments to establish whether or not contamination exists were carried out. These experiments included UV absorption spectroscopy, gas chromatography- mass spectrometry and electron impact mass spectrometry. The results from the aforementioned techniques could not establish the presence of a contaminant in the nitrobenzene sample.

Experiments performed using the REMPI technique revealed unambiguously the presence of benzene contamination in the nitrobenzene sample. In comparison it was concluded that the laser based approach identified the presence of the benzene impurity much more readily than the other techniques.

Chapters 5 and 6 give detailed expositions of the fragments obtained on laser irradiation of nitrobenzene and nitrotoluene. These compounds were found to readily fragment on irradiation of laser light to produce a variety of hydrocarbon groups.

Chapter 5 has been dedicated to a detailed analysis of the NO fragment, which is the most prominent ion in the mass spectra recorded in all of the explosive materials so far investigated. This ion is found to show the largest enhancements in signal size at 226.3nm in the wavelength regions so far studied. By carrying out sensitivity studies at this wavelength, attomole detection of NO containing compounds has been achieved.

The NO ion exhibits strong characteristic wavelength dependent spectra, which can be used as a fingerprint to show the presence of NO containing compounds. The origin of the wavelength dependent ion signals is evaluated as arising from vibrational and rotational bands in the electronic transition. A computer program was written in order to evaluate the theoretical wavelengths of the transitions and compared with the experimental data. This showed good similarity, with the band heads of both spectra matching closely.

Chapter 6 is divided into two main sections; 1) dealing with formation of atomic oxygen and hydrogen in the fragmentation of nitrobenzene; 2) discussing the photodissociation pathways of nitrobenzene.

In section (1) the transitions involved in production of both oxygen and hydrogen ions have been identified, with predictions made regarding the possible pathways leading to formation of neutral oxygen atoms. These predictions also postulate, under certain conditions, the production of excited state oxygen. To date no photoionisation of oxygen from the excited state has been observed. This analysis has, however, verified that significant numbers of both neutral oxygen and hydrogen atoms are liberated in the photodissociation of nitrobenzene.

Section (2) looks in detail at possible pathways which may lead to the formation of the other fragment ions arising during the photofragmentation of nitrobenzene. The fragmentation routes are divided into two main sections. These are dissociation ionisation (DI) and ionisation dissociation (ID) routes, which account for all of the fragment masses observed. The route which dominates is determined by both the wavelength and fluence of the laser beam.

Chapter 7 gives results from preliminary investigations of TNT, DNT, PETN, RDX and EGDN in the TOF mass spectrometer. Studies have involved looking at the variation of the NO intensity with temperature. These experiments have established the lowest temperature at which reliable signals may be detected. Quantitative measurements on the detection of these samples have been investigated which indicate high sensitivity is possible. Measurements based on the detection of the NO ion have indicated that attomole sensitivity can be attained under optimised conditions. Selectivity is possible between some of the samples on inspection of the fragments found in the mass spectra. The fragment ion spectra show features which are characteristic of the class to which the parent molecule belongs, i.e. nitroaromatics, nitrate esters, nitramines.

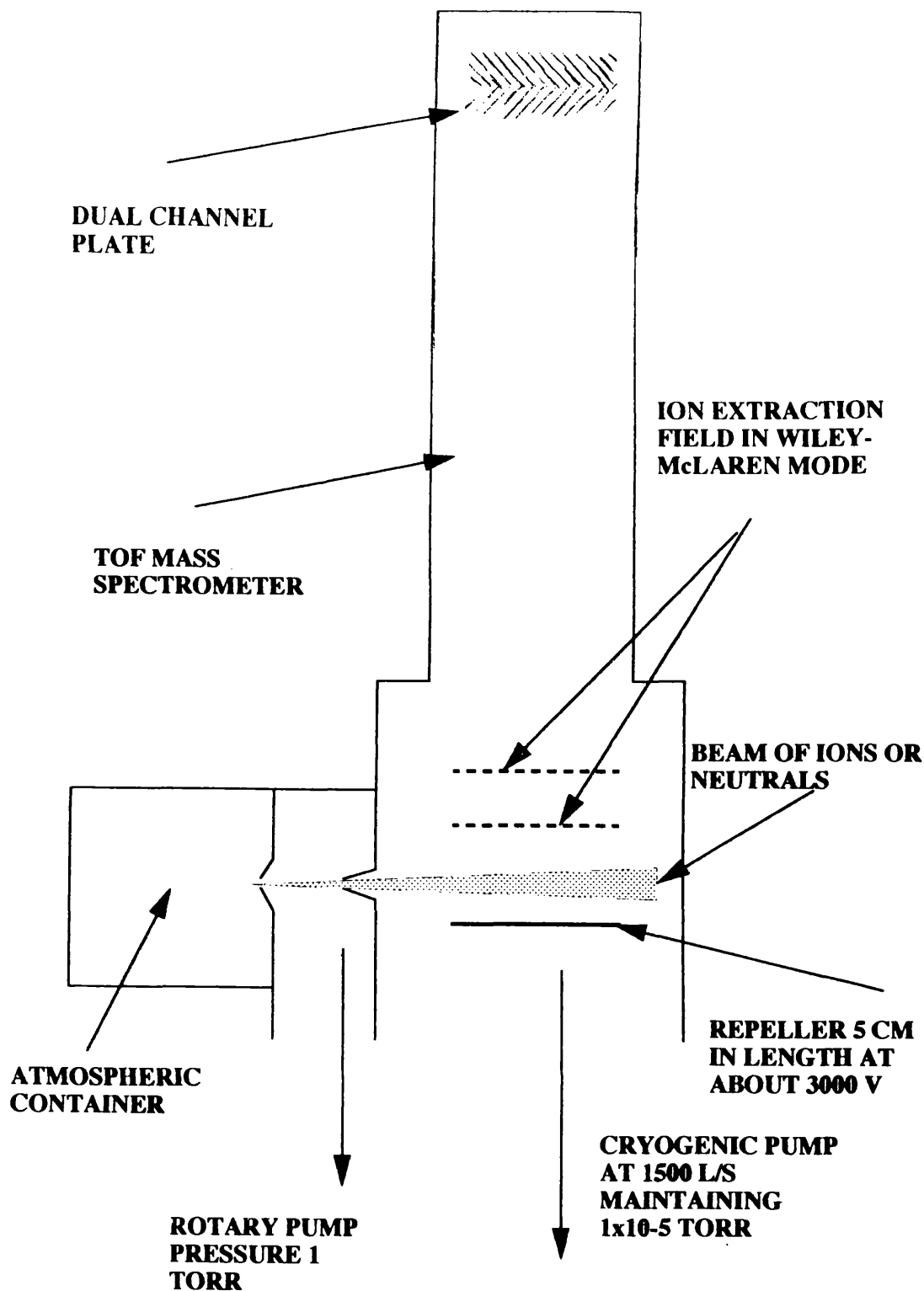
Future

Immediate work is concerned with obtaining the wavelength dependence of the fragment ions obtained from the samples of the more complex explosives. In particular studies on the NO ion will be carried out to establish whether the wavelength dependence of the NO ion yield is the same for all the explosive groups. It is also important to complete the wavelength dependence studies of the mass spectra by extending further into the UV where there are absorption bands for some of the explosives molecules as well as for the NO molecule. By

operating in the deep UV an increase in the fragment ion yield may be observed, thus enhancing the selectivity aspect of the procedure.

Work in the longer term will involve assessing the possibility of interfacing the technique for atmospheric pressure sampling. Developing the combination of laser ionisation and TOF mass spectrometry as a procedure for the detection of explosive compounds would be possible with some modifications to the existing apparatus. This can be brought about by using the laser to ionise the analyte in an atmospheric cell. Any ions produced can then be electrostatically directed towards the TOF system where the direction of the these ions is perpendicular to the flight axis. Once within the TOF spectrometer a pulsed voltage may be applied to the ion optics which would send the packet of ions down the flight tube to the detector where differences in flight time can be used for a mass analysis.(Fig 8.1)

With the above approach a potentially viable system exists for the sensitive and selective detection of specific analyte compounds. These do not necessarily have to be explosive in nature but could include drugs and chemical warfare agents.



8.1) An illustration showing the possibility of interfacing laser ionisation at atmospheric pressure, with a time of flight mass spectrometer.

References

- 1) V.S. Letokhov (1969) Report of the P.N Lebedev Institute, " On the possibilities of isotope separating by the methods of the resonant photoionization of atoms and photodissociation of molecules by laser radiation."
- 2) R.V Ambartsumyan, V.N. Kalinin and V.S. Letokhov (1971) Zh. Eksp. Teor.Fiz. Pisma Red. **13(6)**, pp305.
(English Translation) R.V. Ambartsumyan and V.S. Letokhov (1972), Appl.Opt. **11(2)** pp354.
- 3) G.S. Hurst M.H. Nayfeh and J.P. Young (1977), Appl. Phys. Lett. **30(5)**,pp229
- 4) G.S. Hurst M.G. Payne, S.D. Kramer and J.P. Young (1979), "Resonance Ionisation Spectroscopy and One Atom Detection ", Rev. Mod. Phys. **51(4)**, pp767.
- 5) V.S. Letokhov (1987), Laser Photoionization Spectroscopy. Academic Press Inc. (London) Ltd. **1987**.
- 6) Zhu J, Lustig D, Sofer I and Lubman DM, Anal. Chem. **62** (1990) pp2225
- 7) Haung DH, Kolaitis L, and Lubman DM, Appl. Spec. **41** (1987) pp1371
- 8) Roger Livesey, Electronics & Power , September, **1984**, pp708
- 9) 'Modern Methods and Applications in Analysis of Explosives', Jehuda Yinon and Shmuel Zitrin.

- 10) G.E. Spangler and P.A. Lawless Anal.Chem., **50** (1978) pp884-892.
- 11) S.D. Huang, L. Kolataitis and D.M. Lubman Appl. Spectrosc., **41** (1987) pp1371-1376.
- 12) Lee Grodzins Nuclear Instruments and Methods in Physics Research **B56/57** (1991) pp829-833.
- 13) P.Shea and T. Gozani Nuclear Instruments and Methods in Physics Research **A299** (1990) pp444-448.
- (14) Dermtroder W (1982), Laser Spectroscopy: Basic Concepts and Instrumentation., Springer Verlag, Chemical Physics 5.
- (15) G. S Hurst, M.G. Payne, S.D. Kramer and J.P. Young (1979), " Resonance Ionisation Spectroscopy And One Atom Detection", Rev. Mod. Phys. **51** (4) pp767.
- (16) Zandee, L and Bernstein, R.B. (1979). J.Chem. Phys. **71**, pp1359.
- (17) Vladilen S. Letokhov, "Laser Photoionization Spectroscopy".
- (18) Johnson, P.M. (1980). Acc. Chem. Res. **13**, pp20
- (19) Antonov, V.S., Letokhov, V.S., and Shibanov, A.N. (1981) Appl. Phys. **25**, pp71.
- (20) Andreyev, S.V., Antonov, V.S., Knyazev, I.N., and Letokhov, V.S.(1977). Chem. Phys. Lett. **45**, pp166.
- (21) Johnson, P. M., Berman, M.R., and Zakheim, D. (1975). J. Chem. Phys. **62**, pp2500.
- (22) Petty, G., Tai, C., Dalby, F.W. (1975). Phys. Rev. Lett. **34**, pp1207.

- (23) G.S Hurst, M.G. Payne "Principles and Applications of Resonance Ionisation Spectroscopy".
- (24) W.C. Wiley and I.H. McLaren, Rev. Sci. Instrum. **26**, pp1150 (1955).
- (25) S. Guizard, D. Chapoulard, M. Hortani and D. Gaoyacq Appl. Phys. B47, (1089) pp471.
- (26) J.A. Syage Anal.Chem. **62**(1990) pp505 A.
- (27) D.M. Lubman Anal. Chem. **59**(1987) pp31A.
- (28) J.C. Miller Anal. Chem **58**(1986).
- (29) A. Marshall, A. Clark, R. Jennings, K.W.D. Ledingham, J. Sander and R.P. Singhal, Int. J. Mass Spectrometry Ion Proc., **116** pp143-156, 1992
- (30) A. Clark, K.W.D. Ledingham, A. Marshall, J. Sander and R.P. Singhal, Analyst, June 1993, Vol. **118** pp601
- (31) G.W. Lemire, J.B. Simeonsson and R.C. Sausa, Anal. Chem, **65**,pp529-533, 1993.
- (32) A. Marshall, A. Clark, K.W.D. Ledingham, J. Sander and R.P. Singhal Int. J. Mass Spectrom. and Ion Proc., **125**(1993) R21-R26
- (33) D.B. Galloway, J.A. Bartz, L. Gregory Huey and F.F. Crim. J. Chem. Phys. **98**(1993) pp2107.
- (34) J. Zhu, D. Lustig, I. Sofer and D.M. Lubman Anal. Chem **62**(1990) pp243.

- (35) A. Marshall, A. Clark, R. Jennings, K.W.D. Ledingham, J. Sander and R.P. Singhal, *Int. J. Mass Spectrometry Ion Proc.*, **112** (1992) pp273.
- (36) G.H Atkinson and C.S Parmenter *J.Mol. Spectr.* **73**, (1978), pp52.
- (37) A.Marshall, A.Clark, R.Jennings, K.W.D Ledingham and R.P Singhal *Meas. Sci Technol.* **2**(1991) pp1078-1082.
- (38) N. Ikeda et al. *JAC* **107**, pp3381, (1985).
- (39) Multiphoton Ionisation and Fragmentation Pathways of Polyatomic Molecules: Studies with a Laser Time-Of-Flight Mass Spectrometry.
- (40) News of The Week, March 4, **1991 C & EN**
- (41) H. Zacharias, K. Geilhaupt, K. Meier and K.H. Welge, *J. Chem. Phys.*, **74** (1981) pp218.
- (42) Boesl, U. , Neusser, H.J. , and Schalg, E.W. , *J. Chem. Phys.*, **1980,72**,pp4327.
- (43) Fisanwick, G.J., Eichelberger, T.S., IV, Heath, B.A. ,and Robin, M.B., *J.Chem. Phys.* , **1980,72**, pp5571.
- (44) Hager, J.W., and Wallace, S.C., *Anal. Chem.*, **1988, 60**, pp5.
- (45) Lubman, D.M., Naaman, R., and Zare, R.N., *J. Chem. Phys.*, **1980, 72**, pp3034.
- (46) Rettner, C.T., and Brophy, J.H., *Chem. Phys.*, **1979, 71**, pp1359.

- (47) J.J. Kaufmann, P.C. Hariharn, S. Roszak and M. van Hemert J. Comput. Chem. **8**(1987) pp736.
- (48) E.C Apel and N.S Nogar, Int. J. Mass Spectrom. Ion Processes, **70** (1986) pp243.
- (49) Dermtroder W(1982), Laser Spectroscopy: Basic Concepts and Instrumentation., Springer Verlag, Chemical Physics 5.
- (50) Beta And Gamma Band Systems Of Nitric Oxide,
R. Engleman JR, P.E. Roose, H.M. Peek, V.D. Baiamonte
Los Almos Scientific Laboratory LA 4364 UC -34 Physics TID-4500 (1970).
- (51) Arepalli S, Presser N, Robie D and Gordon R.J. 1985 Chem Phys. Lett. **118**pp88-92.
- (52) Das P, Ondrey G, van Veen N and Borsohn R 1983 J. Chem. Phys. **79** pp724-6
- (53) Matsumi Y, Shafer N, Tonokura K, Kawasaki M, Huang Y and Gordon R 1991 J.Chem. Phys. **95** pp7311-6.
- (54) Tonokura K, Shafer N, Matsumi Y and Kawasaki M 1991 J. Chem. Phys. **95** pp3394-8.
- (55) Whetten R.L, Fu K. J, Tapper R. S and Grant E.R 1983 J. Phys. Chem. **87** pp1484-7.
- (56) Dixit S N, Levin D A and McKoy B V(1988), Phys. Rev. A **37** No. 11, pp4220.
- (57) Slanger T. G, Bischel W. K and Dyer M. J 1983 J. Chem. Phys. **79** pp2231-9.
- (58) Spinelli N, Bruzzese R, Pavese G and Aremenante M 1987 Opt. Commun. **63** 153-8.

- (59) Haas T, Gericke K. H, Maul C and Comes F. J **1993** chem. Phys. Lett. **202** pp108-14.
- (60) Mordaunt D. H, Lambert I. R, Morley G. P, Ashfold M. N. R and Dixon R. N **1993** J. Chem. Phys. **98** pp2054-65.
- (61) G.Porter and B. Ward , Proc. R. Soc. London Ser A **303** , pp139, (1968)
- (62) P.Brown , Org. Mass. Spectrom., **4** , pp533, (1970)
- (63) E.S. Mukhtar ,I.W. Griffiths, F.M.Harris and J.H. Beynon, Org. Mass Spectrom., **15**, pp51, (1980)
- (64) T. L. Bunn, A. M. Richard and T.Baer, J. Chem. Physics, **84** pp1424, (1986)
- (65) V.H. Schuler and A.Woeldike, Phys. Z., **45** , pp171, (1944)
- (66) S.H. Hastings and F.A. Matsen, J.Am. Chem. Soc., **70**, pp3514, (1948)
- (67) H. Budzikiewicz, C. Djerassi, D.H. Williams " Mass Spectrometry of Organic Compounds ", Holden- Day Inc , San Francisco (1967)
- (68) J.B. Simeonsson, G.W. Lemire, and R.C. Sausa, submitted for publication to Applied Spectra.
- (69) P. Brown, Org. Mass Spectrom., **3**, pp1175, (1970)
- (70) J. Beynon, M. Bertrand and R.G. Cooks, J. Am. Chem. Soc., **95**, pp1739, (1972)
- (71) F.W. McLafferty, P.F. Bente III, R Kornfeld, S.Tsai and I. Howe, J. Am. Chem. Soc., **95**, pp2120, (1973)

- (72) I.W. Griffiths, E.S. Mukhtar, F.M. Harris and J.H. Beynon, *Int. J. Mass Spectrom. and Ion Phys.*, **38**, pp333, (1981)
- (73) I.W. Griffiths, F.M. Harris, E.S. Mukhtar, and J.H. Beynon, *Int. J. Mass Spectrom. and Ion Phys.*, **38**, pp127, (1981)
- (74) M. Panczel and T. Baer, *Int. J. Mass Spectrom. and Ion Proc.*, **58**, pp43, (1984)
- (75) T. Nishimura, P.R. Das and G.G. Meisels, *J. Chem. Phys.*, **84**, pp6190, (1986)
- (76) V.M. Matyuk, V.K. Potapov and A.L. Prokhoda, *Russ. J. Phys. Chem.*, **53**, pp538, (1979)
- (77) A. Clark, C. Kosmidis, K.W.D. Ledingham, A. Marshall, J. Sander, R.P. Singhal and M. Campbell, *J. Phys. B*, **26**, ppL665, (1993)
- (78) F. F. Crim - private communication
- (79) W. M. Uselman and E.K.C. Lee, *J. Phys. Chem.*, **65**, pp1948, (1976)
- (80) R.J. S. Morrison and E. R. Grant, *J. Phys. Chem.*, **77**, pp5994, (1982)
- (81) R.J. S. Morrison, B.H. Rockney and E. R. Grant, *J. Phys. Chem.*, **75**, pp2643, (1981)
- (82) T.G. Slinger, W.K. Bichel and M.J. Dyer, *J. Chem. Phys.*, **79**, pp2231, (1983)
- (83) A. Marshall, A. Clark, R.M. Deas, C. Kosmidis, K.W.D. Ledingham, J. Sander, R.P. Singhal, to be published

(84) S.H. Allam, M.D. Migahed and A.El Khodary, Int. J. Mass Spectrom. Ion. Phys., **39**, pp117, (1981)

(85) Volk F, Schubert H, Explosivstoffe **16** (1968) pp2

